Modelling of the human quiet stance with ankle joint complexity

UNIVERSITY OF **Hull**

Amartya Ganguly, B.Tech

School of Engineering

University of Hull

A thesis submitted for the degree of

Doctor of Philosophy

August 2014

This thesis is dedicated posthumously to my loving grandfather, Phanindranath Ganguly who has been a constant source of inspiration. I would also like to dedicate this thesis to my parents for their everlasting love and affection.

Acknowledgements

that has funded this challenging project, and for making my doctoral journey very special.

Abstract

This study derives an inverted pendulum model for quiet stance in humans around the ankle joints with 4×9-element mass-spring-damper (MSD) units as the musculoskeletal connections between the shank and foot bilaterally. The model focuses on the role played by both the stiffness and the damping parameters of muscles, tendons and ligaments about the ankle complex. This model partitions muscles, tendons and ligaments functionally. This novel model is used to study the behaviour of individual components in relation to quiet standing. The Lagrange d' Alembert principle has been used to derive the equations of motion of the system and resulted in eighteen 2nd order differential equations with nine constraints. Four MSD units connects with the shank (tibia and fibula) and foot bilaterally. The units function passively and are representative of the mechanical functionality of muscles, tendons, and ligaments about the ankle complex. The dynamics of the MSD units are considered linear in nature and their stiffness and damping parameters are calculated by finding the slope of the force vs. deformation length curve and force vs. velocity curve reported in the literature.

The simulation results revealed that the torques generated by the internal constraints through the MSD units are significantly greater than the gravitational torque. A case study has been conducted for eyes open vs. eyes closed conditions. It was found that the angular displacement of the shank varied but the overall range of motion of the ankle joint remained constant at $0.6°$. This was expected as there was no external perturbation applied to facilitate any amount of plantarflexion or dorsiflexion at the point of articulation of the ankle joint.

In conclusion, the model derived and analysed in this study explains that the human body was able to maintain its upright posture mechanically during unperturbed quiet standing without the use of an active control system emphasising the importance of damping and its influence on postural balance. Furthermore, this sophisticated model is not limited to only considering the muscle-tendon unit and ligaments play an important role in maintaining balance during quiet stance and are therefore included in the model. This model is physiologically more realistic than previously developed postural models thus providing a deeper insight towards the passive mechanism of postural balance and providing a new approach towards future postural models.

Contents

List of Figures

Nomenclature

α angle of sway of shank

$\dot{\alpha}$ first order time derivative of α

$\ddot{\alpha}$ second order time derivative of α

h vertical distance between the CoM of the upper body and malleoli

f_h height of the foot from the ground

g gravitational acceleration

m total mass of the body

m_a mass of tendon

m_b mass of muscle

m_c mass of ligament

k_a linear stiffness of tendon

k_b linear stiffness of muscle

k_c linear stiffness of ligament

c_a linear viscoelasticity of tendon

c_b linear viscoelasticity of muscle

c_c linear viscoelasticity of ligament

v comprises of l left leg and r right leg

i units 1, 2, 3, and 4

q generalised co-ordinates

$\dot{q}$ first order time derivative of q

$\ddot{q}$ second order time derivative of q

p co-ordiantes transformed from q

$\dot{p}$ first order time derivative of p

$\ddot{p}$ second order time derivative of p

p^{-1} inverse of co-ordinate transform p

$\frac{\partial p}{\partial q}$ partial derivative of p with respect to q

$(\frac{\partial p}{\partial q})^{-1}$ inverse of matrix $\frac{\partial p}{\partial q}$

Q' transpose of matrix Q

$y_{v,i}^{0}$ natural length of MSD unit

$\bar{y}_{v,i}$ change in MSD unit length

$y_{v,i}$ difference between the natural and changed unit lengths

I_a moment of inertia of the whole body

e vector containing segment geometry values

e' transpose of matrix e

E diagonal matrix of e_1

e_1 a 1×2 co-efficient matrix of E with elements 0 and 1

$\bar{E}$ diagonal matrix of $\bar{e}_1$

$\bar{e}_1$ a 1×2 co-efficient matrix of $\bar{E}$ with elements 1 and 0

D diagonal matrix of $\bar{y}_{r,i}$

D^{-1} inverse of matrix D

$\bar{D}'$ transpose of matrix $\bar{D}$

τ_f frictional torque

k_f co-efficient of friction

M symmetric positive definite inertia matrix

$C\dot{q}$ centrifugal and Coriolis torques

$G(q)$ gravitational torques

f vector of dimensional elements

$f(q)$ f is a function of generalised co-ordinates q

F partial derivative of $f(q)$ with respect to q

F' transpose of matrix F

$F'\lambda$ generalised torques induced by the constraints

λ Lagrangian multiplier

Chapter 1

Introduction

1.1 Introduction

Postural balance is maintained when all body segments function synergistically. Nashner and McCollum (1985) described the controlled ankle and hip movements as two postural strategies which help to maintain a balanced posture during external perturbations. In the ankle strategy, substantial sway of the centre of mass (CoM) with respect to the ankle complex occurs. However, the hip strategy involves a combination of the hip and ankle movements, where the hip plays a more dominant role in maintaining balance. Postural balance essentially means that the point of equilibrium of the body is constantly adjusted to prevent the body from a fall, which results in anterior-posterior and medio-lateral sways (Nashner, 1970). Sway is initiated during free stance as a result of inherent unstable properties of the body together with internal and external perturbations (Karlsson and Persson, 1997).

One aspect of postural balance investigations is the study of quiet stance which is usually modelled as an inverted pendulum (Aramaki et al., 2001; Casadio et al., 2005b; Fitzpatrick et al., 1994; Gatev et al., 1999; Karlsson and Persson, 1997; Winter et al., 1996). Among various models of the inverted pendulum, intrinsic stiffness models (Casadio et al., 2005b; Fitzpatrick et al., 1992; Humphrey and Hemami, 2010; Thomas Edwards, 2007) are often used to understand the mechanical contributions of the musculoskelatal system towards postural balance. These

models mainly focus on the mechanical properties of the musculoskelatal system which affect the equilibrium process of the system. However, these postural models have typically considered only a single muscle-tendon acting as a single unit into account, apart from Humphrey and Hemami (2010) which so far remains as the only study that has included ligament for a postural model. The models so far proposed have demonstrated that stiffness properties alone are insufficient to maintain an upright stance in a person subjected to external perturbations.

The aim of this thesis is to consider intrinsic soft tissue mechanical parameters such as stiffness and damping, and their effects during quiet stance. The model has taken into account the muscles, tendons and ligaments, grouping them based on their biomechanical functionality and essentially mapping the outcome of the individual components. This study will show that intrinsic inverted pendulum modelling can maintain the equilibrium position of the body during quiet stance without the involvement of a control system. This thesis hypothesises that during quiet stance, the intrinsic mechanical properties (such as stiffness and damping) of muscles, tendons and ligaments passively affect anterior-posterior sway with respect to the ankle complex. To understand the mechanical attributes of muscles, tendons and ligaments, an inverted pendulum model is proposed which takes into account both the stiffness and damping properties of the soft tissues. It also compares the effects on postural balance when quiet stance is modelled using only muscle-tendon unit versus muscle-tendon-ligament unit.

The following sections set the background of various theories put forward towards understanding postural balance.

1.1.1   Theories proposed to explain quiet stance

The assumption that there is no movement of body segments during quiet stance, and thus is of no tangible consequence showed the lack of research towards postural balance. However, the research in recent years, proved the assumption to be erroneous (Casadio et al., 2005b; Loram and Lakie, 2002; Loram et al., 2005; Morasso et al., 1999a; Thomas Edwards, 2007). Postural stability is extremely important in activities of daily living and is one of the first skills to degenerate due to ageing (Coogler, 1992). A principal requirement to prevent falls and avoiding

bone fractures is the ability of the human body to have stability (Coogler, 1992; Morasso et al., 1998).

Standing, an initial state also acts as a precursor to walking or running, is considered a relatively simple task but in reality, it is not the case as the body needs constant stabilisation which may lead to fatigue (Morasso et al., 1999a). It is interesting to note that people can voluntarily change their centre of pressure (CoP) in order to maintain upright stance which can be defined as a vertical force and the trajectory of the line of action of the same force, intersecting at a point on the base of support (Latash et al., 2003). The human body in its upright posture, has a high CoM maintained over a relatively small base of support which means that the body has a high potential energy and therefore, requires maintaining equilibrium control during quiet stance (Gatev et al., 1999).

1.2   Motivation

This thesis recognises the biomechanical issues that contribute towards maintaining upright stance and investigates the intrinsic mechanical properties of the ankle strategy. This study emphasises the need for detailed modelling of the ankle complex to understand postural balance. In order to justify the orientation and positioning of soft tissues (such as muscles, tendons and ligaments), it is also necessary to study radiograph images of the bones of the human ankle complex before discussing the various mechanical and architectural parameters.

To have a clear understanding of the role played by the ankle in postural stability, it is imperative to formulate a mathematical model to illustrate and explain postural balance with respect to the ankle complex. In this thesis, it has been assumed that the central nervous system is already triggered and hence the muscles are signalled to engage accordingly. This implies that the muscles, tendons, and ligaments facilitate the movement of posture passively.

The mathematical model developed in this thesis is considerably different from the classical single inverted pendulum model. The models so far reported are simplistic with regard to the inherent mechanical properties of the muscles, tendons and ligaments which perform a vital role during quiet stance. Parameterisation of these soft tissues in terms of their mass, stiffness and damping co-efficients has

been taken into account as they affect postural control.

1.3   Thesis overview

The section provides a brief overview of the thesis, highlighting the main points of interest and previous key literature.

1.3.1   Literature review

The focus of this literature review is on the development of the inverted pendulum theory (Fitzpatrick et al., 1994; Karlsson and Persson, 1997; Winter et al., 1996) which has brought about widespread research discussion for several decades (Aramaki et al., 2001; Casadio et al., 2005b; Fitzpatrick et al., 1994; Horak and Nashner, 1986; Humphrey and Hemami, 2010; Latash et al., 2003; Loram et al., 2005; Nashner, 1970; Smith, 1957; Winter et al., 1996). This chapter first introduces the concept of the inverted pendulum with regards to postural balance, and then explores the type of modelling undertaken to explain quiet stance in the absence of external perturbations. Not only does this chapter highlight areas where a consensus is still lacking but it also critically discusses certain discoveries which have proven detrimental to the advancement of postural assessment. The use of experimental practices and protocols are also discussed at length. These are instrumental in evaluation, validation and formation of new conceptual theories to address postural balance.

1.3.2   Mathematical modelling of the ankle complex

An entire chapter has been dedicated to the conceptualisation, formulation and derivation of the mathematical model during quiet stance using the Lagrange D'Alembert principle for dynamic systems. In this case, mass-spring-damper (MSD) units are used as musculoskeletal models to explore the inverted pendulum theory and their role played in postural balance in the anterior-posterior direction. In terms of dimensional parameters (length of MSD units and their angular precision) which were required to derive constrained dynamic equations, the functional geometry of the MSD units plays an important role. The underlying

geometrical changes involved during anterior-posterior sway have been calculated using the basic trigonometry of the shank and ankle setup.

1.3.3 Parameterisation of the proposed model

As the model is largely based on the intrinsic mechanical properties of the muscles, tendons and ligaments (namely stiffness and damping parameters), this chapter investigates these datasets from the published literature. This chapter discusses at length the methods used to calculate these parameters and why they were considered suitable for the proposed postural sway model. These unknown dimensional parameters were calculated from the published data of anatomical literature making extensive use of radiograph images.

1.3.4 Initial simulation of the mass-spring-damper model and testing of model parameters

After the model parameters were determined, this chapter evaluates the said parameters with initial inputs from experimental data from published research. The system's responses under six different types of mechanical conditions namely:

1) damping with 100% stiffness; 2) damping with 75% stiffness; 3) damping with 50% stiffness; 4) damping with 25% stiffness; 5) stiffness only; 6) minimal damping with 100% stiffness.

The object of the simulation study was to determine if the shank would be able to return to its upright equilibrium position which is inherently unstable without any control mechanism. From the simulation, it was inferred that the inverted pendulum model with MSD units would indeed passively retract to its initial biased upright position thus providing an insight into the dominance of the triceps surae muscle group during quiet stance.

The model was linearized in order to see which six conditions would be an ideal combination of parameters for a stable system. Nyquist and Bode diagrams are standard tools which were used to determine stability of the inverted pendulum model described in this thesis.

1.3.5   A preliminary case study for model evaluation

A single healthy subject has been tested in eyes open and eyes closed conditions during upright quiet stance with synchronised EMG and motion capture equipment to measure muscle co-activation of the triceps surae muscle group (gastrocnemius lateralis, gastrocnemius medialis, soleus) and tibialis anterior during quiet standing. The EMG was then compared with maximal voluntary isometric contraction(MVIC) to assess muscle co-activation levels during anterior-posterior sway. Although the MSD model of the inverted pendulum could not distinguish the eyes open from the eyes closed condition, the difference between ankle angular displacement during unperturbed quiet stance was negligible with and without visual input. This ankle angular displacement has then been used as input in subsequent simulations to further evaluate the model simulation.

1.3.6   Mass-spring-damper model simulations with internal perturbation

This chapter evaluates the MSD model further using the participant anthropometrics recorded in the case study. This chapter examines the postural response of the MSD system in the presence internal perturbations. The simulation results show that the internal perturbation applied to the inverted pendulum model did not destabilise the system which further evaluates that the model under damping with 100% stiffness is the most plausible candidate to mimic quiet stance in humans.

1.3.7   Conclusion, limit of the study and future work

In Chapter 8, the main results of this investigation are discussed with reference to the novelty of the research and by highlighting the crucial points of interest to further our understanding of human postural sway with regards to the inverted pendulum theory. The conclusions drawn stress the importance of modelling by using intrinsic mechanical models that focus on the passive torque generated about the ankles. The findings also highlight certain limitations which the model has been subjected to and further ideas that would prove detrimental during

future investigations.

Chapter 2

Postural balance models

2.1 Introduction

The study of postural control encompasses a variety of complex systems within the human body which include the musculoskeletal, somatosensory, vestibular, visual and central nervous systems (Horak and Macpherson, 1996). In order to simplify the problem, studies have focused on one or two systems at a time. To test various hypotheses to explain quiet stance, relatively simple computational and mathematical models were derived (Peterka, 2002; Winter et al., 1998, 2001). These models represented the lower limbs body using single inverted pendulums. The lower limbs, especially the ankle complex have been over-simplified using massless links or triangular wedges (Karlsson and Persson, 1997; Morasso et al., 1999b; Qua et al., 2007). However, in recent years a number of studies (Casadio et al., 2005a; Humphrey and Hemami, 2010; Loram and Lakie, 2002; Morasso and Sanguineti, 2002) investigated the ankle joint as one of the important factors responsible for postural control. Substantial effort has been made to understand the biomechanics of this joint especially its geometrical orientation by developing mathematical and computational models. Such models are mathematically and computationally demanding but on the other hand very suitable for simulating its dynamic behaviour required for postural control.

2.2 Single segment inverted pendulum models

To investigate the adequacy of the single segment inverted pendulum model and the role played by the joints above the ankles to maintain a quiet stance, only two studies have investigated the effect of joint immobilisation above the ankles (Aramaki et al., 2001; Fitzpatrick et al., 1994). Fitzpatrick et al. (1994) measured the amount of postural sway in the anterior−posterior (AP) direction after joint immobilisation, whereas the effect of joint immobilisation on mediallateral(ML) direction was not assessed. They observed that when a rigid splint prevented the movement of all joints above the ankles, the magnitude of angular sway about the ankle increased significantly.

The results of the study by Paulo et al. (2009) revealed that after immobilisation of the knees, hips and trunk, a small but significant increase in postural sway in the AP direction was identified. These results contradict the hypothesis that postural stability in the AP direction can be achieved through minimal joint motion above the ankles and argue against the idea that the single inverted pendulum model can adequately describe quiet stance. These results agreed with Fitzpatrick et al. (1994) who reported a 52% increase in ankle joint sway during joint immoblisation versus sway during unrestricted body segments. These studies (Fitzpatrick et al., 1994; Paulo et al., 2009) argued that during unrestricted body segments, body stability increases by minimising the dependency on the ankle joints for stability during quiet stance.
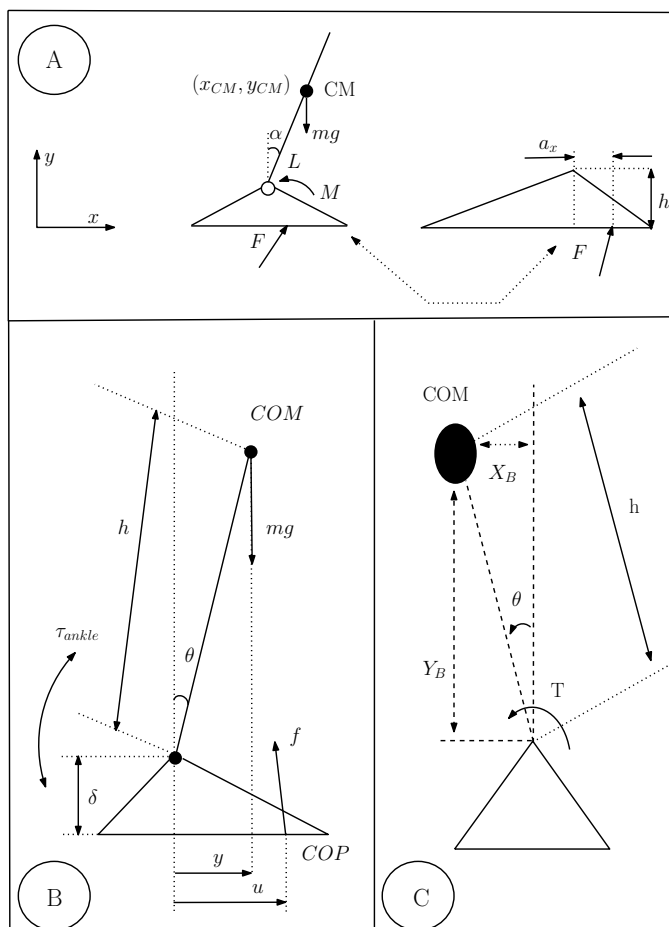
Figure 2.1: Typical single-segment inverted pendulum models. Figure (a) illustrates an inverted pendulum model proposed by Karlsson and Persson (1997) in the saggital plane. The straight line represents a rigid body rotating about the ankle joints. The triangular wedge represents the foot, where h is the distance from the ground to the ankle joint centre in the vertical direction, L is the distance from the ankle joint to the CoM and M is the moment of the force at the ankle joint. Figure (b) illustrates an inverted pendulum model for quiet stance proposed by Morasso et al. (1999b). The triangle here also represents the foot with h as the distance from the ground to the ankle joint centre. δ and u are the vertical and horizontal displacements of the CoP with respect to the ankle joint. Finally, y is the horizontal displacement of the CoM of the system. Figure (c) illustrates a single-segment inverted pendulum model for sway mechanism during quiet stance proposed by Qua et al. (2007). The triangle again is representative of the foot, where h is the height from the ankle joint centre to the CoM of the body, T is the torque generated at the ankle and θ is the sway angle.

10

In Figure 2.1, model A developed by Karlsson and Persson (1997) is an inverted pendulum model of the human body in the sagittal plane. The straight line represents the rigid body rotating about the ankle joints, where (X_{CM}, Y_{CM}) are the coordinates of the CoM. The foot is modelled as a triangle, where h represents the distance from the floor to the ankle joint centre in the vertical direction, L is the distance from the ankle joint to the CoM and a_x as the distance from the CoP to the ankle joint in the horizontal direction. Lastly, F represents the resultant ground reaction force vector. The CoM estimated by both the marker as well as model based method result in a few differences. Firstly, because of the construction of the human ankle joint and the surrounding soft tissues, the human body would not function as a perfect inverted pendulum. The model parameters has contrarieties and positioning of reflective markers is not exactly at the same level as the true CoM. The measures reported in this study are considered important with regard to the extent of the ankle strategy used for postural balance. The model would be applicable only when the system behaves like an inverted pendulum, which is in the sagittal plane when the ankle strategy is adopted.

Model B in Figure 2.1, proposed by Morasso et al. (1999b) considers only AP oscillations. However, the model and the algorithm could be applied to ML oscillations as well. This model shows an inverted pendulum in which the resultant ground reaction force $f = (f_H, f_V)$ has been singled out, where f_H is the resultant horizontal displacement vector and f_V is the resultant vertical displacement vector. The force due to gravity has been given by mg, and the ankle torque τ_{ankle} is generated by the muscles. For the foot, an equilibrium equation is formed: $f_H \delta + f_V u + \tau_{ankle} = 0$, where δ and u represent the vertical and horizontal displacements of the CoP with respect to the ankle. The sway equation obtained for the inverted pendulum, $\ddot{y} = g/h_e(y - u)$ indicates that the CoM-CoP difference is proportional to the horizontal component of the ground reaction force, where $h_e = k_s h + \delta$, with h being the distance of the CoM from the ankle and $k_s = 1$, a shape factor dependent on the distribution of mass in the body and g is the acceleration due to gravity.

Model C in Figure 2.1, proposed by Qua et al. (2007) describes yet another single segment inverted pendulum model. The postural control system is modelled as a feedback control system. The closed loop of the postural control system model

consists of human body dynamics, the sensory system and a neural controller. Sway is restricted to the sagittal plane only and anthropometric parameters are those of an "average" adult male. This model proposes a method for optimising standard sway parameters. Modelling the neural controller as an optimal controller was considered appropriate while incorporating physical quantities relevant to sway into the performance index defined in the optimal controller. The information of body dynamics and sensory systems is passed on to the neural controller to generate the optimal control signal. It was proposed that muscle spindles would sense the joint angular displacement and velocity and concurrently analyse balance strategies for different subject groups(young versus old) by comparing their model parameters (weight, disturbance gain and sensory delay). However, the authors acknowledged various limitations of the model, such as, only few physical quantities that might affect spontaneous sway could be used in the model. The neural controller may not use an optimal control strategy to generate the motor behaviour that induces spontaneous sway. But based on the simulation results, a control strategy might partly explain the neural controller. This model can only be applicable for small amplitudes of AP sway since only ankle torques have been considered contributing factors towards quiet stance. This model is dependent on experimental data to determine the parameters and the same anthropometry has been assumed for both younger and older adults, an indicative limitation in implementation. The genetic algorithm, a heuristic approach and unsuitable for local searching, does not guarantee that the used set of model parameters lead to the global optimum. The real sensory systems are much more complex than those represented in the model, as the time delay is required to be integrated and fed back to the neural controller to maintain quiet stance. However, it has been acknowledged that modelling sensory systems as a time delay has been simplified as the goal was to study the working of sensory systems during quiet stance. Hence, this requires a more complex control system.

In Figure 2.1, insufficient attention has been given to the importance of the mechanical properties of the muscles, tendons and ligaments. However, these models addressed the question of postural response during very small oscillations of the body CoM with respect to the ankle strategy. At small angular displacement the role played by the muscles, ligaments and tendons is known to

be significant and is discussed in the subsequent sections.

The focal interest of this study was to derive a mathematical model based on the single inverted pendulum. The premise of the single inverted pendulum model is that the body behaves as a rigid structure above the ankles. The single inverted pendulum is an unstable system because of the gravitational torque around the ankles, which increases with the angular displacement of the shank and thus requires a restoring force (Bottaro et al., 2005).

2.3 Mechanical characteristics affecting postural control

An important part of the research investigating quiet stance is based on a one-segment inverted pendulum model (Jeka et al., 2004; Loram and Lakie, 2002; Loram et al., 2005; Morasso and Sanguineti, 2002; Peterka, 2002; Winter et al., 1998, 2001). In this model, the human body is represented as a rigid segment with the body CoM located at 50-55% of body height and slightly anterior to the ankle. This model is based on the assumption that postural control is performed about the ankle and that other joints are immobilised. The advantage of this model is that it reduces the system to a single degree-of-freedom system while focusing on the joint for which the destabilising effect of gravity is largest. This destabilising effect of gravity is commonly expressed as the destabilising gravitational stiffness of the ankle (Pietro and Schieppati, 1999). In the context of this model, a prerequisite for local stability at the equilibrium is that the net joint stiffness at the ankle, which arises from both intrinsic muscle properties and neural feedback, is larger than the destabilising gravitational stiffness (Pietro and Schieppati, 1999). During quiet stance the body has often been modeled as a single inverted pendulum, pivoting about the ankle joints. The use of this model to represent balance maintenance during quiet stance has been supported by kinematics, kinetic data (Gage et al., 2004; Karlsson and Persson, 1997), and EMG (Gatev et al., 1999) measures in both the sagittal and frontal plane (Winter et al., 1996).

The stiffness and the damping parameters of the model proposed by Winter et al. (1998) were used to predict the sway patterns of balance control. The

2. Postural Control Models

change in stiffness was thought to be indicative of dynamic changes in muscle stiffness induced by the central nervous system (CNS). These changes were classified as time invariant (stationary) or time variant (non-stationary) (Ferdjallah et al., 1999). It was suggested that the spring and damping properties of the muscles are controlled by activation of fast and slow muscle fibres. The passive (wide frequency and low average signal power achieved by joint or skeletal structure) and active control (muscle activation) phases proposed in the study Ferdjallah et al. (1999), suggested that these control phases are time varying due to random internal disturbances in sway. Although the triggering mechanism remains unclear, it has been hypothesised that the switch from passive to active phase is causal to exaggerated sway requiring dynamic control.

In recent years, measuring the range of net ankle joint stiffness during quiet stance and its regulation have received much needed attention (Casadio et al., 2005a; Lakie et al., 2003; Loram and Lakie, 2002; Loram et al., 2005; Morasso and Sanguineti, 2002; van der Kooij et al., 2005; van Soest et al., 2003; Winter et al., 2001). It has been shown that the stiffness of the Achilles tendon during standing is lower than the gravitational stiffness (Loram and Lakie, 2002; van Soest and Rozendaal, 2008). This finding led Loram and Lakie (2002) to conclude that quiet stance was intrinsically unstable under purely muscle stiffness considerations. For a single-segment inverted pendulum, Loram et al. (2005) postulated that an anticipatory control mechanism was likely used. However, it has been argued by Loram et al. (2005) that the local stiffness at the ankle joint, required for stability is much lower than the gravitational stiffness for a multi-segment model as assumed by van Soest and Rozendaal (2008). In other words, modelling assumptions have room for extensive studies (modelling and experimental) to understand control strategies used during quiet stance.

2.3.1 Ankle stiffness and its effect on postural balance

During quiet stance the triceps surae musculature generates an intrinsic mechanical stiffness across the ankle joint. Such stiffness provides an instantaneous torque response changing the ankle angle without any appreciable CNS involvement (Grillner, 1972; Horak and Macpherson, 1996; Winter et al., 1998). If the

ankle stiffness is less than the gravitational torque per unit angle, then the body CoM is mechanically unstable facilitating the need for neural modulation to stabilise the system (Morasso et al., 1999a; Pietro and Schieppati, 1999).

Morasso and Sanguineti (2002) further investigated the concept of the stabilisation of human posture with regard to the muscle stiffness about the ankle joint. They argued that 8.8% of ankle stiffness (Winter et al., 2001) is not a sufficient margin to explain the natural frequency of sway. In a spring-mass model, the following relation links the natural frequency ω_n, the moment of inertia I, and the total stiffness of the system: $\omega_n^2 = K_{total}/I$. In the case of quiet stance, $K_{total} = K_a - mgh$ (mg is the body weight vector and h is height of the CoM from the ground) if the natural frequency is 0.5 Hz and moment of inertia is 80 kg.m^2, 8.8% margin of K_a i.e ankle stiffness with respect to the stiffness value of ankle required for stabilisation would be insufficient, thereby making the measurement technique for ankle stiffness flawed (Winter et al., 2001). Although, it is true that the stiffness of a given body is the slope of the stress-strain characteristic curve, but the related measurements would be only valid if the following conditions were met.

1) during measurement, the system must operate under open-loop conditions, making it the only source of energy transmitted through the system, also known as test disturbance;

2) stress and strain have to be measured under static or quasi-static conditions or time-dependent forces are selectively taken into consideration;

Morasso and Sanguineti (2002) argued that during quiet stance, both above mentioned conditions, can be ignored for the following reasons:

1) the assumption that the level of activation of the motor-neurons should remain constant throughout the measurement time. Although, the activation levels are not short they include a number of postural oscillations. These changes in active muscle torques are not accounted for locally while calculating the net torque.

2) the recorded total ankle torque is not exclusive of viscous and inertial components which depend not only on the velocity but also on the acceleration of angular sway. These components are not explicitly accounted leaving room for ambiguous interpretation.

A study by Thomas Edwards (2007), used Lagrangian equations of motion to explain multi-segment models and described the inherent characteristics of standing stability. This was achieved by assigning segment mass, damping and stiffness parameters and the interaction of such a system was observed under external load conditions. The study calculated the limits of stability for a range of lower extremity joint stiffnesses by varying the body mass values. The damping matrix in the Lagrangian equation was considered to be zero however the author Thomas Edwards (2007) acknowledged the fact that damping or torques that were proportional to the angular velocity of joints were necessary for stability.

2.3.2   Postural response with regards to damping

The effect of damping on human postural balance has not been given sufficient recognition in the recent past. Winter et al. (1998) developed an inverted pendulum model with damping parameters, but damping effects were not clarified fully. Nevertheless, more recently damping effects are being researched in order to fully understand postural balance in humans. Bonnet et al. (2011) used Lagrange's equations to calculate the inverse dynamics of the human body system. The passive damping and stiffness parameters were taken into consideration as they facilitated in restoring the double inverted pendulum model into the upright position. Although, their model was not based solely on the ankle joint, it was one of the few investigations that have used the Lagrangian dynamics and have taken into account the importance of damping parameters. The model however, is overly-simplistic and does not capture the full essence of the role played by the antagonistic musculature of the shank.

In a study by Suzuki et al. (2012), an intermittent control model ("off-off model") of a double inverted pendulum was developed that simulated movements of the ankle and hip joints during human upright stance. In particular, small passive viscoelasticity at the ankle and hip joints was assumed, which made the upright equilibrium unstable without neural control. In this particular model, although quite detailed in nature, could not consider the viscoelastic values of the ankle and the hip to be realistic. However, the authors have acknowledged that higher damping values are required to stabilise the model.
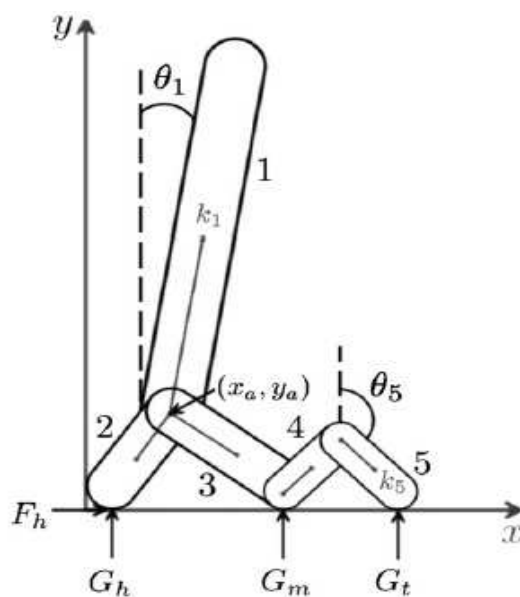
Figure 2.2: An inverted pendulum saggital model consisting of 5 rigid links proposed by Humphrey and Hemami (2010). Link 1 represents the head, arms and torso; link 2 represents the calcaneus; link 3, the metatarsals, navicular, cuneiforms, and cuboid; link 4, the proximal and intermediate phalanges of all the toes; and link 5 the distal phalanges of toes. All connections are assumed to be bilaterally symmetrical. K_i is the distance from the end of link i to the center of mass as illustrated.

Humphrey and Hemami (2010) developed a computational model (Figure 2.2) which was quite different from the typical single segment inverted pendulum model. This model uses one rigid link to represent the body above the ankle, similar to an inverted pendulum model. The point at which links 1, 2, and 3 are connected can be considered roughly the talus or ankle joint. The foot makes contact on the ground at the bottom of the calcaneus or heel, the head of the metatarsals or forefoot, and the head of the distal phalanges of the toes. Simple muscle models operated the movements of this inverted pendulum by producing net torque on the segments at their attachment points. These muscle models were viscoelastic circular springs that generated torque. Passive effects due to friction at the joints and stretching of ligaments were not taken into consideration in this particular model. However, this model is the only model so far that has

17

considered the effects of ligaments while modelling an inverted pendulum with regard to postural balance. The equations of motion describing the dynamics of the model have been described using Euler-Lagrange equations (Humphrey and Hemami, 2010). The damping effects of the soft tissues have been acknowledged as well (Humphrey and Hemami, 2010). However, the parametric values may not be realistic enough. Links 4 and 5 of the model representing the metatarsals and the phalanges of the foot were also not realistic as the longitudinal arch appeared to be over-emphasized. The effects of Achilles tendon as well as the gastrocnemius muscle have been over-looked as the model focused mainly on the soleus. The model is however, very different from others reported so far. The model does show the need for consideration of the viscoelastic as well as the stiffness parameters while explaining postural balance during quiet stance.

Imagawa et al. (2013) used the electromyogram-weighted averaging method (EWA) method to investigate the contribution of individual muscles to postural control in each direction(AP and ML). The study indicated that the gluteus medius muscle would have acted in the anterior direction with tibialis anterior acting as controller in the posterior direction during quiet stance. This implied that postural control in the experiment performed was implemented using an ankle strategy. Moreover, the small contribution of gluteus medius during quiet stance in the anterior direction could not have been estimated from EMG activity alone. This finding is contradictory to the results obtained by Kutch et al. (2010) where the gluteus medius was estimated to be the controller for maintaining quiet stance in the anterior direction. The study revealed that muscle synergy played an invaluable part during quiet stance. Therefore, in motor tasks in which many muscles are involved, there would also be insufficient to investigate muscle coordination solely by using the EWA method. Furthermore, postural balance was suggested to occur, not by gluteus medius, but through co-activation of tibialis anterior, soleus, and gastrocnemius muscles.

It is evident that muscle co-activation affects postural balance, hence, the 2×4 9-element MSD model developed in this thesis as described in the subsequent chapters incorporates such muscle functioning while defining the four units attached to the shank.

Chapter 3

Mathematical modelling of the ankle complex

3.1 Introduction

The ankle joint is a complex joint hence modelling it with all its physiological aspects and functionality increases the mathematical complexity beyond the scope of this study. However, this investigation takes into account the role played by the ankle joints in postural balance during quiet standing, specifically in anterio-posterior sway. Postural balance with respect to the ankle joint is modelled by using the Lagrange d'Alembert Principle (Udwadia, 2000). The model is basically an inverted pendulum where the shank of either lower extremities act as pendulums articulated at the base which is the foot. This pendulum has four mass-spring-damper (MSD) units attached symmetrically to one another. The functioning of the MSD units is passive which is representative to the mechanical functionality of muscles, tendons and ligaments which is discussed later in subsequent sections. This chapter discusses the formulation of the mathematical model detailing out the functional geometry of the ankle during forward and backward sway. The modelling has been carried out while keeping in mind the musculo-skeletal structure of the ankle joint and the mechanical movements associated with it.

3.2 Functional anatomy explaining mechanical construction of mass-spring-damper units
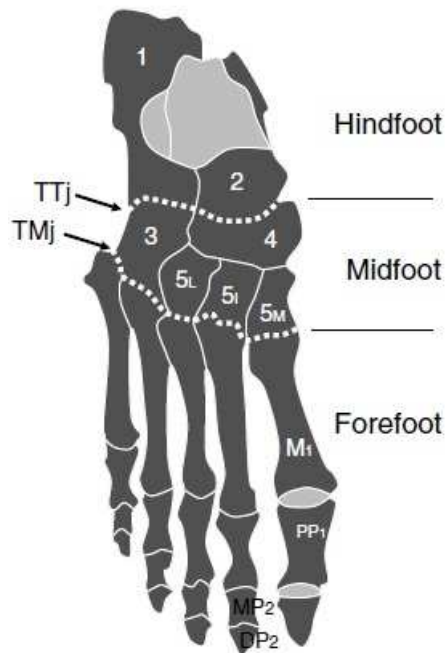
Figure 3.1:   Schematic drawing of a dorsal view over the foot illustrates: the hindfoot made up of the calcaneus (1) and the talus (2); the midfoot composed of the cuboid (3), the navicular (4), and the lateral (5L), middle (5I), and medial (5M) cuneiforms (5); and the forefoot, made up of the metatarsals (M) and phalanges (proximal, PP; middle, MP; distal, DP). The hindfoot is separated from the midfoot by the transverse tarsal joint (TTj), the midfoot from the forefoot by the tarsometatarsal joint (TMj). This figure has been reproduced from (Bianchi and Martinoli, 2007).

The ankle is a functional and enduring joint. Ankle anatomy is comprised of the tibia, talus, and fibula. The three bones articulate at the ankle joint stabilised by a number of ligaments and an interosseous syndesmosis. The tibia and fibula form a mortise in which the talus resides. The tibia is the dominant weight-bearing bone in the lower leg. The medial malleolus is essentially an extension

of the tibia and provides medial support for the ankle mortise. The talus, wider anteriorly, provides a more inherent stability with the ankle during dorsiflexion as opposed to plantarflexion. Ankle joint movement is primarily plantarflexion and dorsiflexion. The deltoid ligament makes up the medial ankle ligamentous support. It consists of a deep layer, which runs from the medial malleolus to the talus, and a superficial layer, which originates on the medial malleolus attaching to the medial aspect of the calcaneus. Anterior fibres attach to the talus and navicular while posterior fibres attach predominantly to the talus.

The lateral ligament complex is comprised of the anterior talofibular ligament (ATFL), calcaneofibular ligament (CFL), and posterior talofibular ligament (PTFL). The ATFL originates at the anterior aspect of the lateral malleolus and runs nearly parallel to the axis of the foot. It attaches to the talus anteriorly and is the primary ligamentous restraint to inversion stress at the ankle. It becomes taut with the ankle in slight plantarflexion. The ATFL is the most commonly injured ligament in the body. The CFL is stronger than the ATFL and spans the tip of the lateral malleolus to the lateral surface of the calcaneus. The PTFL originates on the posterior tip of the lateral malleolus and attaches to the posterior talus.

The high ligaments consist of the anterior inferior tibiofibular ligament, posterior inferior tibiofibular ligament, and interosseous syndesmosis. The bones of the foot are divided into the hindfoot, midfoot, and forefoot. The talus and calcaneus make up the bones of the hindfoot. The calcaneus is the largest and strongest bone in the foot. It serves as the attachment for the Achilles tendon and as the origin of the plantar fascia. The talus and calcaneus have three articulations. This subtalar or talocalcaneal joint permits inversion and eversion of the foot. The bones of the midfoot include the cuboid, navicular, and three cuneiforms. The navicular is on the medial aspect of the foot and serves as the attachment for the posterior tibialis tendon. The forefoot is comprised of the metatarsals and their corresponding five phalanges. The great toe has a proximal and distal phalanx. The other four toes have proximal, middle, and distal phalanges. The sesamoids are two pea-sized bones in the substance of the flexor hallucis brevis tendons. Their positioning on the plantar aspect of the first metatarsalphalangeal (MTP) joint help function to increase the mechanical advantage of the flexor tendons, as

well as to disperse forces with gait and stance.
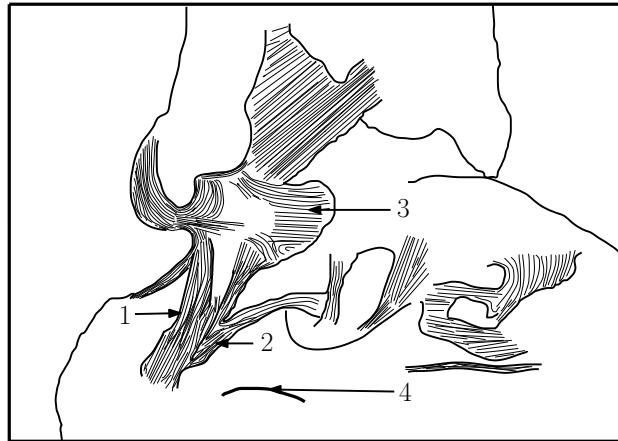
Figure 3.2: Osteoarticular dissection. Relationship of the calcaneofibular ligament with the lateral talocalcaneal ligament. 1 Calcaneofibular ligament; 2 lateral talocalcaneal ligament; 3 anterior talofibular ligament; 4 peroneal tubercle. This figure has been reproduced from (Golano et al., 2010).

Muscles of the foot and ankle can be principally divided into three compartments: the anterior, lateral,and posterior. The interosseous membrane and anterior crest of the tibia form the boundaries between these compartments. The extensor hallucis longus, extensor digitorum longus, and anterior tibialis make up the anterior compartment and primarily dorsiflex the ankle. The anterior tibialis attaches to the first cuneiform and metatarsal and inverts the foot. The lateral compartment comprises of the peroneus longus and brevis. The peroneal brevis attaches to the base of the fifth metatarsal. The longus crosses the sole of the foot to attach on the first cuneiform and base of the first metatarsal. The peroneals evert the foot. The posterior compartment has superficial and deep groups. The triceps surae is the superficial group and includes the gastrocnemius, soleus, and plantaris. The deep compartment includes the flexor hallucis longus, flexor digitorum longus, and tibialis posterior muscles. These muscles function to plantar flex the ankle, flex the toes, and invert the foot. There are many intrinsic muscles of the foot analogous to the intrinsic muscles of the hand. The plantar fascia runs from the inferior aspect of the calcaneus to the forefoot. It has a role in support

of the longitudinal arch of the foot.

3.2.1   Ankle movements

The muscles considered for postural control have very specific movements which can be divided into two types of movements planterflexion and dorsiflexion which is typical in backward and forwards sway mechanism as portrayed in Table 3.1.

Table 3.1: Actions of the muscles of the foot and ankle complex (Pierrynowski, 1995)

Extrinsic Muscles	Action Involved
Tibialis anterior	Prime mover of dorsiflexion and inversion
Extensor digitorium longus	Prime mover of dorsiflexion and eversion
Extensor hallucis longus	Assisting in dorsiflexion and inversion
Gastrocnemius	Prime mover of plantarflexion
Plantaris	Assisting in plantarflexion
Soleus	Prime mover of plantarflexion
Peroneus longus	Assisting in plantarflexion and prime mover of eversion
Flexor digitorum longus	Assisting in plantarflexion and inversion
Flexor hallucis longus	Assisting in plantarflexion and inversion
Tibialis posterior	Assisting in plantarflexion and prime mover of inversion
Peroneus brevis	Assisting in plantarflexion and prime Mover of eversion

3.2.2   Model derivation

In order to model the ankle joints for postural balance it is of paramount importance to first explain the construction and representation of soft tissue connections to the joints keeping in mind that the tendons connect muscle to bone and ligaments connect bone to bone. AB, CD, EF, and GH are four units connecting the shank (tibia and fibula) to the phalanges of the foot, posterior of the calcaneus, lateral side of the calcaneus and to the medial side of the calcaneus respectively as shown in Table 3.2.

Table 3.2: Muscle, Tendon and Ligament representation of units AB, CD, EF and GH

Units	Muscles	Tendons	Ligaments
AB	tibialis anterior	peroneus brevis	anterior fibulotalar (AFTL)
CD	tricep surae	Achilles Tendon	
	tibialis posterior	plantaris	
EF	flex.dig.long	flex.hal.long	calcaneofibular (FCL)
			tibiocalcaneal (TCL)
GH	ext.dig.long	peroneus longus	anterior tibitalar (ATTL)
			posterior tibiotalar (PTTL)
			tibionavicular (TNL)

The musculoskeletal system plays an equally important role in postural control along with the nervous system. Both these systems are dependent on each other. This study focuses on the musculoskeletal system and its contribution towards postural stability. Four mass-spring-damper units are associated with one ankle, each representing a group of muscles, tendons, and ligaments as shown in Figure 3.3.
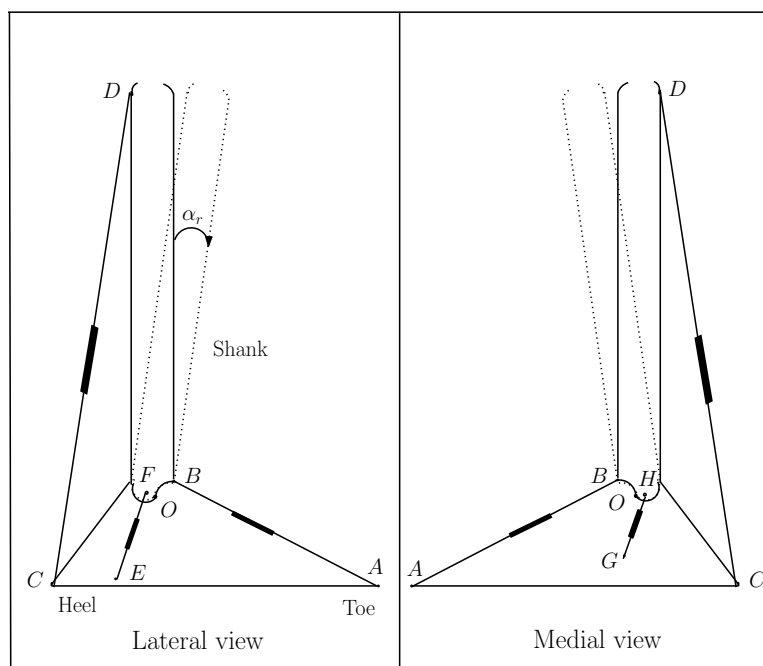
Figure 3.3: A sagittal model for anterior-posterior sway where α_r is the angular displacement of the right shank and O is the point of articulation of the shank and foot acting as the fulcrum. The model shows the orientation of AB, CD, EF and GH units.

3.2.3 Sway referenced geometrical illustration of the ankle

Figure 3.4 illustrates the geometrical alignment of the four units, namely AB, CD, EF and GH connecting the shank to the foot. However, the figure is not drawn to scale but gives a clear indication of the orientation of the units at its natural position and after the onset of sway resulting in the change of geometrical parameters. Unit AB forms a crucial angle, α_1 forms when the talar declination angle intersects perpendicular lines from the axis of the collum tali, which bisects the head and neck of the talus, the plane of support is same as the horizontal angle of the talus as described by Vanderwilde et al. (1988), and which quantifies the anterior tibiotalar impingement. Unit CD forms an angle α_2, called the tibiotalar angle formed by the axis of the tibia and the axis of the talus. EF and GH units forms α_3 and α_4 in the lateral and medial side respectively, which are the posterior

facet inclination angles (Sarrafian, 1993), the angle formed by two intersecting lines along the surface of the posterior facet and along the upper surface of the calcaneal tuberosity. Both these angles are equal. The model presented in Figure 3.4 does not take into any deformation of the foot during quiet stance and all the units function passively. The model takes a three dimensional to two dimensional representation where the two ankles are parallel to each other.
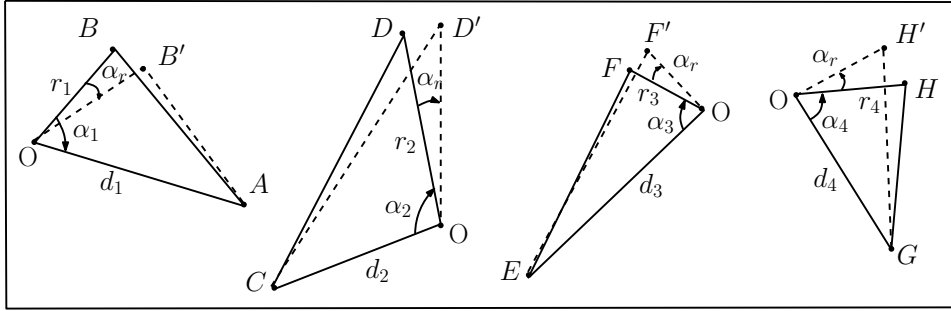
Figure 3.4: Geometries of length changes of units AB, CD, EF, and GH

In case of unit AB, let r_1 and d_1 be the lengths of BO and AO respectively, and α_1 the angle between BO and AO. During postural forward and backward sways, when the shank moves around the point O by an angle α_r, B moves to a point, B'. Note that $OB = OB' = r_1$ and $OA = d_1$ remain unchanged before and after shank's movement.

The unit length changes from AB to AB'. Using law of cosines, the length of the unit represented as:

$$\bar{y}_{r,1}^2 = d_1^2 + r_1^2 - 2d_1 r_1 \cos(\alpha_r - \alpha_1). \tag{3.1}$$

Clearly, when $\alpha_r = 0$, (3.1) gives the natural length of the unit, denoted by $y_{r,1}^0$. Later when dealing with dynamics of the unit, the length difference $y_{r,1} = \bar{y}_{r,1} - y_{r,1}^0$ will be used as well.

Enumerate unit AB, CD, EF and GH as unit 1, 2, 3 and 4. In a similar way, the lengths of the other three units, denoted by $y_{r,i}$ for $i = 2, 3, 4$, can be determined as

$$\bar{y}_{r,i}^2 = d_i^2 + r_i^2 - 2d_i r_i \cos(\alpha_r + \alpha_i). \tag{3.2}$$

The natural lengths, denoted by $y_{r,i}^0$, of units CD, EF and GH can be obtained from (3.2) for $\alpha_r = 0$ and respectively $i = 2, 3, 4$.

Table 3.3 lists the ranges of constant geometric parameters, namely r_i, d_i and α_i of the units AB, CD, EF, and GH. These geometric parameters are constant for any given subject. In the case of unit CD, averaging the dimensional values of muscles and tendons is involved in the length calculation performed, while ligaments are ignored, as they do not play as vital a role as in units EF and GH. In (3.1) and (3.2) r_1 represents the difference between the absolute foot height and the calcaneal facet height, r_2 represents the tibial length to the articulation point with the calcaneus, r_3 and r_4 are the distance between the point O (the articulation point of the shank to the foot) F and H (the superior attachment point of EF and GH) respectively, d_3 and d_4 represent the facet height laterally as well as medially.

Table 3.3: Geometrical dimensions of units AB, CD, EF and GH (Devanshu and David, 2006; Gentili et al., 1996; James et al., 2006; Schepers et al., 2007; Vanderwilde et al., 1988)

Length of MSD unit (mm)	Length from origin (mm)	Angular precision (°)
d_1=110-128.47	r_1=21.20-34.90	α_1=26.88-54.66
d_2=36.10-74.47	r_2=332-467	α_2=102-152
d_3=71.61-79.76	r_3=19.10-32.50	α_3=55-75
d_4=47.23-58.37	r_4=19.10-32.50	α_4=55-75

3.2.4 Mass-spring-damper dynamics

Each of the four MSD units represents some particular groups of the combined muscles, tendons and ligaments. These three types of tissues have different mechanical properties, forming the three mass-spring-damper sub-units. Two of the three sub-units in series connection, and the third in parallel as shown in Figure 3.5, based purely on the functional anatomy of the muscles, tendons, and liga-

ments as explained in section 3.2.3. The first sub-unit counts for tendons, second for muscles and third for ligaments, denoted by (m_d, c_d, k_d) for $d=a, b, c$.
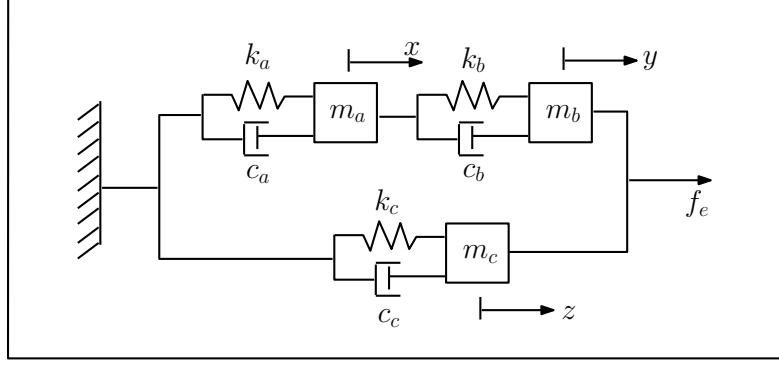
Figure 3.5: 9-element model

This study investigates the anterior and posterior sway with the absence of the bending of the knee. In unit AB, although the 9-element MSD model is applicable it is necessary to clarify the effect of ligaments shown in Figure 3.5, where the actions of the ligaments are in parallel to the series connection of the muscle-tendon unit.

Assuming that the external force $f_e = 0$ and as $y = z$, and following the Lagrange-d'Alembert principle (Udwadia, 2000), equations governing the movement of the units are as follows

$$
\begin{aligned}
m_a\ddot{x} &= -c_a\dot{x} - k_a x + c_b(\dot{y} - \dot{x}) + k_b(y - x)\,, \\
m_b\ddot{y} &= -c_b(\dot{y} - \dot{x}) - k_b(y - x) + \lambda_c\,, \\
m_c\ddot{z} &= -c_c\dot{z} - k_c z - \lambda_c\,,
\end{aligned}
$$

where λ_c is the Lagrange multiplier with respect to constraint $y - z = 0$.

After eliminating λ_c, substituting z by y and rearranging the above equations, x and y equations are reduced to

$$
\begin{aligned}
m_a\ddot{x} + (c_a + c_b)\dot{x} + (k_a + k_b)x - c_b\dot{y} - k_b y &= 0\,, &&(3.3) \\
(m_b + m_c)\ddot{y} + (c_b + c_c)\dot{y} + (k_b + k_c)y - c_b\dot{x} - k_b x &= 0\,. &&(3.4)
\end{aligned}
$$

It is clear that the unit length is $y_r = y + y_0$, where y_0 is the natural length of the unit. Applying formulae (3.3) and (3.4) to units AB, CD, EF and GH results in the unit dynamics, for $i = 1, 2, 3, 4$,

$$m_{a,i}\ddot{x}_{r,i} + (c_{a,i} + c_{b,i})\dot{x}_{r,i} + (k_{a,i} + k_{b,i})x_{r,i} - c_{b,i}\dot{y}_{r,i} - k_{b,i}y_{r,i} = 0, \quad (3.5)$$
$$(m_{b,i} + m_{c,i})\ddot{y}_{r,i} + (c_{b,i} + c_{c,i})\dot{y}_{r,i} + (k_{b,i} + k_{c,i})y_{r,i} - c_{b,i}\dot{x}_{r,i} - k_{b,i}x_{r,i} = 0, \quad (3.6)$$

where, for the CD unit,

$$m_{c,2} = 0, \quad c_{c,2} = 0, \quad k_{c,2} = 0. \quad (3.7)$$

It is noticed that unit CD does not have extensive use of ligaments as compared to AB, EF and GH as it is attached directly from the calcaneus to the tip of the tibia where the main soft tissues are the Achilles tendon and the triceps surae which play a more dominant role.

Recall that the unit lengths $\bar{y}_{r,i} = y_{r,i} + y^0_{r,i}$ for $i = 1, 2, 3, 4$. So far the right ankle has been considered. The modelling directly applies to the left ankle as well.

If both the shanks are devoid of all kinds of connections, they will independently influence the angular sway, α_l and α_r, pivoted at their respective ankle joints. This would result in unrestricted anterior and posterior sway of the CoM of the body, governed by

$$\bar{I}\ddot{\alpha}_r - \bar{g}\sin\alpha_r = 0, \qquad \bar{I}\ddot{\alpha}_l - \bar{g}\sin\alpha_l = 0, \quad (3.8)$$

where $\bar{I} = \frac{1}{2}[(h - f_h)^2 m + I_{zz}]$ and $\bar{g} = \frac{1}{2}mgh$, h is the vertical distance between the CoM of the upper body and ankles, f_h is the height of the foot from the ground, m the total mass of the body, I_{zz} the (3,3) element of the whole body moments of the inertia I_a around the mass centre of the body rotating in the sagittal plane, and g the gravity acceleration. It is evident that if merely the ankle movements are permitted, only forward and backward sways are possible, and the left and

right ankle angles must be equal to each other, namely $\alpha_l = \alpha_r$, where the angles are defined naturally according to the shank movements as shown in Figure 3.3.

3.3 Constrained dynamics

Again, following the Lagrange-d'Alembert principle (Udwadia, 2000), the individual dynamic equations and the associated constraint equations can be combined to form a complete mathematical model of the open stance. In this particular case, the vector consisting of all variables of interest is defined as:

$$
q = \begin{bmatrix} \alpha_l \\ q_l \\ \alpha_r \\ q_r \end{bmatrix}, \quad q_v = \begin{bmatrix} x_{v,1} & y_{v,1} & x_{v,2} & y_{v,2} & x_{v,3} & y_{v,3} & x_{v,4} & y_{v,4} \end{bmatrix}' \quad (3.9)
$$

where, $v = l, r$ corresponding to the left or right side ankle joint.

In a standard form, the general equations with constraints are given by

$$
M\ddot{q} + C\dot{q} + G(q) = F'\lambda, \tag{3.10}
$$

$$
f(q) = 0. \tag{3.11}
$$

Here, M represents the inertia matrix (which is symmetric positive definite), $C\dot{q}$ is the centrifugal and Coriolis torques, $G(q)$ represents the gravitational torques, $F = \frac{\partial f(q)}{\partial q}$, and λ is the Lagrange multiplier. Term $F'\lambda$ represents the generalised torque induced by the constraints.

The relevant matrices and vectors have the following specifications under the assumption of body's symmetry.

$$
M = \mathrm{diag}\,(\bar{I}, M_0, \bar{I}, M_0),
$$

$$M_0 = \text{diag}\,(m_{a,1},\ m_{b,1} + m_{c,1},\ \cdots,\ m_{a,4},\ m_{b,4} + m_{c,4}),$$

$$C = \text{diag}\,(0, C_0, 0, C_0), \quad C_0 = \text{diag}\,(C_1, C_2, C_3, C_4),$$

$$C_i = \begin{bmatrix} c_{a,i} + c_{b,i} & -c_{b,i} \\ -c_{b,i} & c_{b,i} + c_{c,i} \end{bmatrix}, \quad (i = 1, \cdots, 4)$$

$$G = \text{diag}\,(0, K_0, 0, K_0)q + \begin{bmatrix} g'_l & g'_r \end{bmatrix}',$$

$$g_v = \begin{bmatrix} -\bar{g}\sin\alpha_v & 0 & \cdots & 0 \end{bmatrix}', \quad (v = l, r),$$

$$K_0 = \text{diag}\,(K_1,\ K_2,\ K_3,\ K_4),$$

$$K_i = \begin{bmatrix} k_{a,i} + k_{b,i} & -k_{b,i} \\ -k_{b,i} & k_{b,i} + k_{c,i} \end{bmatrix}, \quad (i = 1, \cdots, 4),$$

$$f = \begin{bmatrix} \alpha_l - \alpha_r \\ f_l \\ f_r \end{bmatrix},$$

$$f_v = \begin{bmatrix} (y_{v,1} + y_{v,1}^0)^2 - d_1^2 - r_1^2 + 2d_1 r_1 \cos(\alpha_v - \alpha_1) \\ (y_{v,2} + y_{v,2}^0)^2 - d_2^2 - r_2^2 + 2d_2 r_2 \cos(\alpha_v + \alpha_2) \\ (y_{v,3} + y_{v,3}^0)^2 - d_3^2 - r_3^2 + 2d_3 r_3 \cos(\alpha_v + \alpha_3) \\ (y_{v,4} + y_{v,4}^0)^2 - d_4^2 - r_4^2 + 2d_4 r_4 \cos(\alpha_v + \alpha_4) \end{bmatrix}, \quad (v = l, r).$$

With $f_r = 0$, $f_l = 0$ is equivalent to $f_l - f_r = 0$ which corresponds to $(y_{l,i} + y_{l,i}^0)^2 = (y_{r,i} + y_{r,i}^0)^2$ for $i = 1, \cdots, 4$ due to $\alpha_l = \alpha_r$, and further $y_{l,i} + y_{l,i}^0 = y_{r,i} + y_{r,i}^0$ because unit lengths are always positive. This means that the constraint vector in (3.11) can be reduced to

$$f = \begin{bmatrix} \alpha_l - \alpha_r \\ f_{l,r} \\ f_r \end{bmatrix} \quad \text{with} \quad f_{l,r} = \begin{bmatrix} y_{l,1} + y_{l,1}^0 - y_{r,1} - y_{r,1}^0 \\ y_{l,2} + y_{l,2}^0 - y_{r,2} - y_{r,2}^0 \\ y_{l,3} + y_{l,3}^0 - y_{r,3} - y_{r,3}^0 \\ y_{l,4} + y_{l,4}^0 - y_{r,4} - y_{r,4}^0 \end{bmatrix}, \tag{3.12}$$

and f_r being defined before. Accordingly, F in (3.10) should be determined from f defined in (3.12).

3.4 Free dynamics

In total there are 18 2nd-order differential equations with 9 constraints in (3.10) and (3.11). It is desirable to derive free dynamics by eliminating constraints. This shall facilitate numerical simulations of the derived mathematical model of the posture because most numerical solvers provided in the majority of software tools are for simulating dynamic systems described by ordinary differential equations without constraints.

Define a coordinate transformation as $p = \begin{bmatrix} p_1 \\ p_2 \end{bmatrix}$ with $p_2 = f$, where f is defined in (3.12),

$$p_1 = \begin{bmatrix} \alpha_l \\ p_{1,l} \\ p_{1,r} \end{bmatrix}, \quad p_{1,v} = \begin{bmatrix} x_{v,1} & x_{v,2} & x_{v,3} & x_{v,4} \end{bmatrix}', \quad (v = l, r). \tag{3.13}$$

The inverse of the transformation can be easily determined as given in Appendix C and denoted by $q = p^{-1}(p)$ from which

$$\dot{q} = Q(p)\dot{p}, \qquad \ddot{q} = \dot{Q}(p)\dot{p} + Q(p)\ddot{p}, \tag{3.14}$$

where $Q = \left(\frac{\partial p}{\partial q}\right)^{-1}$. Substituting these relations into (3.10), left multiply (3.10) by Q', and note that $p_2 = 0$ and $FQ = \begin{bmatrix} 0 & I \end{bmatrix}$. In the p-coordinates, the system of (3.10) and (3.11) becomes

$$M_1(p_1)\ddot{p}_1 + C_1(p_1, \dot{p}_1)\dot{p}_1 + G_1(p_1) = 0, \tag{3.15}$$
$$C_2(p_1, \dot{p}_1)\dot{p}_1 + G_2(p_1) = \lambda, \tag{3.16}$$
$$p_2 = 0, \tag{3.17}$$

where

$$M_1 = Q'_1 M Q_1 \,, \quad C_1 = Q'_1 (CQ_1 + M\dot{Q}_1) \,, \quad G_1 = Q'_1 G \,,$$
$$C_2 = Q'_2 (I - MQ_1 M_1^{-1} Q'_1) M\dot{Q}_1 + Q'_2 CQ_1 - Q'_2 MQ_1 M_1^{-1} C_1 \,,$$
$$G_2 = Q'_2 (I - MQ_1 M_1^{-1} Q'_1) G$$

with $Q = \left[\begin{array}{cc} Q_1 & Q_2 \end{array} \right]$ and Q_1 and Q_2 containing nine columns each. The component expressions of these coefficient matrices and vectors are given in Appendix A. The free dynamics of the system are described by the nine 2nd-order differential equations in (3.15). The free dynamics can be numerically simulated by some standard solvers of ordinary differential equations. The Lagrange multiplier can then be calculated from (3.16). Finally, from the inverse of the coordinate transformation $p = p(q)$, the variables in q can be obtained.

3.5 Linearisation of the model

The model developed so far is a nonlinear system. Stability analysis of a nonlinear system normally requires Lyapunov stability theory, which could be very involved and there is no general constructive procedure for carrying out the analysis. Linearisation of the nonlinear system can lead to effective evaluation of the stability of the system under various conditions due to changing values of the overall stiffness and damping parameters. Since the ankle angles and tendon length variations of the open stance during swings are very small, linearisation of the nonlinear model around zero value of these variables will give rise to a very good approximation of the original system. Stability of the system will be assessed by examining the Nyquist and Bode plots of the linearised model, which are shown in detail in Chapter 5. This section deals with linearisation of the nonlinear model and clarification of the Nyquist stability criterion applied to the linearised model. The clarification is needed because as a result from complex variable theory known as the Cauchy's argument principle (Franklin et al., 2010), the Nyquist stability criterion is normally stated for closed-loop systems, namely systems having a feedback control that associates system's output to its input. The nonlinear model developed in this thesis is a passive system because the

mass-spring-damper units as internal feedback controls are already included in the system's model. The nonlinear system is an open-loop system and so does its linearised counterpart.

In order to perform stability analysis using frequency response methods developed by Nyquist and Bode, a transfer function needs to be derived for the linearised model of the system. First of all, an input and output of the system need to be defined. It is well known from control theory that selections on system's input and output with respect to a particular transfer function have no effects on system's stability. The left ankle angle α_l is chosen as the output, denoted by y, of the system, and a disturbance torque, denoted by u, acting about the left ankle as the input.

In this case, by linearising the terms on the left-side of dynamic equation (3.15) around $p_1 = 0$ and $\dot{p}_1 = 0$, adding $\bar{B}u$ to its right, and introducing $y = \alpha_l$, the following linear system's equations are obtained

$$\bar{M}_1 \ddot{p}_1 + \bar{C}_1 \dot{p}_1 + \bar{G}_1 p_1 = \bar{B}u \,, \tag{3.18}$$

$$y = \bar{C}q_1 \,. \tag{3.19}$$

where,

$\bar{M}_1$ is linearised mass matrix

$\bar{C}_1$ is linearised stiffness matrix

$\bar{G}_1$ is linearsied torque matrix

$\bar{B}$ is an input matrix, and

$\bar{C}$ is an output matrix

3.5.1 Transfer function realisations and stability analysis

The derivation of the above equations and specifications of these coefficient matrices are given in Appendix C. Routine operations of taking Laplace transform with zero initial conditions and algebraic manipulations lead to the required transfer function

$$T(s) = \bar{C}(s^2 \bar{M}_1 + s\bar{C}_1 + \bar{G}_1)^{-1}\bar{B} = \frac{N(s)}{D(s)} \,, \tag{3.20}$$

where $N(s)$ and $D(s)$ are two polynomials in s. This transfer function presents a 18th-order system with a single input and single output. After parameterisation of the system's model, this transfer function is explicitly given by equation (5.4) in Chapter 5.

It is well known that an open-loop linear system is stable if and only if all its poles, namely solutions of the characteristic equation $D(s) = 0$, have negative real parts. Without calculating the poles, the stability of the system can be determined from the Nyquist plot of the transfer function of the system, and the Nyquist plot also indicates relative stability in terms of gain and phase margins. Precisely, the stability analysis is for the closed-loop system formed by using the unity negative output feedback control, which is not directly applicable here. To remedy this, rewrite $D(s) = 0$ as $1 + \bar{D}(s) = 0$ with

$$\bar{D}(s) = \frac{d(s)}{D(s) - d(s)}, \tag{3.21}$$

where $d(s)$ is an arbitrary polynomial of an order less than 18 and it should be so chosen that $D(j\omega) \neq d(j\omega)$ for all real number ω. This selection of $d(s)$ ensures that $\bar{D}(j\infty) \neq -1$ and $\bar{D}(s)$ has no poles on the imaginary axis of the complex plane. Now, $\bar{D}(s)$ can be considered as the transfer function of a pseudo open-loop system and $1 + \bar{D}(s) = 0$ as the characteristic equation of the corresponding closed-loop system. Applied to this particular system, the Nyquist stability criterion is: the point $(-1 + j0)$ will be encircled clockwise for $n_z - n_p$ times, where n_z and n_p are respectively the number of poles of $T(s)$ and $\bar{D}(s)$ inside the right-hand of the complex plane.

If the selection of $d(s)$ ensures additionally that $\bar{D}(s)$ has no poles inside the right-hand of the complex plane, which is again always possible, the Nyquist stability criterion is simply: The linearised system described by (3.18)-(3.19) or equivalently by (3.20) is stable if the Nyquist plot of $\bar{D}(s)$ does not encircle point $(-1 + j0)$. This will also facilitate relative stability analysis in terms of gain and phase margins.

One particular selection of $d(s)$ is given here, which satisfies all the requirements mentioned above. Let, without loss of generality, $D(s) = s^{18} + \bar{d}(s)$ with $\bar{d}(s) = \Sigma_{i=1}^{18} a_{i-1} s^{i-1}$. The particular selection of $d(s)$ is $d(s) = \bar{d}(s) - \Sigma_{i=1}^{18} b_{i-1} s^{i-1}$

with b_is being the coefficients determined from $\prod_{i=1}^{18}(s + p_i)$, where p_is are arbitrary stable real or complex conjugate numbers.

It is worth noting that, although selections of $d(s)$ have no effects on conclusions on stability of the system (3.20), since $\bar{D}(s)$ is dependent on $d(s)$, relative stability of the system in terms of gain and phase margins of the Nyquist plot of $\bar{D}(s)$ is bound to be influenced by $d(s)$. It is however hypothesised that different selections of $d(s)$ will not alter the trends and orders of changes in terms of gain and phase margins in relative stability analysis of the system (3.20). This aspect will be explored through simulation studies shown in Chapter 5. A theoretical proof of this hypothesis is nevertheless beyond the scope of the research presented in this thesis.

3.5.2 Model reduction

Model reduction of the initial 18 order linear system has been carried out based on the method detailed in (Moore, 1981). Model reduction approximations are necessary to evaluate "weakness" of any variables on the system dynamics. This means that the change in the dynamics of a system minimal or negligible. This has been carried out through the realisation of stable poles of the original system. For stable systems it is a close approximation of conrollability and observability of Gramians are equal and diagonal forming Hankel singular values. This concept was implemented in MATLAB as detailed in Chapter 5 where non-linear, linearised 18 order system and reduced order systems have been compared.

Chapter 4

Parameterisation of the proposed model

4.1 Introduction

In order to justify the orientation and position of soft tissues (muscles, tendons and ligaments), radiographic analysis of the bones of the human ankle complex is necessary. This chapter subsequently proceeds to explain the mechanical properties of the soft tissues, from various published papers which report collection and analysis of data necessary for model parameterisation. The viscoelastic properties of human soft tissues were studied, recorded and inferred by various authors which involved a number of coefficients and parameters, dependent on the methods and devices used (Belaya, 1979; Vasyukov, 1967; Zilbergleit et al., 1984) and it is therefore practically impossible to compare results obtained by different researchers.

4.2 Anatomical angles created by ankle bones using radiographic images
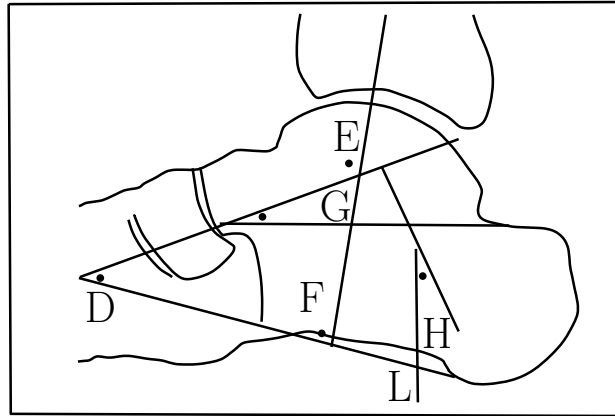
Figure 4.1: Anatomical angles of the ankle joint (Schepers et al., 2007).

Certain angles in the human ankle complex are of interest in this study in order to gain a geometrical insight of the ankle complex with respect to quiet stance. Fig.4.1 shows the posterior facet inclination (angle L) which is the angle formed by the intersection of two lines drawn along the surface of the posterior facet and along the upper surface of the calcaneal tuberosity.

The lateral talocalcaneal angle (angle D), is be formed by the calcaneal axis and the collum tali axis. The angle decreases when there is varus angulation of the hindfoot or when the foot is in dorsiflexion. The talocalcaneal angle increases with valgus or plantar flexion (Vanderwilde et al., 1988). There are two ways of measuring this angle. Some authors (Buch et al., 1996; Rammelt et al., 2004) use the centre line of the calcaneus as axis while others use the line formed by the most inferior part of the calcaneal tuberosity and the most inferior point of the calcaneocuboid joint (Bryant et al., 2000; Gentili et al., 1996). The latter is less likely to be affected by inter-observer variability, because of the use of fixed points.

The tibiotalar angle (angle E) on the radiograph is formed by the axis of the tibia and the axis of the talus. The tibiocalcaneal angle (angle F) is formed by the axis of the tibia and the axis of the calcaneus. The angle increases with plan-

tarflexion and subsequently decreases with dorsal flexion of the foot (Vanderwilde et al., 1988). The talar declination angle (angle H) is formed by the intersection of perpendicular lines drawn from the axis of the collum tali, which bisects the head and neck of the talus, and the plane of support. This line is essentially the same as the horizontal angle of the talus (angle G), as described by (Vanderwilde et al., 1988) who quantified the anterior tibiotalar impingement.
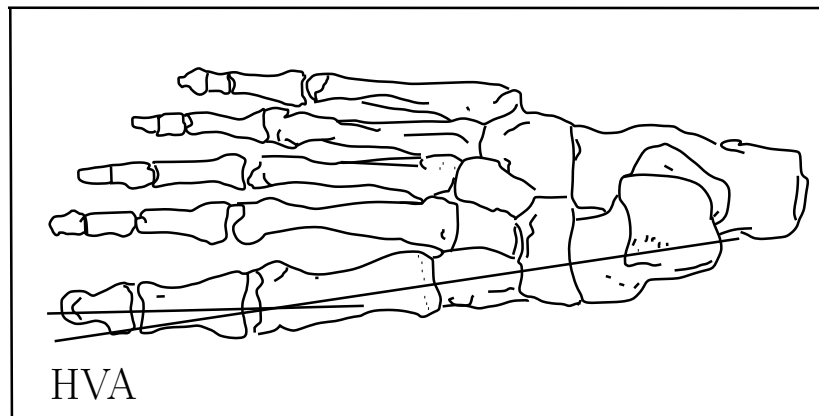
Figure 4.2: The hallux valgus angle (HVA), reproduced from Gentili et al. (1996).

The hallux abductus or hallux valgus angle (HVA) in Figure 4.2 is formed by the longitudinal axis of the first proximal phalanx and the longitudinal axis of the first metatarsus (Karasick and Wapner, 1990; Laporta et al., 1974; Mann, 1989) (normal: 5°-15°). Hallux abductus valgus would be mild at HVA 16°-25°, moderate at HVA 26°-35°, and severe at HVA greater than 35° (Karasick and Wapner, 1990; Laporta et al., 1974; Mann, 1989). In hallux varus or adductus, the HVA would be less than 0° (Karasick and Wapner, 1990; Laporta et al., 1974; Mann, 1989).
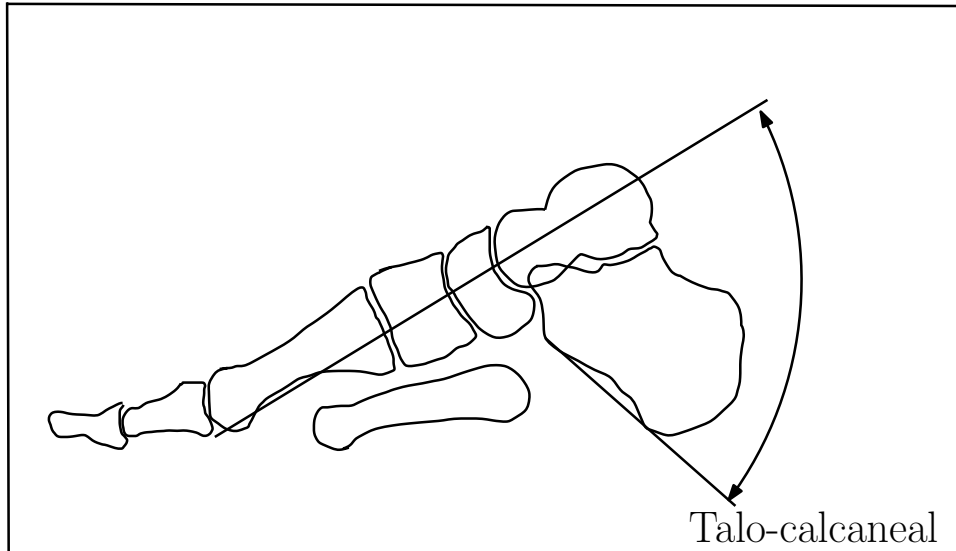
Figure 4.3: Measured angles in the lateral view (James et al., 2006).

Talocalcaneal in Figure 4.3 would be the angle formed by a line perpendicular to a line connecting the anterior-dorsal and anterior-plantar extremes of the talar head and line from the most anterior-plantar point of the calcaneal tubercle to the most anterior-plantar point of the calcaneus at the calcanealcuboid joint (James et al., 2006).
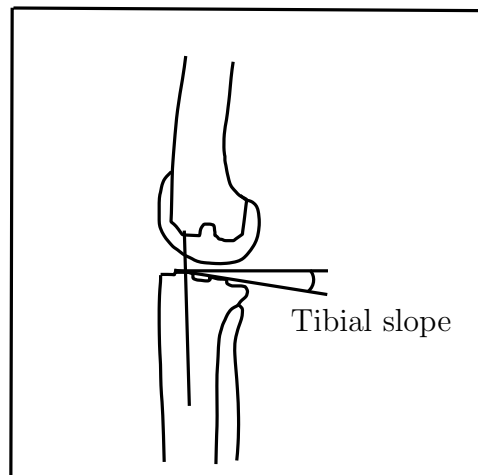
Figure 4.4: Tibial slope (Devanshu and David, 2006).

Figure 4.4, depicts a schematic representation of the slope measurement method.

A vertical line is drawn representing the longitudinal axis of the tibia. A horizontal line is drawn perpendicular to the vertical longitudinal. A third line is drawn along the superior margin of the proximal tibia representing its slope. The angle formed by the horizontal perpendicular and the proximal tibial margin represents the slope angle (Devanshu and David, 2006).

4.3   Mechanical parameters

The nine element MSD model is a derivation of the classical Kelvin-Voigt model (Thomson, 1865; Voigt, 1892) which can be assumed to have an amalgamation of a dissipative fluid and an elastic solid. This facilitates model development wherein implicit relationships can be derived for both the dissipative as well as the elastic response. The classical one-dimensional KelvinVoigt model is basically a mechanical analog of a spring and dashpot in parallel reflecting the fact that the Kelvin-Voigt model considers both the linear properties of an elastic solid and a linear viscous fluid that function with no relative motion between either the solid and the fluid. Classical linearised elasticity (linearised viscoelasticity) can be expressed as either the stress or strain in terms of each other, in general, nonlinear theories of elasticity, the stress is usually expressed as a function of the nonlinear strain even though implicit relation are not uncommon for viscoelastic fluids (the Oldroyd-B fluid (Oldroyd, 1950) or Burgers fluid (Burgers, 1996)).

Thus, it would be possible to generalize the classical KelvinVoigt solid as a mixture of more general elastic solids and viscous fluids. Such a model leads to a number of interesting observations. Since, stress cannot be substituted in terms of the strain or the strain rate, implicit constitutive relations come into play. (Rajagopal, 2009) solved the constitutive relations and the balance equations for mass and linear momentum, simultaneously which leads to a system of partial differential equations where the constitutive relations are a part of that very system. The model developed in this thesis involves muscles, tendons and ligaments grouped together as a unit. The mechanical properties of these three soft tissues should be first considered individually before taking into account their combined effect in the model.

4.3.1 Muscles-tendons-ligaments

Research which focuses primarily on specific muscle groups and their mechanical effects, warrants an accurate description of muscle geometry and the joints involved. The geometry of the musculoskeletal system would define the moment arms and the length of the muscles. The moment of a muscle can therefore generate a force at the joint in question. To date, several anatomical studies (Brand and Crowinshield, 1982; Spoor et al., 1991; Weber, 1851; Wickiewicz et al., 1983) have been published which contain information for the various musculoskeletal models for the lower extremity.

However, (Klein et al., 2007) has given calculated details of the muscle parameters which had been lacking so far and is a valuable addition to muscle parameter database, as summarised in Table 4.1. The muscles were dissected and weighed, after removing the tendon, fat and excessive connective tissue, using a scale with an accuracy of 0.1g. Muscle belly, tendon and muscle fibre length were measured with a palpator, by calculating the distance between origin and insertion points. The length of at least five representative fibres was measured depending on the size of the muscle. Standard deviation in fiber length within a muscle was found to be around 0.5cm.

Table 4.1: Optimal fibre length (Lopt), tendon length (Lten) and mass of selected postural muscles (Klein et al., 2007)

Muscles	L(opt)(cm)	L(ten) (cm)	Mass(g)
Extensor digitorium longus	6.0	30.1	34.1
Flexor digitorium longus	3.8	16.6	26.7
Flexor hallucis longus	2.6	23.4	83.7
Gastrocnemius latralis	5.7	23.4	144.0
Gastrocnemius medialis	6.0	21.2	278.0
Peroneus brevis	2.7	6.4	53.9
Peroneus longus	3.4	15.9	86.0
Peroneus tertius	4.3	10.0	28.0
Plantaris	4.8	35.0	12.0
Popliteus	2.4	1.0	27.0
Soleus (medial)	2.4	8.5	238.5
Soleus (lateral)	2.6	8.5	238.5
Tibialis anterior	4.6	23.5	129.0
Tibialis posterior(medial)	2.4	11.0	55.9
Tibialis posterior (lateral)	2.4	11.0	55.9

The tendons basically mechanically transfer the force of the muscle to the bone (Wang, 2006), which in turn induces locomotion and enhances joint stability. Tendons are living tissues which alter their structural and mechanical properties when they bear large forces. Several factors affect the mechanical forces on tendons during normal locomotion and postural control. Firstly, different tendons are subjected to different levels of mechanical loads. For example, the Achilles tendon withstands higher tensile forces than that of the tibialis anterior (Maganaris, 2002; Paul, 2002). Secondly, both the level of muscle contraction and the tendons relative size affect the mechanical forces on a tendon. It can be inferred that the greater the cross-sectional area of a muscle, the higher is the force produced and the larger is the stress a tendon undergoes (e.g., patellar tendon vs.hamstrings tendons) (Kellis, 1998). Thirdly, a variety of activities produce different levels of forces, even on the same tendon (Korvick et al., 1996; Malaviya et al., 1998).

If one studies the tendon, it can be seen that it has a multi-unit hierarchical structure composed of collagen molecules (see Fig 4.5), fibrils, fiber bundles, fascicles and tendon units that run parallel to the tendons long axis. Collagens in the matrix are cross-linked (Bailey and Light, 1985; Eyre et al., 1984). This cross-linkage increases the Youngs modulus of the tendon and subsequently reduces its strain during failure (Thompson and Czernuszka, 1995). Tendons are subjected to dynamic mechanical forces *in vivo* which shows that the tendons have fibre patterns and viscoelastic properties producing their unique mechanical behavior. A study in (Maganaris and Paul, 1999) estimates the *in vivo* structural and mechanical properties of the human tibialis anterior (TA) tendon. It was determined that the tendon stiffness and Youngs modulus at maximum isometric load were 161 N/mm and 1200 MPa, respectively. Because of their viscoelasticity, tendons are liable to deform more during lower rates of strain. This suggests that the tendons absorb more energy, but are less effective in transferring loads. At higher strain rates, tendons have a higher degree of stiffness and are more effective in moving large loads (Jozsa and Kannus, 1997).

Recently, (Leardini et al., 1999a,b) and (O'Connor et al., 1998) described motion path of the ankle joint in the unloaded state and further more have also analysed ligament shape changes and articular contact throughout the range of
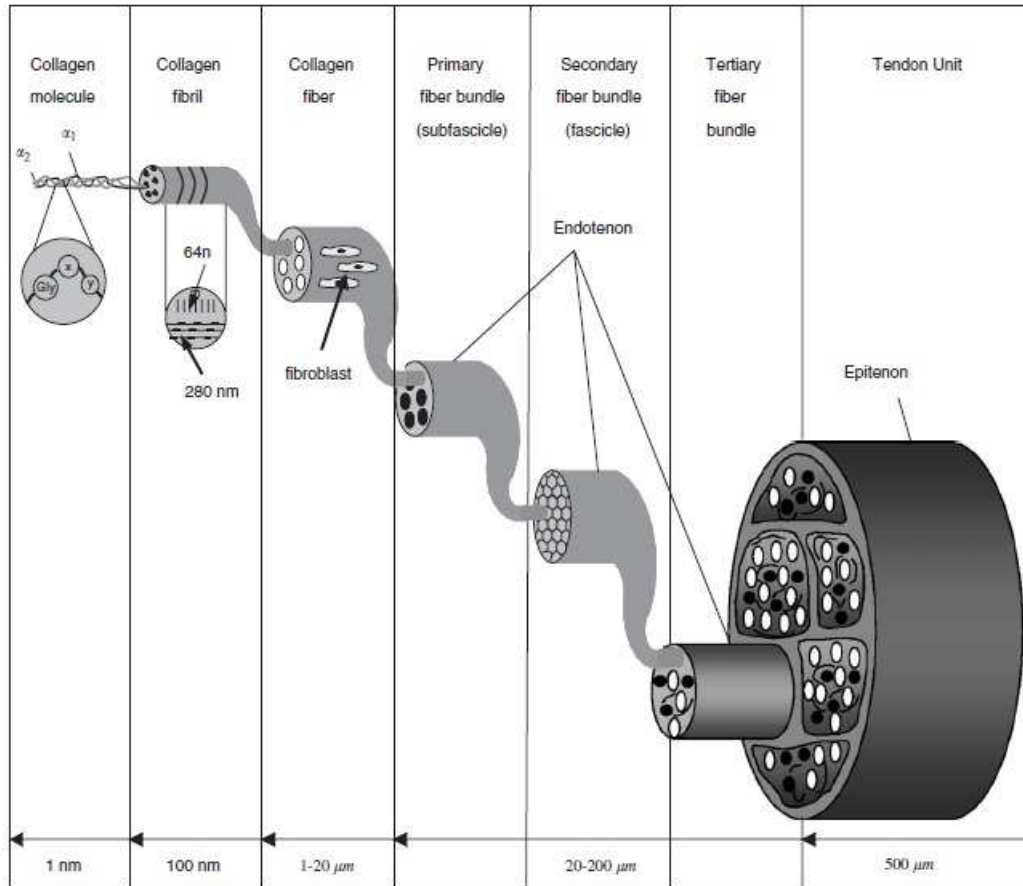
Figure 4.5: Tendon structure (Wang et al., 1998)

flexion (Corazzaa et al., 2003). These studies show considerable insight into developing a mathematical model for postural stability at the ankle region where ligaments are one of the main factors. Ligaments are responsible for providing physical restraints to unwanted movements at joints which in turn provides stability. Testing would basically rely on moving the particular joint so much into the position of instability that maximum tension is placed within the ligament. This would clearly identify if the ligament in question is absent or damaged, and naturally the joint becomes unstable when the unwanted position is attained. These tests would of course depend on a detailed knowledge of anatomy and joint biomechanics. Similar to the tendon testing, problems arise in joints where a complex arrangement of ligaments tend to generate multi-directional stability

so much that a complete assessment of individual ligaments is impossible (David et al., 2000).

4.3.2   Calculation of model parameters

Table 4.2: Mean mechanical muscle parameters (Babic and Lenarcic, 2004; Datta et al., 1952; Edith and Scott, 2011; Klein et al., 2007; Kubo et al., 2002; Lichtwark and Wilson, 2005; Lintz et al., 2011; Pearsall et al., 2003; Robert et al., 2005; Samuel et al., 2009; Tammy et al., 2002; Wakeling et al., 2003)

Muscles and Tendons	Mass (Kg)	Stiffness (10^5 N/m)	Damping (10^5 Ns/m)
Triceps surae	0.225	4.400	0.299
Achilles tendon	0.067	3.640	0.299
Plantaris	0.012	3.640	0.128
Popliteus	0.027	0.837	33.910
Flexor hallucis longus	0.084	0.433	24.830
Flexor digitorium longus	0.027	0.478	24.830
Tibialis posterior	0.056	3.790	33.910
Tibialis anterior	0.129	4.600	34.120
Peroneus brevis	0.054	0.436	24.830
Peroneus longus	0.086	3.460	24.830

Assumptions have been made as to the selection of tendons because of lack of availability of data. Muscles have tendonous parts attached at their ends and these skeletal muscles also tend to differ in their masses because of the amount of tendonous material attached together with the number of pennations. Muscles which have a greater tendonous part have been selected as tendons for example plantaris. In most experiments, the mass of muscle-tendon unit is measured rather than the muscle belly which adds to the change in mass. It is quite difficult to obtain data which gives the mass, stiffness and damping co-efficients separating the muscle belly and the tendonous tissue.

The structural and material properties specifically the stiffness constant of tibialis anterior and posterior have been determined from a plot of load versus elongation. Both the specimens were equivalently elongated and the slope of the elongation at 50% and 70% of failure load determined by basic regression technique (Tammy et al., 2002). (Pearsall et al., 2003) investigated the material

properties of tibialis anterior, tibialis posterior and peroneus longus using the double loop fashion. The specimens were prepared and average initial measuremt was recorded. They were subjected to maximum failure load with a loading rate of 1mm/s. The slope of this graph gave the damping values of the soft tissues in question. The change in the length of the peroneus longus under maximal failure load gave the stiffness constant resulted the stiffness co-efficient as mentioned in Table 4.2.

Testing of the popliteus complex structures was performed by first testing the popliteofibular ligament (Robert et al., 2005), while the popliteus tendon and its attachments were wrapped in a moist, saline-soaked gauze. Once testing was completed on the popliteofibular ligament, testing on the popliteus tendon was performed. Before tensile testing was performed, several preconditioning cycles were performed by slowly cycling the specimens from an unloaded state to the linear portion of their load deformation curve and back to zero load. Each specimen was then rapidly loaded to failure at more than 100%/s to obtain the ultimate tensile strength. Force displacement graphs were recorded, and mechanical propertieswere calculated.

The procedure for measuring the viscoelastic properties of the triceps surae MTC consisted of two parts (Babic and Lenarcic, 2004). Soleus and Achilles tendon stiffness and viscosity were determined in the first part (Flexion trial) while the gastrocnemius stiffness and viscosity were determined in the second part (Extension trial). In both parts of the measurement procedure, subjects inserted their foot in a movable stirrup. The foot was fixed in the stirrup with a strap. The stirrup was attached by steel wire to a weight and force sensor (JR3, model 45E15A) via a pulley system. The MTC viscoelastic properties for different MTC loads were determined by varying the load from 0 to 50 kg. The measurement device and procedure were designed to minimise the movement of human body segments during the measurement. (Lichtwark and Wilson, 2005) measured the damping co-efficients of Achilles tendon and the Triceps surae using a motion capture system at 25 frames/second subjected to an average maximal force.

All specimens of plantaris were first preconditioned by being stretched once up to approximately 5% strain at a rate of 6mm/min, once up to 10% strain at a

rate of 12mm/min (to detect any slipping in the clamps) before being stretched to failure at 36mm/min for an avarage failure load of 7.7N (Lintz et al., 2011) and lastly the mechanical properties of flex.Hal.Long, flex.Dig.Long, peroneus brevis and longus have been deemed to be similar (Hoy et al., 1990). The stiffness and damping parameters have been calculated using the slope of the load versus deformation length and load versus velocity graphs respectively from the papers cited Table 4.2.

Table 4.3: Mean mechanical parameters of ligaments (Bandak et al., 2001; Mkandawire et al., 2005; Siegler et al., 1998; Wei et al., 2011)

Ligaments	Volume (m^3)	Density (kg/m^3)	Mass (Kg)	Stiffness (10^5 N/m)	Damping (10^5 Ns/m)
AFTL	0.0023	1.9376	0.0044	1.418	43.585
ATTL	0.0105	1.9376	0.0203	0.700	8.811
FCL	0.0027	1.9376	0.0052	1.266	5.759
PFTL	0.0045	1.9376	0.0088	1.643	7.842
TCL	0.0162	1.9376	0.0313	0.700	8.811
PTTL	0.0054	1.9376	0.0104	2.343	8.811
TNL	0.0030	1.9376	0.0057	0.391	2.251

The AFTL, FCL and PFTL form the lateral collateral ligaments while the ATTL, TCL, PTTL and TNL form the medial collateral or the deltoid ligaments. A tensile test at low stretch rate of 0.32cm/min was performed on collateral ankle ligaments to study their elastic response on different loading conditions (Siegler et al., 1998). The ATTL and the TCL damping co-efficients were difficult to obtain. The value of PTTL was used keeping in mind that all three are of the same type and the ATTL and TCL have the same stiffness co-efficients (Wei et al., 2011).

The deformation of the specimens (muscle, tendon and ligament) from their initial length under same loading conditions determines the stiffness properties of the collateral ligaments. The mechanical property values are very much dependent on factors like age, preparation, sample used, stretching rate and loading conditions, which therefore makes it increasingly difficult to gauge the range of mechanical properties of these soft tissues. The stiffness and the damping co-efficients also change depending upon the type of physical activity performed. In

this study the stiffness and damping dynamics have been considered to be linear in nature, but in order to gain a further understanding of the functioning of these soft-tissues a non-linear model would be more suitable.
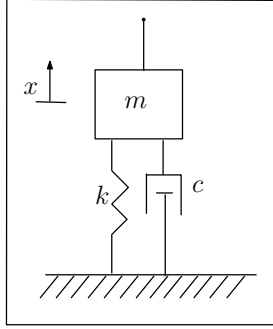
Figure 4.6: Simple mass-spring-damper model

The damping is called viscous because it models the effects of an object within a fluid. The proportionality constant c is called the damping coefficient and has units of force over velocity (N s/m).

Dynamics of the MSD unit in Figure 4.6 are described by the following ordinary differential equation:

$$m\ddot{x} + c\dot{x} + kx = 0. \tag{4.1}$$

The type of solutions to this equation depends on the amount of damping. To characterise the amount of damping in a system a ratio called the damping ratio (also known as damping factor or percentage critical damping) is used. This damping ratio given by $\xi = \frac{1}{2}\frac{c}{\sqrt{km}}$, is just a ratio of the actual damping over the amount of damping required to reach critical damping, whereas the angular frequency of the system is given by $\omega_d = 2\pi f_d$ with $f_d = \omega_n\sqrt{1-\xi^2}$ being the frequency (Hz) of the system's response, and $\omega_n = \sqrt{k/m}$, the natural frequency of the system. If the damping is small ($\xi < 1$) the system's response vibrates, but eventually, over time, will approach zero. This case is called under-damping. If the damping increases just to the point where the system no longer oscillates the point of critical damping ($\xi = 1$). When the damping is increased past the critical damping the system is said to be over-damped, ($\xi > 1$). The critical damping occurs in the mass spring damper model when $c = 2\sqrt{km}$.

During the calculation of the damping co-efficient where the frequency value f_d is imperative and certain assumptions had to be made. Finding data for individual muscles, tendons and ligaments was proven difficult because not much data was available. The frequency for muscles ranged between 28.62 ±1.22Hz for the force acting in the direction of the normal in case of the tibialis anterior muscle and the frequency ranged from 44.89 ±2.10Hz in case of the triceps surae muscle group. However in the axial or the medio-lateral direction the frequencies values appear to be same. It was found upon calculation that there was not much change in the damping ratio ξ. The same set of frequency values were used in case of the other muscle groups which is assumed to have similar damping ratios (Wakeling et al., 2003).

In case of ligaments one frequency, 5Hz (Bonifasi-Lista et al., 2005) from the range of 0.01-15Hz was used. Here, the ligaments were oscillated at different frequency values so as to test it dynamic stiffness response. The results showed that the long-time relaxation behavior and the short-time dynamic energy dissipation of ligament can be controlled by various types of different viscoelastic mechanisms but yet these mechanisms may affect tissue viscoelasticity similarly under different loading conditions (Rasch and Burke., 1965).
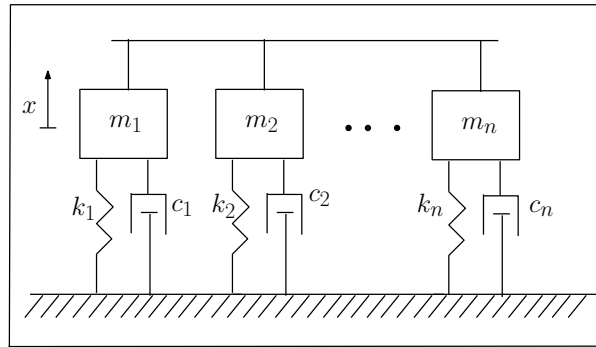
Figure 4.7: Multiple MSD units representing equivalence of muscles, tendons and ligaments

Since each of the mass-spring-damper unit represents one particular soft tissue namely muscle, tendon or ligament which is basically a collection of individual soft tissues grouped together in Figure 4.7 as AB, CD, EF and GH. So, the equivalent mass, stiffness and damping co-efficients can be represented as

$$(m_1 + m_2 + ... + m_n)\ddot{x} + (c_1 + c_2 + ... + c_n)\dot{x} + (k_1 + k_2 + ... + k_n)x = 0 \quad (4.2)$$

where n is the number of muscles, tendons or ligaments in each of the groups.

Figure 4.7 shows the representation of each muscle, tendon or ligament group. The equivalent equation determines the mass, stiffness and damping co-efficients for each MSD sub-unit in AB, CD, EF and GH units. These parameters are summarised in Table 4.4. They have been determined following the discussions in this section. It is quite clear that it follows the structure presented in Fig 4.7 and the calculation of mechanical properties of the soft tissues have been followed in accordance with (4.2).

Table 4.4: Mechanical unit parameters

Parameters	AB	CD	EF	GH
m_a (kg)	0.054	0.079	0.084	0.086
m_b (kg)	0.129	0.281	0.034	0.026
m_c (kg)	0.004	0	0.036	0.035
k_a (N/m)	43300	369710	43300	43600
k_b (N/m)	460000	819000	43300	43300
k_c (N/m)	142000	0	197000	109100
c_a (Ns/m)	48.35	164.45	60.31	61.23
c_b (Ns/m)	243.60	460.32	38.37	33.55
c_c (Ns/m)	23.83	0	71.78	99.76

Since many different sources were used to collect this data a range was expected, but because different types of experiments were used with different subjects both living and cadavers data has been selectively chosen. The next chapter which discusses the simulation of the MSD model will further elucidate the parameter selection and its effects on postural balance.

Chapter 5

Initial simulation of the mass-spring-damper model and testing of model parameters

5.1 Introduction

In this study, the inverted pendulum model derived in Chpater 3 has been used to explain the anterior and posterior sway of the human body with respect to the ankle under a static condition, in other words no external perturbation has been applied to generate exaggerated sway patterns. The unit connections are made bilaterally between the shanks and feet by four of mass-spring-damper (MSD) units. This would be instrumental in analysis and numerically simulate anterior-posterior sway in open stance (feet apart at a natural stance) during quiet standing, where the ankle acts as a fulcrum. There are four units connecting the shank (tibia and fibula) to the phalanges of the foot, the posterior aspect of the calcaneus and the lateral and medial sides of the calcaneus, respectively. Each unit represents a group of muscles, tendons and ligaments which are represented by a 9-element MSD model. The series connection represents the muscle-tendon unit and the parallel unit represents the ligaments. The anterior-posterior sway results in geometrical changing of length from the initial orientation of the four units. As detailed Chapter 3, the Lagrange d' Alembert principle has been used to derive

eighteen ordinary differential equations, along with nine algebraic equations to describe the human body dynamics of anterior-posterior sway with respect to the ankle complex. As detailed in Chapter 4, the model has been parameterised with respect to the length changes, mass, stiffness and damping co-efficient of every muscle, tendon and ligament groups responsible for maintaining quiet stance with respect to the movements about the ankle joints. The numerical simulations are based on the free dynamics of the system described by equation (3.15) associated with the original dynamics described by equations (3.10) and (3.11).

This chapter discusses the response of the system during quiet stance. MAT-LAB function blocks were used in SIMULINK to incorporate the mathematical equations derived in Chapter 3. A variable-step solver was chosen as it dynamically adjusts the time step size, causing it to increase when a variable changes slowly and to decrease when the variable change is rapid. This behavior causes the solver to take many small steps in the vicinity of a discontinuity because rapid variable change in this region. This tends to improve accuracy of the simulation whilst the simulation is sped up even during slow change of the variables. Numerical solver ordinary differential equation-15s (error tolerance of $1e^-9$) was used to run the simulations as it is a variable-order solver for stiff problems. It is based on the numerical differentiation formulae (NDFs). The NDFs are generally more efficient than the closely related family of backward differentiation formulas (BDFs), also known as Gear's methods.

5.2 SIMULINK model
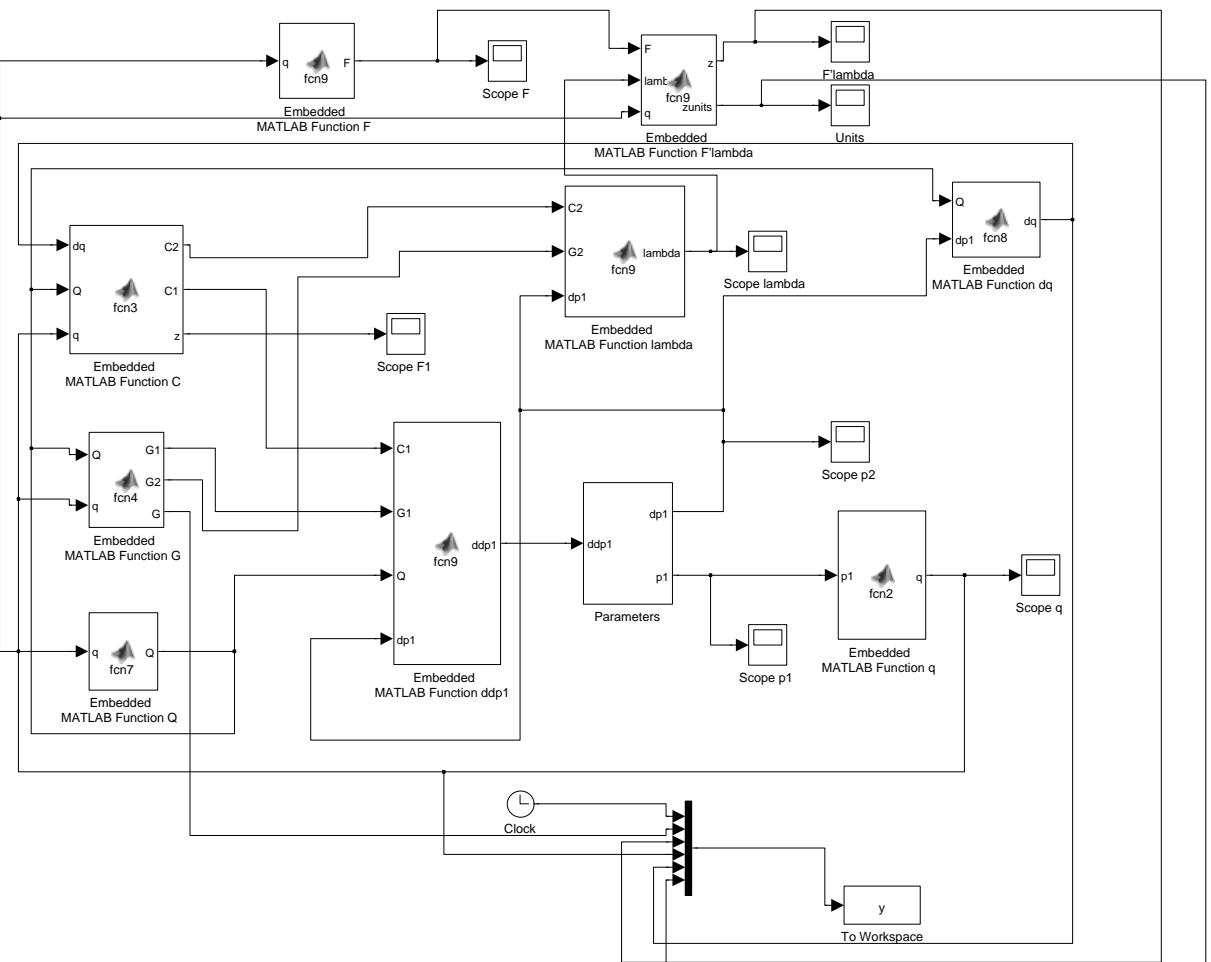
Figure 5.1: SIMULINK block diagram

Figure 5.1 illustrates the function block diagram of dynamic equations previously described in Chapter 3 of the thesis. The simulation in MATLAB and SIMULINK

consists of two parts namely, global parameter assignment and variable solving linkage. The code for simulation is given in Appendix D.

5.2.1 Global parameter assignment

A MATLAB script file was created where the anthropometric, mass, stiffness and damping parameters are listed. Initial condition of α is also given. The initial geometrical conditions are calculated in this file. This file would be then called from various MATLAB embedded function blocks in SIMULINK.

5.2.2 Variable solving linkage

From the block diagram in Figure 5.1 the linkage of different blocks is based on identification of variables which would serve as input, output and global parameters. The global parameters are called in these blocks to facilitate the calculation of constrained dynamics described in Chapter 3. The inverse mapping shown in Appendix B is calculated in Embedded MATLAB function block q, where the output q, a vector of size 18, consists of constraint variables of both the left and the right leg.

The vector q is then linked to Embedded MATLAB function block C, Embedded MATLAB function block G, Embedded MATLAB function block Q, Embedded MATLAB function block F and Embedded MATLAB function block $F'lambda$. The Embedded MATLAB function block C calculates the component matrices of $C1$ and $C2$ which are used in the calculations of the free dynamics and Lagrange multiplier of the dynamic equations. The Embedded MATLAB function block G, calculates the induced gravitational torque values for anterior-posterior sway. The Embedded MATLAB function block Q, calculates the Jacobian matrix associated with the coordinate change from q to p forming an 18×18 matrix. The free dynamics of the system are described by the nine 2nd-order differential equations in (3.15) and the Lagrange multiplier could then be calculated according to equation (3.16) in Embedded MATLAB function block F and Embedded MATLAB function block $F'lambda$ which is the internal torque generated by the constraints. The output of the function blocks are then fed into the workspace with respect to time.

5.3 Response of the system with an initial small angle of the inverted pendulum

In the case of quiet stance, the intended equilibrium position is a slight forward tilt of the body and the instability is gravity-driven. The rate of growth of the toppling torque (i.e. the toppling torque per unit angle) is indicative of the amount of stiffness required to avoid the need for neural intervention. Below the level of critical stiffness, an active stabilisation mechanism is necessary for compensating the inadequate stiffness and restricting the residual oscillations to a small region surrounding the unstable equilibrium position. However, the 2×4 9-element MSD model developed in this study shows that stiffness alone cannot stabilise the posture but the damping parameters play a crucial role to maintain an upright stance of the human body.

5.3.1 System equilibrium calculation

Mechanical perturbation can be caused due to external forces or generated internally, but both displace the body segments which in turn displaces the total system CoM and the human body attempts to regain its upright position. This position is the equilibrium position.

From equation (3.15) representing the free dynamics obtained by eliminating the constraint equations, the equilibrium of the system can be derived. When $G_1 = 0$, from $g_{1,l} = 0$ and $g_{1,r} = 0$, the relationship between $y_{v,i}$ and $x_{v,i}$ is obtained as $k_{b,i} y_{v,i} = (k_{a,i} + k_{b,i}) x_{v,i}$, for $v = l, r$ and $i = 1, 2, 3, 4$. Here, $g_{1,l}$, $g_{1,r}$ and g_1 given below along with other constants and variables are specified in Appendix A

Finally, $A \sin \alpha + B \cos \alpha = 0$ can be derived from $g_1 = 0$, where

$$
\begin{aligned}
A &= \beta_1 \cos \alpha_1 + \beta_2 \cos \alpha_2 + \beta_3 \cos \alpha_3 + \beta_4 \cos \alpha_4 - 2\bar{g}\,, \\
B &= -\beta_1 \sin \alpha_1 + \beta_2 \sin \alpha_2 + \beta_3 \sin \alpha_3 + \beta_4 \sin \alpha_4
\end{aligned}
$$

with, for $i = 1, 2, 3, 4$,

$$\beta_i = \frac{d_i r_i}{\bar{y}_{r,i}} \left[(k_{b,i} + k_{c,i})(y_{l,i} + y_{r,i}) - k_{b,i}(x_{l,i} + x_{r,i}) \right] .$$

Since β_is are functions of α, the latter cannot simply be obtained as $\alpha = -\tan^{-1}\frac{B}{A}$.

For simplicity, assume, with a minor loss of generality, $y_{l,i} = y_{r,i}$ which implies $x_{l,i} = x_{r,i}$ as muscle, tendon and ligament attachment to bone have been considered symmetrical for left and right ankle joint to reduce complexity of the mathematical formulation. Under this assumption, β_i is reduced to

$$
\begin{aligned}
\beta_i &= 2\frac{d_i r_i}{\bar{y}_{l,i}} \left[(k_{b,i} + k_{c,i})y_{l,i} - k_{b,i}x_{l,i} \right] \\
&= 2d_i r_i \frac{k_{a,i}k_{b,i} + k_{a,i}k_{c,i} + k_{b,i}k_{c,i}}{k_{a,i} + k_{b,i}}(1 - \frac{y_{l,i}^0}{\bar{y}_{l,i}})
\end{aligned}
$$

with

$$\bar{y}_{l,1} = \sqrt{d_1^2 + r_1^2 - 2d_1 r_1 \cos(\alpha - \alpha_1)}, \quad \bar{y}_{l,i} = \sqrt{d_i^2 + r_i^2 - 2d_i r_i \cos(\alpha + \alpha_i)},$$

for $i = 2, 3, 4$. Now, it can be seen that $A\sin\alpha + B\cos\alpha = 0$ becomes an equation with the single variable α and all other quantities are known constant parameters. In general, an analytical solution to this equation does not seem possible, but the equation can be solved numerically. Once α is obtained, $\bar{y}_{l,i}$ and further $y_{l,i}$ can be calculated using the equations given above, and finally $x_{l,i}$ as $x_{l,i} = \frac{k_{b,i}}{k_{a,i} + k_{b,i}}y_{l,i}$ for $i = 1, 2, 3, 4$. The calculation of equilibria is completed by recalling the assumption $y_{l,i} = y_{r,i}$ and hence $x_{l,i} = x_{r,i}$.

5.4   Simulation results

The damping parameters play a critical role in the stabilisation of the human body. Since, in this particular model the individual muscles, tendons and ligaments have been considered, their mechanical properties have to be taken into account in order to explain balance of the quiet human stance. The model devel-

oped can be used to analyse the mechanical influence of these soft tissues on the behaviour of the postural sway. Hence, the force-velocity and the force-length changes of individual components of units AB, CD, EF and GH affect the sway pattern of the body about the angle region. The system was simulated with an initial angle of $\alpha(0) = 0.01$ rad (Loram et al., 2005) for 100s.
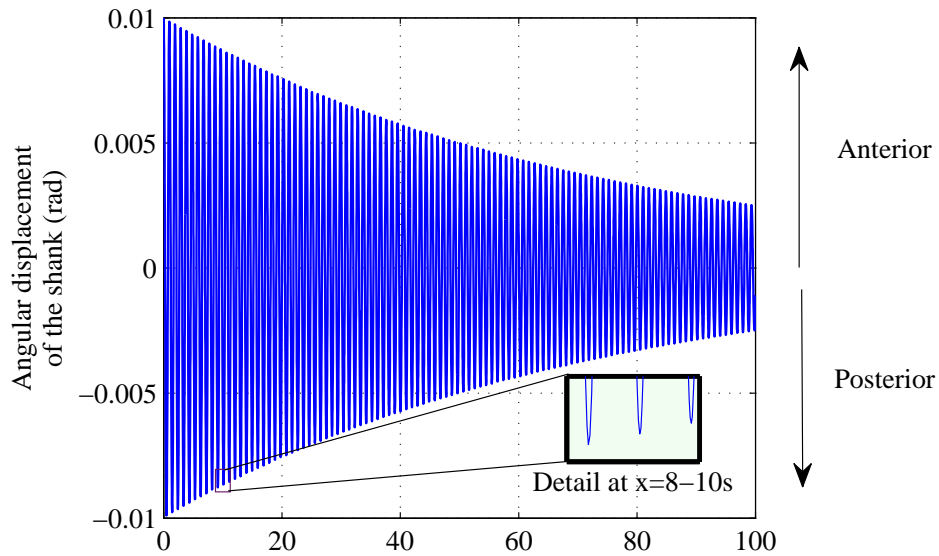
Figure 5.2: Angular displacement of the system with initial angular position $\alpha(0) = 0.01$ rad. This figure depicts the response of the system with damping and stiffness values as listed in Table 4.4.

Figure 5.4, depicts the angular displacement of the shank for 100s. It can be observed that the angular sway of the shank initially starts at $\alpha(0) = 0.01$ rad and then converges slowly towards $\alpha(0) = 0$ rad. The maximum anterior sway was 0.01 rad and the maximum posterior sway was -0.01 rad. The magnifier in the Figure 5.4 shows that for 8-10s there are three posterior oscillations of the inverted pendulum which portrays a realistic sway response of the human anterior-posterior sway during quiet stance. The frequency of number of oscillations occurring are rapid but slowly converge to $\alpha = 0$ rad. This type of response is consistent with Figures 5.3, 5.4, 5.5 and 5.6
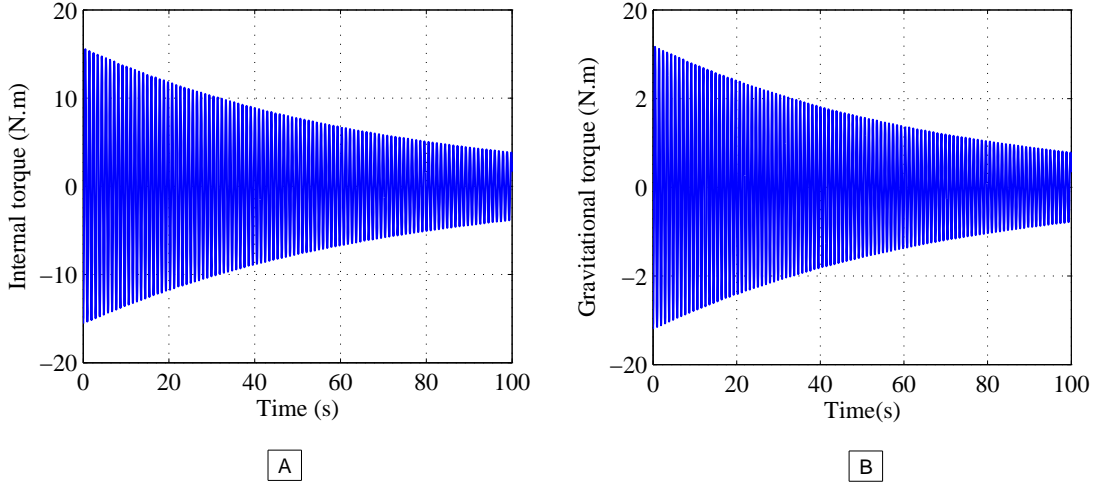
Figure 5.3: Gravitational and internal torque comparative graphs illustrating the
onset of anterior and posterior sway when $\alpha(0) = 0.01$ rad.

The simulation results shown in Figure 5.3 draw a comparison between the
internal and gravitational torque for $\alpha(0) = 0.01$ rad. During anterior-posterior
sway of the system the maximum internal torque measured was 15.55 N.m whereas
the maximum gravitational torque measured was 3.17 N.m. The mean internal
and gravitational torques measured were -0.12 N.m and -0.03 N.m respectively.
The minimum internal and gravitational torques generated were -15.57 N.m and
-3.20 N.m respectively. The values are summarised in Table 5.1.

Table 5.1: Comparison of internal and gravitational torques during anterior-
posterior sway for $\alpha(0) = 0.01$ rad.

	Internal torque (N.m)	Gravitational torque (N.m)
Maximum	15.55	3.17
Minimum	-15.57	-3.20
Mean	-0.12	-0.03

5.4.1 System response without ligaments

So far, it is clear that the model used in this thesis is an intrinsic parametric model
of an inverted pendulum. Ligaments were also considered in units AB, EF and

GH. But, ligaments in unit CD were discounted because it was believed that the triceps surae muscle group along with the Achilles tendon play a dominant role during plantarflexion, thus overriding the passive action of the ligaments induced by anterior-posterior sway during quiet standing. The following results draw a comparison between muscle-tendon-ligament and muscle-tendon only behaving passively as a single unit.
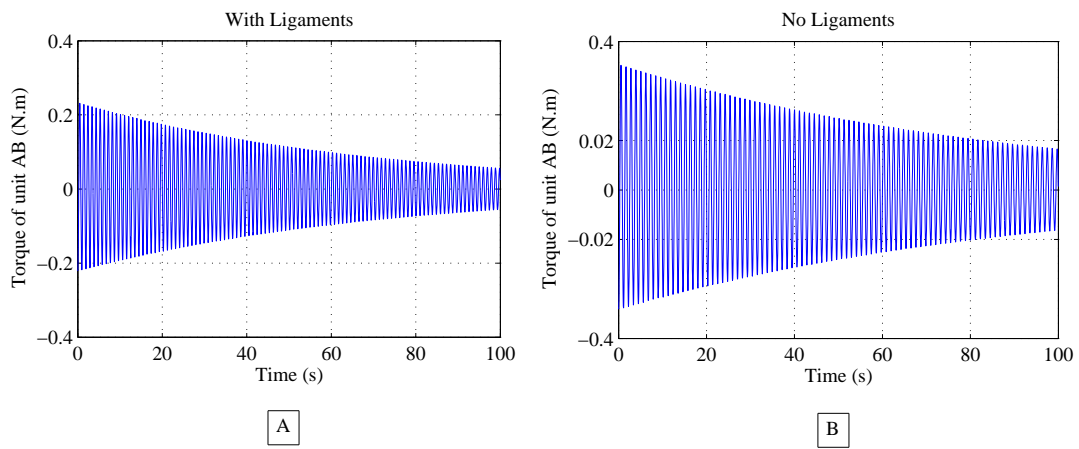
Figure 5.4: Torque of unit AB with (A) and without ligaments (B) at $\alpha(0) = 0.01$ rad.

In the case of unit AB as shown in Figure 5.4, in the absence of ligaments i.e the AFTL is discounted in this particular simulation leaving only the muscle tendon unit of peroneus brevis and tibialis anterior and the maximum and minimum torque produced was 0.05 N.m and -0.04 N.m, respectively. However, maximum and minimum torques produced in unit AB were found to be 78.20% and 78.23% less than the torques produced in the same unit while considering muscle, tendon and ligaments for anterior-posterior sway respectively.
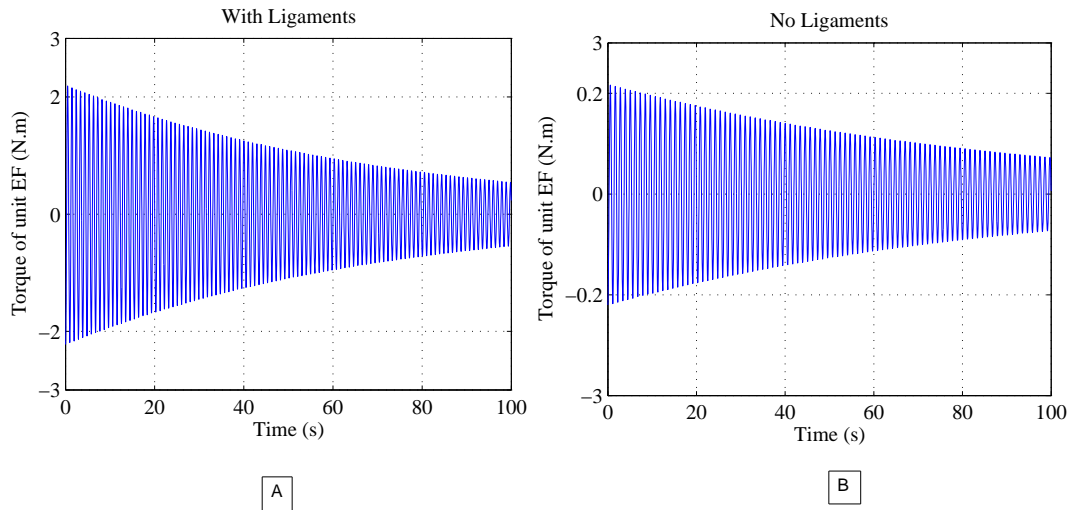
Figure 5.5: Torque of unit EF with (A) and without ligaments (B) at $\alpha(0) = 0.01$ rad.

Figure 5.5, where unit EF consists of only the muscle-tendon unit of flexor digitorium longus and flexor hallucis longus, showed that the maximum and minimum torques produced was 0.22 N.m and -0.22 N.m, respectively. The absence of ligaments in unit EF showed that the maximum and minimum torques were 90.10% and 90.11% less than the torques produced when ligaments were considered in the same unit.
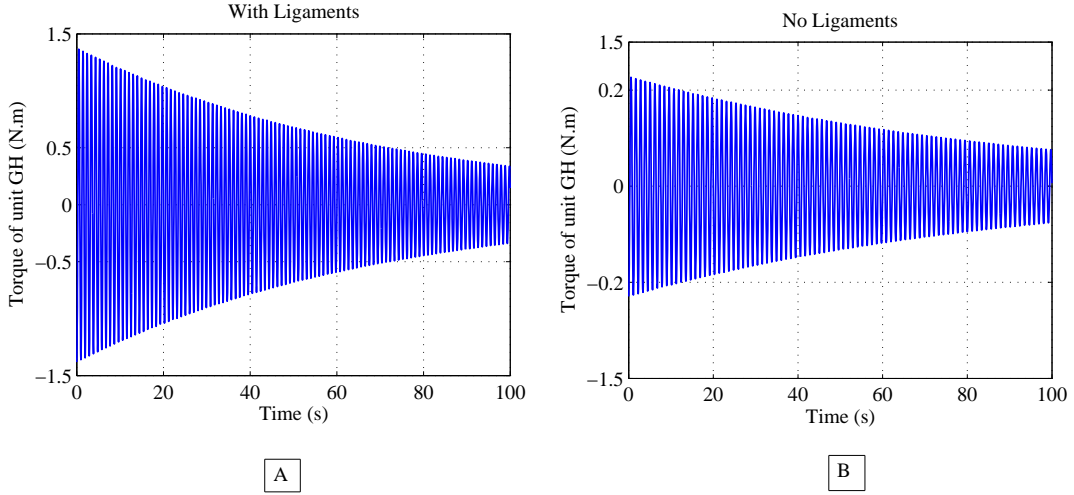
Figure 5.6: Torque of unit GH with (A) and without ligaments (B) at $\alpha(0) = 0.01$rad.

Finally, Figure 5.6, where unit GH consisting of only the muscle-tendon unit, extensor digitorium longus and peroneus longus showed the maximum and minimum torques measured were 0.23 N.m and -0.23 N.m, respectively. However, the measured maximum and minimum torques were 83.40% and 83.41% less than the torques produced when ligaments were considered in the same unit.

5.5 Effects of friction at the ankle joints

So far, in the rigid body dynamics of the inverted pendulum, friction has been ignored. Friction, in this case is considered at the articulating point of the shank and the foot. As the shank moves anteriorly and posteriorly there is a definite sliding friction over the talus of the ankle joint. Now, the ankle joint is classed as a synovial joint which allows relative sliding of surfaces with low friction and negligible wear, while load is transferred with minimal damage to peripheral structural components (Medley, 1981). Based on this argument, during quiet stance, which elicits small anterior-posterior sway which would allow the shank to slide on its pivot generating an opposing frictional torque τ_f.

$$\tau_f = k_f v \tag{5.1}$$

where,

$$v = l \cos \alpha_s \dot{\alpha}_s \tag{5.2}$$

$k_f = 0.01$ is the co-efficient of friction, which is frictional torque generated at a point during translatory motion of the synovial joint normalised to the total torque generated for a given motion (Medley, 1981). l is the absolute distance from the CoM to the ground and α_s is the angular position of the shank attached to the ankle joint.

So, when introducing the torque generated by friction to equation (3.10) it is now represented as

$$M\ddot{q} + C\dot{q} + G(q) \;\; = \;\; F'\lambda - \tau_f \tag{5.3}$$

5.5.1 Simulation of system dynamics with friction
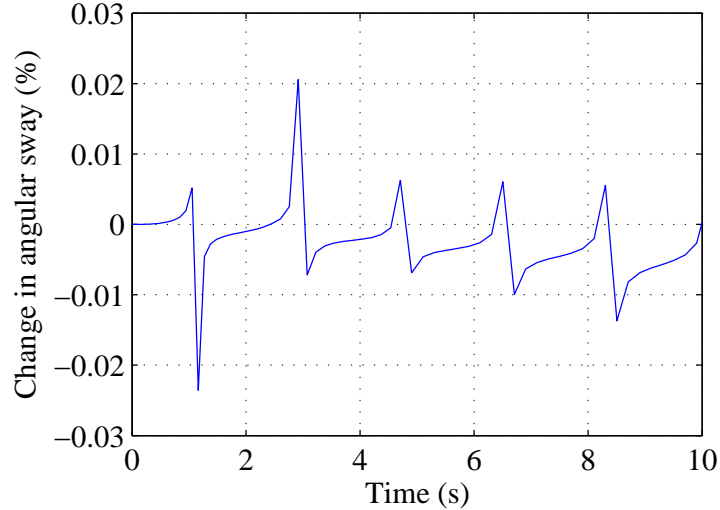
Figure 5.7: Percentage change in angular sway for $\alpha(0) = 0.01$ rad.

Figure 5.7 shows the percentage difference between a frictionless and a system incorporating friction for angular sway for quiet stance. The ankle joint, a synovial joint having a very low co-efficient of friction, it has been expected that the change in angular sway would be very small. The maximum angular change in the anterior direction was 0.02% and the maximum posterior angular change was 0.023% in the negative direction. The mean angular sway change was 0.001%.

5.6 Model linearisation

Chapter 3 discussed the non-linear modelling of the inverted pendulum about the ankle joints. In this section, the model is being linearised to assess the stability of the system using the Nyquist stability criterion. To sketch the Nyquist plot deriving the transfer function is required which has been calculated using MATLAB, using equations from Chapter 3.

The transfer function is obtained as:

$$T(s) = \frac{N(s)}{D(s)} \tag{5.4}$$

with

$$N(s) = 0.01705s^{16} + 531.6s^{15} + 7.58e06s^{14} + 6.566e10s^{13} +$$
$$3.872e14s^{12} + 1.651e18s^{11} + 5.284e21s^10 + 1.301e25s^9 +$$
$$2.509e28s^8 + 3.832e31s^7 + 4.66e34s^6 + 4.503e37s^5 +$$
$$3.42e40s^4 + 1.994e43s^3 + 8.522e45s^2 + 2.428e48s + 3.639e50$$
$$D(s) = s^{18} + 3.118e04s^{17} + 4.447e08s^{16} + 3.852e12s^{15} +$$
$$2.271e16s^{14} + 9.686e19s^{13} + 3.1e23s^{12} +$$
$$7.632e26s^{11} + 1.472e30s^{10} + 2.248e33s^9 + 2.734e36s^8 +$$
$$2.642e39s^7 + 2.007e42s^6 + 1.17e45s^5 + 5e47s^4 +$$
$$1.424e50s^3 + 2.136e52s^2 + 4.814e51s + 6.544e53$$

5.6.1 MATLAB code snippets to explore Nyquist plotting for stability analysis

This section describes in detail how to manipulate Nyquist plot in MATLAB to give a meaningful result and assess stability conditions for the inverted pendulum system described in this thesis.

The following code snippets and figures give a step by step account of how Nyquist plot has been used to analyse the open-loop inverted pendulum system for quiet stance about the ankle joints.

% MATLAB code snippet for Nyquist plot generation (complete coding in Appendix C) %

≫ nyquist(T) % Gives the full Nyquist plot%
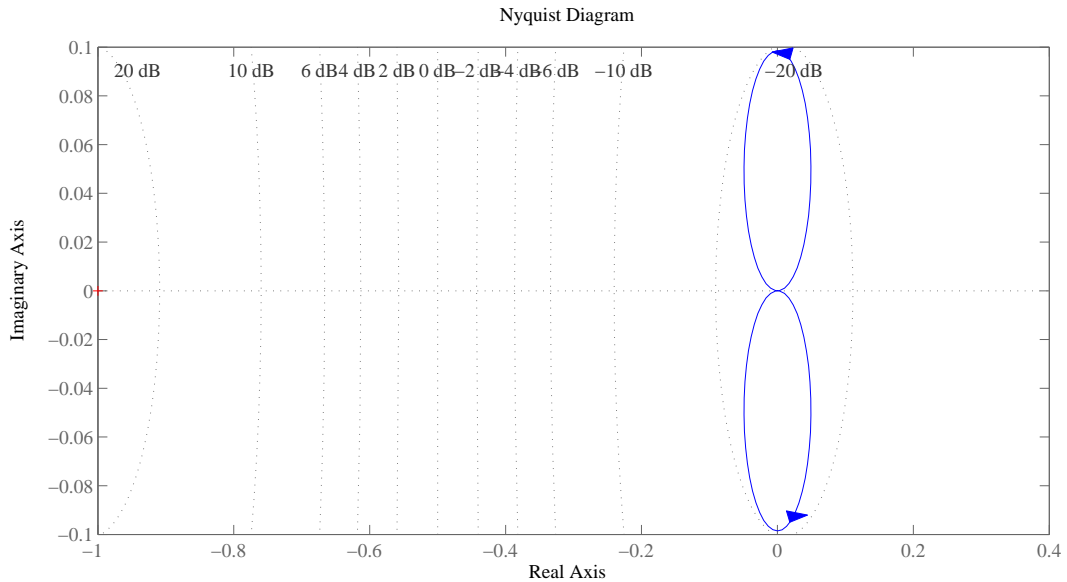
Figure 5.8: Initial Nyquist plot for the transfer function generated from equation 5.4.

≫ [re,im,w]=nyquist(T); % Mapping only positive imaginary axis%

≫ [Gm,Pm, Wg,Wp]=margin(T) % Simple analysis of Nyquist plot of the system%

where,

Gm = Inf

Pm = Inf

Wg = Inf

Wp = NaN

Gm= Gain margin, Pm= Phase margin, Wg= frequency of gain margin and Wp= frequency of phase margin. In this case Gm, Pm and Wg are infinite which means that the open loop inverted pendulum system is inherently stable.

5.7 Model reduction and system stability analysis for different stiffness and damping conditions

Model reduction concept has been briefly described in Chapter 3 based on the method detailed in (Moore, 1981). Model reduction usually incorporates a composition between model order and the degree to which the characteristics of the system are projected by the model. Since, the relative importance of various system variables is dependent on its application there cannot be an universal algorithm. The main principle of model reduction is to remove variables which do not significantly change the dynamics of the original system. The model is reduced from the original system described in equation (5.4) which is given by the subsequent transfer function.

$$\tilde{T}(s) = \frac{\tilde{N}(s)}{\tilde{D}(s)} = \frac{2.046e - 14s^2 + 3.534e - 12s + 0.01705}{s^2 + 0.02718s + 63.42} \tag{5.5}$$

An inbuilt MATLAB function was used which computes a reduced order approximation of a linear time invariant system.

% MATLAB code snippet for model reduction %
≫ rsys = balred(T,2); % MATLAB function used for model order reduction%
≫ [num1,den1] = tfdata(rsys,'v');

The MATLAB code snippet above gives the equation (5.5).
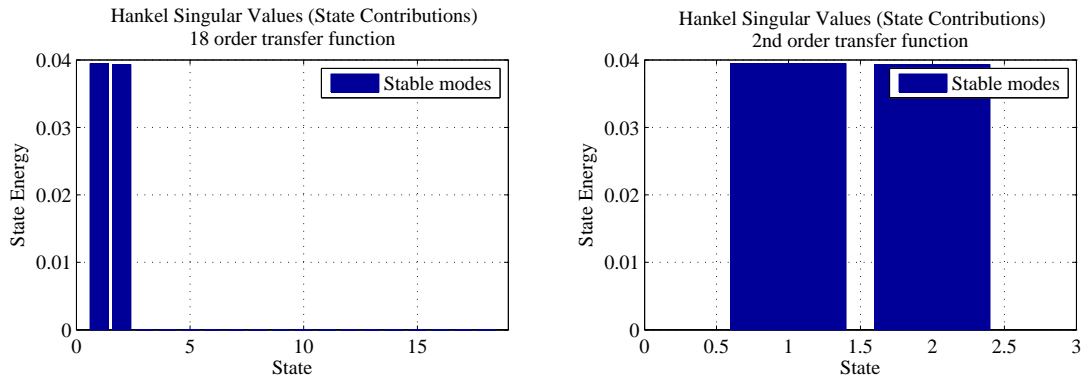
Figure 5.9: Plot of Hankel singular values of 18 order linearised system in comparison with 2nd order minimal realisation system.

Figure 5.9 shows the comparison between the Hankel singular values of the original 18 order system which clear shows which are the dominant poles. The remaining 16 state values are approximately zero, hence have negligible contribution to the system dynamics. This shows the choice of the 2nd order system whose state values exactly match with the original 18 order system.
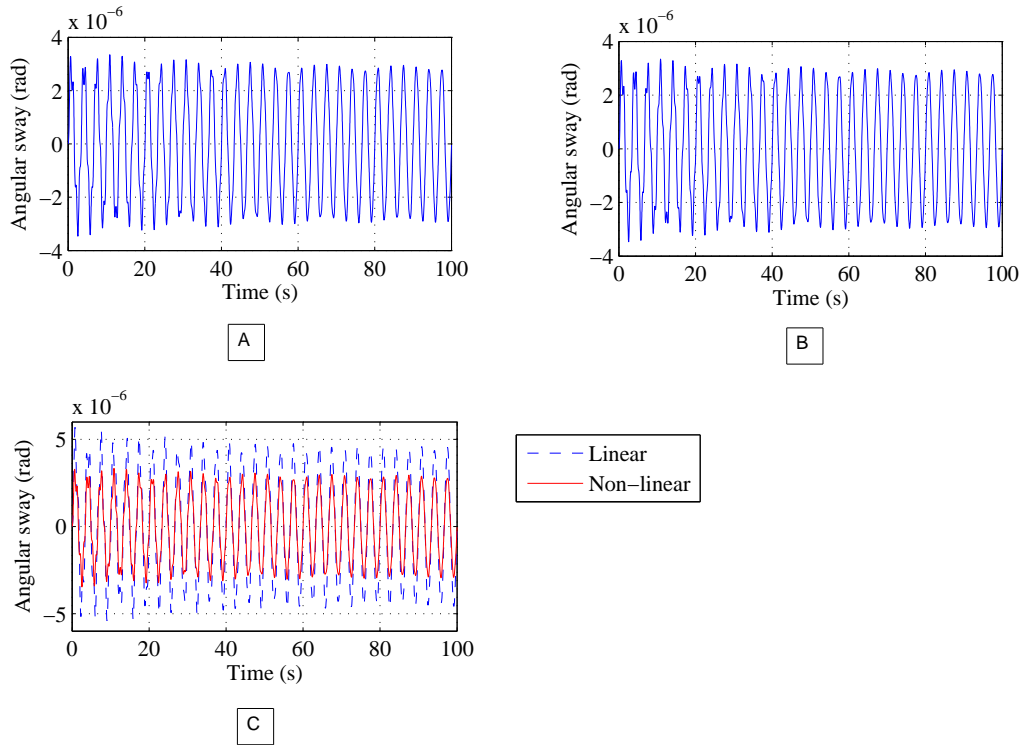
Figure 5.10: Linearised system responses

Figure 5.10A shows the response of the 18 order linearised system as defined in equation (5.4). The response of the system is exactly the same when the 18 order system was reduced to a 2nd order system as shown in figure 5.10B. However, figure 5.10C shows negligible difference between linear and non-linear system.
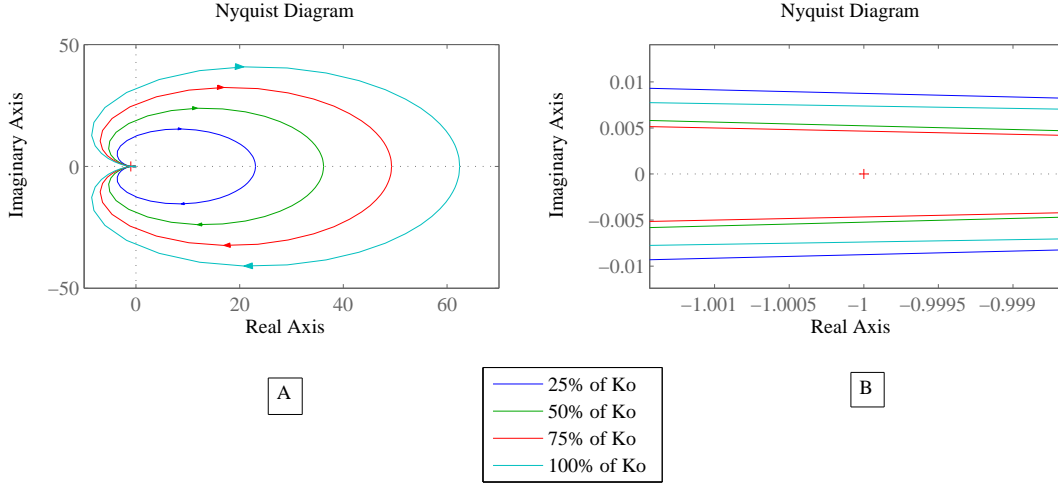
Figure 5.11: Nyquist plot for different stiffness and damping conditions

The original system defined by equation (5.4) has been reduced to a 2nd order system as described in equation (3.21). Figure 5.11B shows the magnified Nyquist plots around (-1,0) of figure 5.11A showing the full view of the Nyquist plots. It can be seen that in figure 5.11 none of the mechanical conditions of K_o (overall stiffness of the system) encircle the (-1,0) point ascertaining stability of the system. The mechanical conditions and their respective transfer functions are listed in Table 5.2.

Table 5.2: Reduced order transfer functions for mechanical conditions as shown in Figure 5.11

Conditions	Transfer function	Colour
100% of K_o	$\frac{-1.973s+62.42}{s^2+2+1}$	cyan
75% of K_o	$\frac{-1.973s+49.29}{s^2+2+1}$	green
50% of K_o	$\frac{-1.973s+36.17}{s^2+2+1}$	red
25% K_o	$\frac{-1.973s+23.04}{s^2+2+1}$	blue

69

Table 5.3: A list of gain margin(Gm), phase margin (Pm), gain margin frequency (Wg) and phase margin frequency (Wp) for a 2nd order reduced linear system listed in Table 5.2

Conditions	Gm (db)	Pm (deg)	Wg (rad/s)	Wp (rad/s)	Remarks
100% of K_o	1.01	0.19	8.02	7.96	stable
75% of K_o	1.01	0.22	7.14	7.08	stable
50% of K_o	1.01	0.26	6.14	6.09	stable
25% K_o	1.01	0.33	4.93	4.89	stable

From table 5.2 it is observed that that the changes of K_o will not affect the first order term of $\tilde{D}(s)$ and the gain margin has remained constant at 1.01 db for the listed conditions of K_o. One explanation could be that the minimal realisation theory of higher order transfer functions are not exact but approximations which in theory removes variables whose effects are negligible to the system as a whole. This is tested when the input and output of the system operate during rest, at equilibrium points. The question then arises to find existing lower order models of the same system which will simulate exactly the characteristics of the whole system. The signals need to be small in order for the minial realisation theory to work. In this particular case, during passive bipedal quiet stance the angular sway of the shank is relatively small $\alpha=0$ rad. A second order model was the best approximation of the initial 18 order linearised system. However, this raises two very important questions:

(1) In what way does the lower order model relate to the original model ?

This question can be answered by injecting a signal into the original system and simulate the dynamics of the original as well as the reduced model. The original system was found to gave to two "dominant poles" which basically means that the response matrix formulated (state-space realisation of a 2nd order system) was similar to the original 18 order system. If the similar realisation cannot be formulated the minial realisation theory would not be possible and erroneous conclusions could be drawn.

(2) Will the lower order system fully explain the dynamics of the system ?

To answer this question, the definition of dominance has to be clearly understood which was proposed by (Moore, 1981). However, it is very easy to confuse between internal dominance of a subsystem and actual dominance of the original system. In this particular case, an 2nd order system, which is nothing but an approximation of the 18 order system will not be able to justify the physical meaning of variables used in an 18 order system. In this case only the angular sway parameter was analysed which was a close match between the linear and non linear system however, the missing torque variables show that 2nd order system is not well suited to explain the relationship between internal torque and gravitational torque of the original model.

5.8 Discussion

In intrinsic parametric models (Casadio et al., 2005b; Clifford and Holder-Powell, 2010; Gatev et al., 1999; Gurfinkel et al., 1974; Jeka et al., 2004; Morasso and Sanguineti, 2002; Winter et al., 2001), only muscle-tendon units were considered and ligaments were left out as it might not play a major role in explaining postural balance. The cases of muscle-tendon units only and those combined with ligaments have been considered and compared in this study. In Unit CD, ligaments were not considered on the grounds that the plantarflexors were strong enough to mask the effects of the posterior ligaments joining the shank with the calcaneus. Unit AB only had one ligament that functionally helped in ankle dorsiflexion and inversion. Units EF and GH had the highest concentration of ligaments in the lateral and medial directions, respectively. Based on the simulation results, it was found that the muscle-tendon-ligament unit produced significantly greater torque at the unit level compared to a muscle-tendon unit alone during quiet stance.

In the context of ligaments' role as bone connectors and tendons' as muscle to bone connectors, the work by Hicks (1953, 1955); Ker et al. (1987); Wright et al. (2012) showed that muscles, tendons and ligaments together formed a functional unit for a static foot where the body weight was distributed about the ankle joint. Supporting the body weight in an erect posture not only involved balancing against the gravitational torque, but also maintaining equilibrium and thus

emphasising its inherent dynamic properties. They found that postural control theories should not be limited suprapedally involving only a muscle-tendon unit.

Having thus established the importance of a biomechanically functional unit of muscle, tendon and ligament, the next objective of this study was to determine the effects of stiffness and damping parameters of such an unit on the postural dynamics. The data collected from the literature reported mainly long range stiffness values (Babic and Lenarcic, 2004; Hoy et al., 1990; Lichtwark and Wilson, 2005; Lintz et al., 2011; Pearsall et al., 2003; Robert et al., 2005; Tammy et al., 2002) where the concept and range of long range stiffness values was defined by Lakie et al. (2003). The current study showed that higher intrinsic stiffness values exhibited a more rapid response for anterior-posterior sway. This demonstrated better maintenance of the angular position of the shank, which is in agreement with previous experimental studies of Alexandrov et al. (2005); Johansson et al. (1988). The overall stiffness values of muscles, tendons and ligaments used in the current study were within the range of stiffness values reported in an in-vivo study (O'Brien et al., 2010).

In the current model the effect of friction was also tested. The velocity induced friction introduced into the system, has been known to have a damping effect on postural dynamics (van Soest and Rozendaal, 2008). However, simulation results show Figure 5.7 that during quiet stance velocity induced friction had negligible effect on postural dynamics. This is so far the only work which has considered frictional effects during quiet stance. Nevertheless, it is possible that velocity induced friction may affect sway during exaggerated anterior-posterior excursions of the CoM.

To control quiet stance, the alignment of the vertical projection of the COM with respect to the base of support has been investigated previously (Winter et al., 1998). This implies that, not only is the body's geometry represented in the postural scheme, but the distribution of body mass must be considered. The main rationale for this control is to adjust the equilibrium constraints. These require that, under static conditions, the COM vertical projection should remain within the base of support. Various studies indeed argue in favour of this hypothesis (Horak and Nashner, 1986; Massion, 1998). In the case of quiet stance, the intended equilibrium position of the body is tilted slightly forward and the

instability is gravity-driven. The rate of growth of the gravitational torque (i.e. the gravitational torque per unit angle) is indicative of the amount of stiffness required to avoid the need for neural intervention. The calculations of the system equilibrium were based solely on the stiffness parameters of the model with only one equilibrium point, ($\alpha = 0$ rad) as shown in Section 5.3.1. The model developed in the current study can be used to analyse the mechanical influence of these soft tissues on the behaviour of postural sway. Hence, the force-velocity and the force-length changes of individual components that make up units AB, CD, EF and GH affect the sway pattern of the body about the ankle joint angle.

The model presented in this study showed that when the body was tilted anteriorly, the torque generated was posterior, which leads to the suggestion that unit CD, consisting of the triceps surae and the Achilles tendon, was instrumental in preventing the body from falling. This was in agreement with the study by Loram et al. (2007). Hence, at any angular position the reflex mechanism of the musculoskeletal system pulls the body about the line of its COM preventing the body from toppling over. Since the muscles responsible for upright stance of the human body function in an antagonistic manner, unit AB was responsible for preventing the body from falling in the posterior direction which was in agreement with the conclusions drawn by Day et al. (2013). When the sway mechanism was initiated, primarily in the anterior direction, the internal torque was maximum on the posterior side as shown in Figure 5.3(A). As a result, the distance between the calcaneus to the fulcrum of the ankle joint was smaller than the distance from the latter to the toe. This suggests an even smaller base of support for stability and that the stiffness co-efficients were higher in unit CD as compared with units AB, EF and GH, respectively. Moreover, the higher internal torque values for unit CD reported in the current study also confirmed these findings. The model in this study not only demonstrated the functional importance of the calf musculature, represented by unit CD, but also suggested that the mediolateral side of the ankle played an equally important role during the stabilisation of quiet stance as a considerable amount of torque was generated by units EF and GH.

Linearisation of the original model was undertaken, where the mathematical realisation has been detailed in Chapter 3. The main goal for model linearisation was to assess stability of the system under various mechanical conditions.

5.Initial simulation of the mass-spring-damper model and testing of model parameters

Linearised model original produced an 18 order system and calculation Hankel singular values yielded that there can be a reduced order model by eliminating state variables which offer negligible change in overall system dynamics which is clearly shown in Figure 5.9. It was found that a second order system would indeed show a similar response as am 18 order linear system as shown in Figure 5.10. However, question arises that whether a second order reduced model can capture the changes in parameters of the system thus altering its dynamic response since Table 5.2 and Figure 5.11 shows little change in system dynamics when overall stiffness parameters were changed.

Chapter 6

A preliminary case study for model evaluation

6.1 Introduction

The primary goal of the experiment is to determine the ranges of gravitational torque values and the angular rotation of the shank at the ankle region during quiet stance. It was hypothesised that the experiment would show predominance of triceps surae muscle group over tibialis anterior during quiet stance where angular rotation of the shank would be small. The experiment recorded angular rotation of the shank for quiet stance and simultaneously measured EMG activity of gastrocnemius lateralis, gastrocnemius medialis, soleus and tibialis anterior. The EMG activity of the said muscles were then compared against the maximal voluntary isometric contraction (MVIC) of the same muscles in a static position.

It is common practice that the measures of static balance are extrapolated during quiet stance, where the accelerations of the body segments and their corresponding inertial forces and torques are deemed to be negligible (Panzer et al., 1995; Prieto et al., 1996). Under such circumstances, muscle forces act antagonistically to counteract the destabilising effects of the gravitational forces, thereby facilitating stability in stance by aligning the horizontal locations of CoM.

6.2 Methodology

6.2.1 Participant

One male subject (age 27; height 173cm; and mass 84kg), gave written informed consent to participate in this study. The participant filled in and signed a pre-excercise medical questionnaire and was deemed healthy and free from any musculo-skeletal injuries. Ethical approval for this study was sought through the Department of Sport, Health and Exercise Science at University of Hull. The participant was barefoot and wore tight fitting clothing to reduce movement of markers attached onto the body.

6.2.2 Equipment

In order to measure muscle activity during quiet stance the TeleMyo 2400 EMG system (Noraxon, Scottsdale, Arizona, USA) was synchronised via a 64-channel AD board with the motion capture system (Qualisys system, Gothenburg, Sweden). Two (one for each lower limb) 400x600 mm Kistler plates 9286AA (Winterthur, Switzerland) were used measure the kinetic data. The calibration of the motion capture system was carried out by using a 750mm calibration wand and L-frame reference object for 100s which was instrumental in identifying the origin of the laboratory where the experiment was conducted. The three dimensional tracking parameters had a prediction error of 30 mm, maximum residual of 10 mm, acceleration factor of 50,000 mm/s^2 and noise factor of 10 mm. The calibration results are shown in Table 6.1 and reliability tests have been carried out to ascertain the accuracy of equipment used which is detailed in Appendix D.

Table 6.1: Calibration results for the motion capture system where X,Y and Z represents the position of the trajectory in the current frame. The coordinates use the coordinate system of the motion capture system set up during calibration. The average residual (the residual of an observed value is the difference between the observed value and the estimated function value) can be defined as the mean of different residuals of the 3D point. This is a quality check of the points measured position (Qualisys User Manual 2011, Gothenburg, Sweden).

Cameras	X (mm)	Y (mm)	Z (mm)	Average Residual (mm)
01	-2879.48	8237.98	3843.52	0.39757
02	580.96	8177.05	3342.09	0.44031
03	4072.65	8129.05	3802.09	0.56613
04	4927.45	2722.54	2092.04	0.33378
05	5153.45	-3563.56	2205.35	0.38378
06	3423.34	-6780.78	3284.22	0.64616
07	402.80	-6806.70	2812.14	0.45712
08	-2527.83	-6796.25	3308.00	0.37735
09	-4296.39	-2877.96	2209.17	0.47538
10	-3809.72	3898.39	1874.80	0.36868

Motion signals were sampled at 100 Hz, and force signals were sampled at 2000 Hz. Twenty one reflective markers (14 mm) were attached bilaterally onto the bony landmarks of the participant's body according to the six degrees of freedom (6 DOF) marker set (Buczek et al., 2010; Cappozzo et al., 1995) as listed in Table 6.2.

Table 6.2: Reflective marker positions on bony landmarks

Segment	Marker positions (Bilateral)
Pelvis	lateral and medial anterior superior iliac spine (ASIS)
	lateral and medial posterior superior iliac spine (LPSIS and MPSIS)
	Greater trochanter (GT)
	Iliac crests
Thigh	Thigh clusters (4 markers)
	Femoral lateral epicondyle (LKNEE)
	Femoral medial epicondyle (MKNEE)
Shank	Shank clusters (4 markers)
Foot	Fibula apex of lateral malleolus (LANK)
	Tibia apex of medial malleolus (MANK)
	1st, 2nd and 5th metatarsal heads (1st MTH, 2nd MTH, 5th MTH)

Isokinetic Dynamometer Biodex System 3 (Shirley, New York, USA) was used to measure MVICs of tibialis anterior, soleus, gastrocnemius lateralis and gastrocnemius medialis.

6.2.3 Protocol

Before commencing the experiment, limb dominance was determined by asking the participant to kick a football. The participant's dominant leg (left) muscles were palpitated, namely, tibialis anterior, soleus, gastrocnemius lateralis and gastrocnemius medialis in order to locate appropriate sites to fix surface EMG electrodes. For accuracy of placement of EMG electrodes, guidelines described by Rainoldi et al. (2004) were followed as represented in Table 6.3.

Table 6.3: Reference lines, anatomical landmarks, and IZ locations (Rainoldi et al., 2004)

Muscles	Reference lines and anatomical land-marks	IZ locations
Gastrocnemius medialis	The percentage distance from the medial side of the popliteus cavity to the medial side of the Achilles tendon insertion, starting from the Achilles tendon	$50.3 \pm 5.7\%$
Gastrocnemius lateralis	The percentage distance from the lateral side of the popliteus cavity to the lateral side of the Achilles tendon insertion, starting from the Achilles tendon	$61.2 \pm 5.1\%$
Tibialis anterior	The percentage distance from the tuberosity of tibia to the inter-malleoli line, starting from the tuberosity of tibia	$15.5 \pm 4.2\%$
Soleus	The percentage distance from the tuberosity of tibia to the medial side of the Achilles tendon insertion, starting from the Achilles tendon	$76.3 \pm 3.7\%$

The guidelines mentioned in Table 6.3 were used because Rainoldi et al. (2004) described the importance of innervation zone (IZ, which is the location where nerve terminations and muscle fibers are connected) and placement of the electrodes on the IZ would result in data variability and ambiguous EMG values. According to Rainoldi et al. (2004), the optimum site for electrode placement would be areas between IZ and tendon terminations.

6.2.4 Recording, processing and normalisation of surface EMG

Having marked the appropriate sites, the skin was prepared by lightly shaving the marked region and wiping it with 70% alcohol wipes. Circular surface electrodes in a bipolar configuration (Ag/AgCl, 10 mm diameter, 20 mm interelectrode dis-

tance) were firmly affixed to the dominant leg of the participant. The participant was then seated in a Isokinetic Dynamometer Biodex System 3 (Shirley, New York, USA) with his upper body firmly braced. For familiarisation, a warm-up, specific to the MVIC movements (plantarflexion and dorsiflexion at $0 \pm 15°$ ankle angular positions) and at least one practice contraction was completed (Rutherford et al., 2011). When the participant reported satisfactory familiarisation, three five-second maximal isometric contractions were completed for each exercise. His dominant foot was on the foot rest and was asked to perform MVICs by plantarflexing and dorsiflexing at $0 \pm 15°$ ankle angular positions (Rutherford et al., 2011). Verbal encouragement was given to the participant to fascilitate maximal effort during each recording with a five-second rest between each trial.

An eight-channel TeleMyo 2400 EMG system (Noraxon, Scottsdale, Arizona, USA) was used to record surface EMGs from the triceps surae muscle group and tibialis anterior during MVICs and quiet stance (eyes open and eyes closed conditions). The surface EMG signal was amplified with a gain of 1000. Common mode rejection rate and input impedance were 100 dB and 1 MΩ, respectively. The raw EMG signals were band-pass filtered online using a fourth-order, Butterworth filter, with cut-off frequencies of 1 and 500 Hz.

EMG signals were corrected for bias, full wave rectified and low-pass filtered (Butterworth, 4th order, cut off frequency, 1 Hz). A 100 ms moving-average window, advancing one sample at a time identified the maximal EMG amplitude for each muscle in all trials of three MVIC exercises (Hubley-Kozey et al., 2006). The peak amplitude regardless of the exercise was considered the MVIC used to normalize the EMG data from the standing trials.

6.2.5 Lower extremity three dimensional (3D) modelling and signal processing

After the MVIC test the participant was prepared for the motion capture experiment. Before the the experiment was performed two 400x600 mm Kistler plates 9286AA (Winterthur, Switzerland) were placed adjacent to each other on a flat level surface in focus of 10 infrared camera systems (Qualisys system, Gothenburg, Sweden). The participant was then instructed to stand on the Kistler force

plates (one leg on each plate with a distance of 0.16m from right medial malleolus to the left medial malleolus) for 100s in their natural stance and to stand as still as possible with eyes open and arms at their sides.
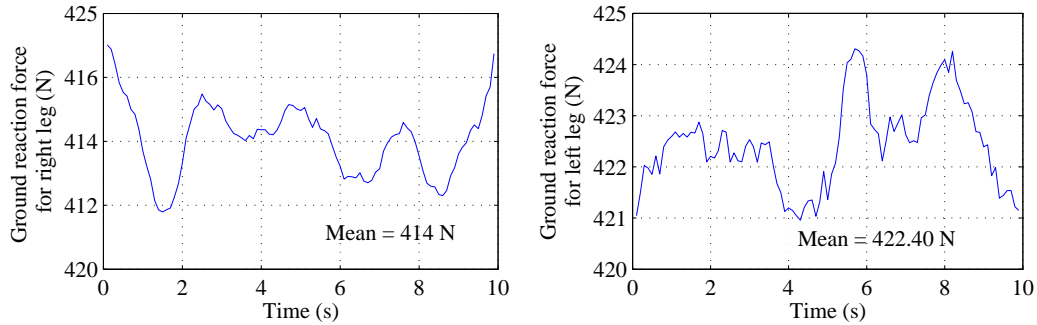
Figure 6.1: Static trial vertical ground reaction force (GRF) for (A) right leg and (B) left leg during quiet stance for 10s.

A static trial for 10s with the participant's eyes open was undertaken to ascertain the participant maintained approximately equal loading on each leg as shown in Figure 6.1.

Standardised positioning between trials was ensured by marking the outline of the participants feet on the force platform. Three trials alternating between eyes open and eyes closed were recorded with 2 min breaks for every second trial.

After acquiring the raw data from Qualisys Track Manager (QTM v2.8) it was exported to Visual 3D v5 (C-Motion, Rockville,US) in .C3D format for 3D model building and signal processing. This section gives an insight towards signal processing, 3D model building and the outputs generated from this software.

The modelling procedure involved identification and monitoring the trajectory of segmental movement in the X,Y,Z plane of the laboratory. This was achieved by making use of rigid clusters which defined the segments in the static trail. The markers not only identified proximal and distal aspects of the segments but also the lateral and medial aspects of each joint. The data gathered from marker positions was used to compute individual segmental parameters as listed in Table

6.4

Table 6.4: Segmental parameters, definition and orientation used in modelling quiet stance in Visual 3D.

Parameters		Segment			
		Pelvis	Thigh	Shank	Foot
Proximal	Lateral	LPSIS	GT	LKNEE	LANK
	Joint	n/a	Hip Joint	n/a	
	Medial	MPSIS	n/a	MKNEE	MANK
Distal	Lateral	GT	LKNEE	LANK	5th MTH
	Joint	n/a			
	Medial	GT	MKNEE	MANK	1st MTH
Segmental geometry		Cylinder	Cone	Cone	Cone
Segmental mass (proportion to total patient mass)		0.142	0.1	0.0465	0.0145

For ease of modelling it was assumed that each segment was a rigid structure. Segment definition based on marker-based information allowed modification for various aspects of each segment. Estimation of segmental mass was done by calculating the percentage of the total subject mass using regression equations developed by Dempster (1955). Segment geometry assessment with their inertial values were selected from previous anthropometric reports (de Leva, 1996). Once each segment had been defined, a skeletal model was generated for the static file. The model acted as a template when assigned to the eyes open and eyes closed dynamic files.

After the skeletal model was built which processed some of the raw data signals, marker trajectories were interpolated via a cubic spline algorithm with a maximum frame gap of ten. The raw kinetic data and the marker trajectories were rigorously filtered to remove high frequency noise using a low pass Butterworth filter with a cut-off frequency of 1.5 Hz (Gage et al., 2004). Relative

orientation of the local coordinate systems of two segments making up a joint and an X,Y,Z cardan sequence was used to define kinematic measures in Visual 3D. Joint moment was calculated based on the dynamics of the mathematical model described in Chapter 3.

6.3   Results

This section presents the outcome of the experiment carried during quiet stance. The experimental results show that during quiet stance the ankle range of motion remains unchanged bilaterally for eyes open and eyes closed condition. Angular sway of the shank (α) described in Chapter 3 was used as initial starting point for model simulation in Chapter 5 has been measured and presented in this section. The gravitational torque was also calculated together with the amount muscle activity during quiet stance. Although, a relationship between force generated and EMG has not been established in this study, the EMG values during quiet stance were compared against MVICs values to gauge the percentage activity of triceps suare muscle group and tibialis anterior which are the dominant muscles of units CD and AB, respectively in the MSD model described in Chapter 3.
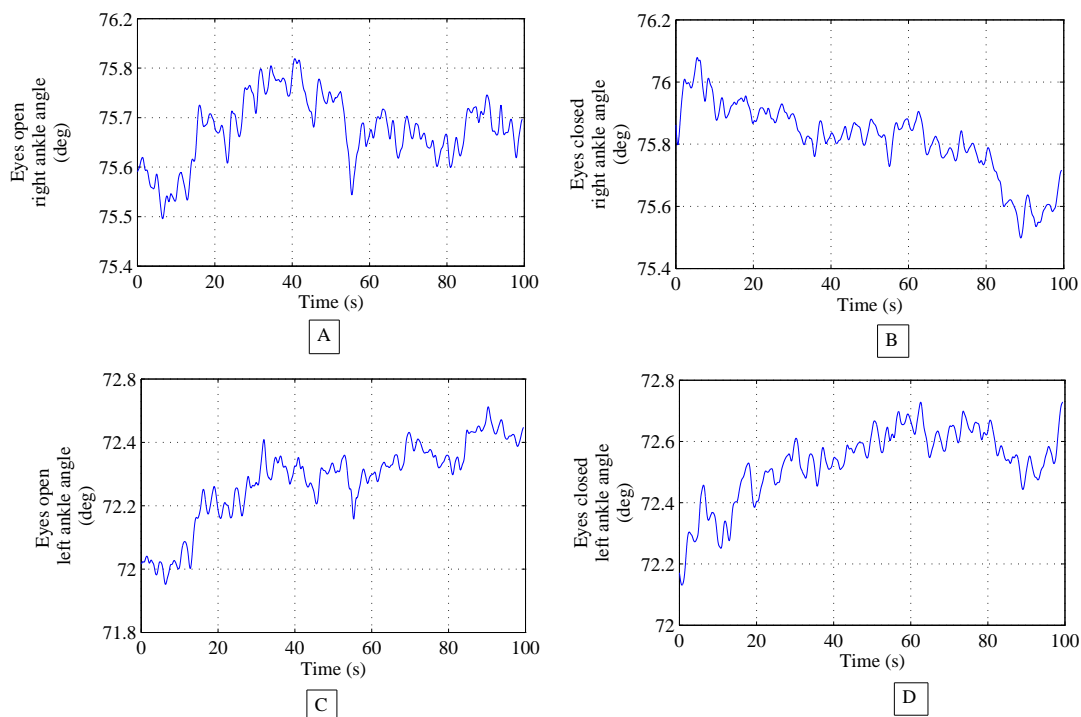
Figure 6.2: Mean ankle joint trajectory for three trials during quiet stance measured bilaterally. Figure A illustrates eyes open mean right ankle joint trajectory with a standard deviation of 0.1; Figure B illustrates eyes closed mean right ankle joint trajectory with a standard deviation of 0.2; Figure C illustrates eyes open mean left ankle joint trajectory with a standard deviation of 0.1 and Figure D illustrates eyes closed mean left ankle joint trajectory with a standard deviation of 0.1.

Figure 6.3 shows the angular trajectory of the ankle joint during quiet stance for conditions eyes open and eyes closed. During eyes open condition as shown in Figure 6.3A, the maximum and minimum ankle angular displacement of the right ankle is 75.82° and 75.50° respectively. For eyes closed condition as shown in 6.3B, the maximum right ankle angular displacement is 76.10°, however, the minimum right ankle angular displacement remains unchanged at 75.50°. Similarly in figure 6.3C, maximum and minimum left ankle angular displacement for eyes open condition are 72.51° and 71.95° respectively. But for the eyes closed condition as shown in figure 6.3D, the maximum and minimum left ankle angular

84

displacement recorded 72.73° and 72.13°, respectively. The ankle range of motion (bilateral) for eyes open and eyes closed condition was 0.6°.
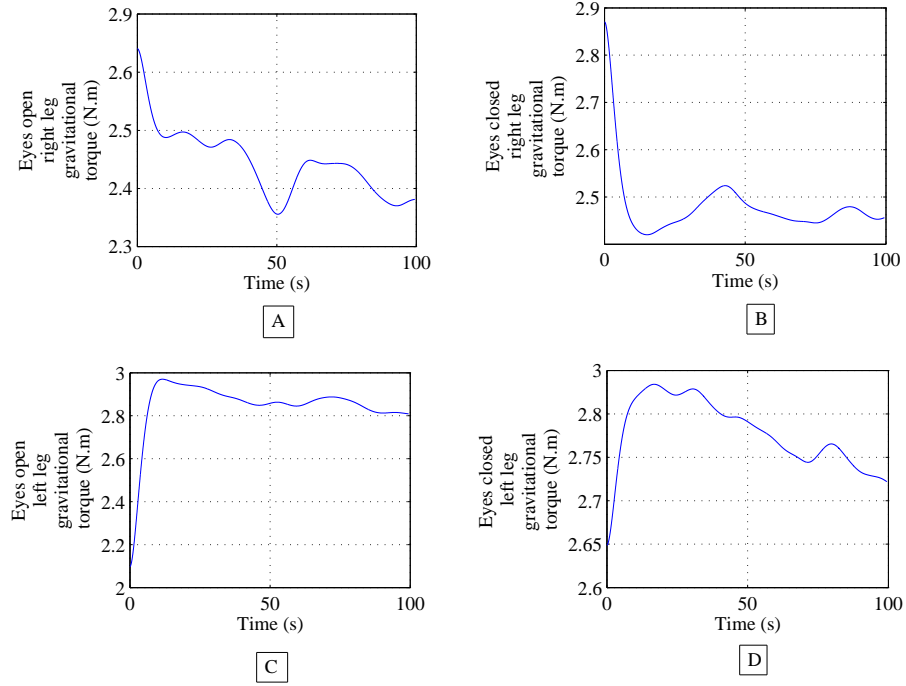
Figure 6.3: Torque induced by gravity during quiet standing for eyes open and closed conditions for the angle range of motion of 0.6°.

Figure 6.3 shows the gravitational torque produced during quiet stance for eyes open and eyes closed condition of both the right and left lower extremities. For eyes open condition, the right foot recorded a maximum posterior gravitational torque of 2.64 N.m as shown in Figure 6.3A and a maximum anterior gravitational torque of 2.35 N.m. The right foot, as shown in Figure 6.3B for eyes closed condition, measured a maximum posterior gravitational torque of 2.87 N.m and a maximum anterior torque of 2.42 N.m. Similarly, for the left foot as shown in Figure 6.3C, for eyes open condition, the maximum posterior and anterior gravitational torque of 2.83 N.m and 2.52 N.m, respectively; whereas for eyes closed condition as shown in Figure 6.3D the maximum posterior and anterior gravitational torques were 2.97 N.m and 2.64 N.m, respectively.

Table 6.5: Gravitational toppling torque bilateral comparison during quiet standing for eyes open and closed conditions.

Sway	Right foot eyes open (N.m)	Left foot eyes open (N.m)	Right foot eyes closed (N.m)	Left foot eyes closed (N.m)
Maximum Anterior	2.64	2.83	2.87	2.97
Maximum Posterior	2.35	2.52	2.42	2.64
% difference >maximum anterior	12.34	12.30	18.60	12.50
Mean torque	2.44	2.77	2.48	2.85

Table 6.5 summarises the gravitational torque values of anterior-posterior sway during eyes open and eyes closed conditions. It was observed that during eyes open condition, the posterior torque was 12.34% and 12.30% less than the torque generated anteriorly in the right and left foot, respectively. Similarly, for eyes closed condition the posterior torque was 18.60% and 12.50% less than the anterior torque for right and left foot, repsectively. The overall mean torque (3 trials) in the right foot for eyes closed condition was 1.64% greater than the mean torque generated during eyes open condition. Similarly, for the left foot eyes closed condition, the overall mean torque (3 trials) was 2.88% greater than eyes open condition.
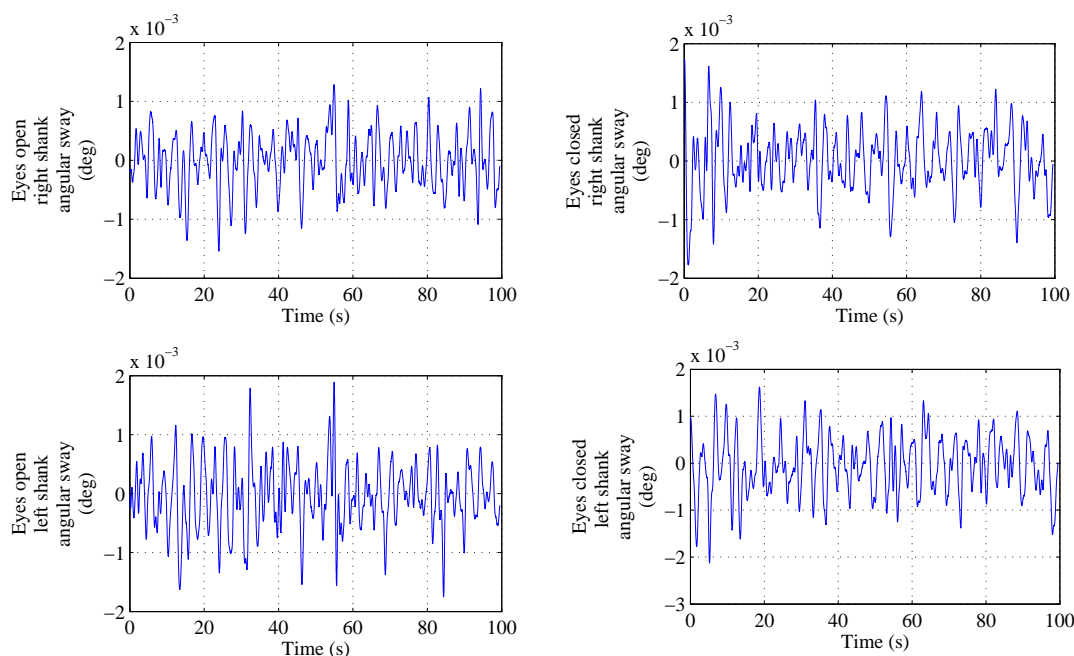
Figure 6.4: Bilateral angular sway of the shank during quiet stance for eyes open and eyes closed conditions.

Figure 6.4 shows the angular sway (anterior-posterior) of the body during quiet stance for eyes open and eyes closed conditions. As there was no application of external perturbation, the maximum anterior and posterior sway angles were relatively small at $0.002°$ and $0.001°$, respectively. The calculation of angular of angular sway can be represented as difference between the initial and final position of the rotation of the ankle joint with respect to the shank segment. The angular sway angle should not be confused with the range of motion of the ankle joint during quiet stance which is the difference between the maximum and minimum ankle joint angles.
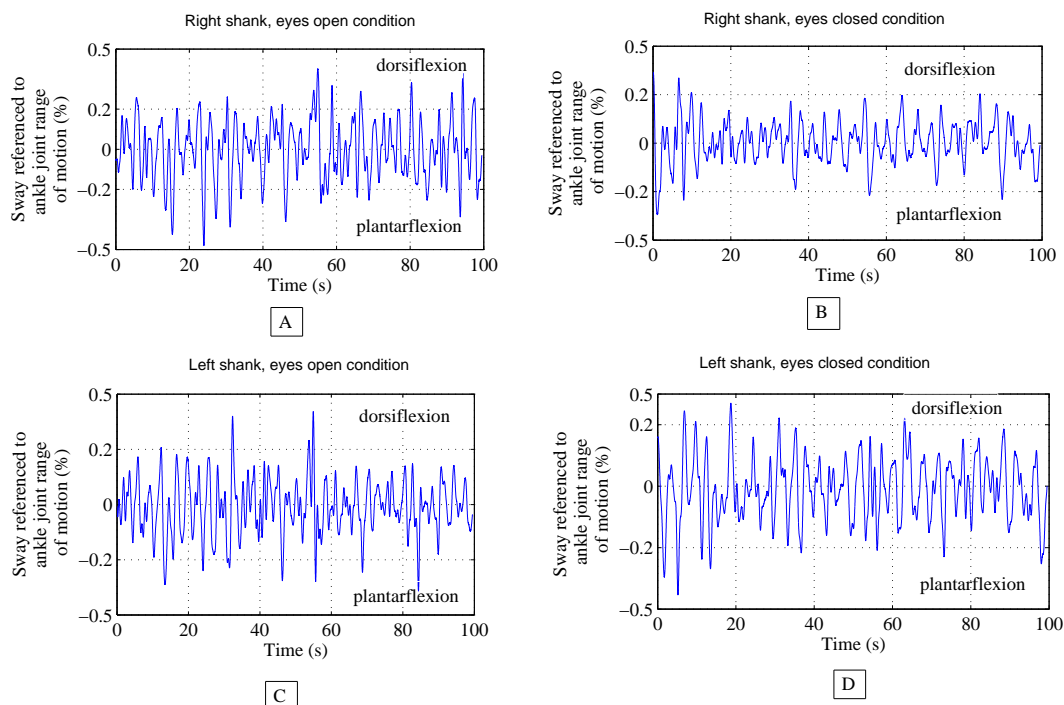
Figure 6.5: Amount of plantarflexion and dorsiflexion during anterior-posterior sway of the shank for eyes open and eyes closed conditions during quiet stance.

Figures 6.5A and B show a sway pattern of the right shank during the eyes open and eyes closed conditions having an unchanged ankle range of motion of 0.6°. The maximum plantarflexion for eyes open condition was 0.4% and dorsiflexion peaked at 0.48% of the ankle range of motion. Similarly, for eyes closed condition, the maximum dorsiflexion was 0.29% and the maximum plantarflexion peaked at 0.28% of the ankle range of motion.

Figure 6.5C illustrates the sway pattern of the left shank for the eyes open condition during quiet stance where the maximum dorsiflexion achieved was 0.34% and maximum plantarflexion was measured at 0.32% of 0.6° range of motion of the ankle joint.

Similarly, Figure 6.5D illustrates the sway pattern of the left shank for eyes closed condition during quiet stance within the range of motion of the ankle joint. The response starts with shank moving in the posterior direction which evokes a plantarflexion response of the ankle joint. Once it has reached its peak, the shank

proceeds to complete the second half of the postural response by dorsiflexing, causing the shank to move in the anterior direction. The maximum amount of dorsiflexion of the ankle joint is 0.36% of the ankle joint range of motion (0.6°) during postrior sway of the shank. The maximum plantarflexion achieved in the same context was 0.27% of the ankle range of motion.

EMG measurements were recorded, synchronised with the motion capture time for eyes open and eyes closed conditions during quiet stance. The EMG measurements (filtered and processed, refer to Section 6.2.4) were then compared with the maximal voluntary isometric contractions for tibialis anterior, gastrocnemius latralis, gastrocnemius medialis and soleus muscles, comparisons of which is given in Table 6.6.

Table 6.6: Filtered electormygraphical activity during quiet stance compared with maximal isometric voluntary contraction (MVIC). The data presented in this table is the overall average of 3 trials. The standard deviation (S.D.) is presented alongside the mean values.

Muscles	Peak MVIC (μV)	Peak Eyes Open (μV)	Mean(S.D.) Eyes Open (μV)	Peak Eyes Closed (μV)	Mean(S.D.) Eyes Closed (μV)
Gastrocnemius latralis	237.73	6	3.52(0.63)	6	3.46(0.51)
Gastrocnemius medialis	194.62	12	2.77(0.45)	11	2.87(0.48)
Soleus	285.47	8	5.13(0.10)	12	5.58(0.82)

The tibialis anterior muscle was found to be "silent" during both eyes open and eyes closed condition, but the triceps surae group consisting of (gastrocnemius lateralis, gastrocnemius medialis and soleus) exhibited a fair amount of activity with maximum values of 6, 12 and 8μV, respectively for eyes open condition and 6, 11 and 12μV, respectively for eyes closed condition during 100s of quiet stance. The overall mean EMG activity during the duration of the experiment for gastrocnemius lateralis, gastrocnemius medialis and soleus was 3.52, 2.77 and 5.13μV, respectively for eyes open condition whereas for eyes closed condition the overall mean EMG activity for the same were 3.46, 2.87 and 5.58μV. The gastrocnemius lateralis activity showed 2.10%, while gastrocnemius medialis

and soleus evoked 2.05% and 3.15% in relation to MVICs during eyes open condition. A similar comparison was conducted for eyes closed condition which showed the gastrocnemius lateralis, gastrocnemius medialis and soleus 2.52%, 5.65% and 4.20% activity of MVICs.

6.4 Discussion

During quiet stance in the experiments, for eyes open and eyes closed conditions, the ankle range of motion remained constant at 0.6° which was expected as there was no external perturbation applied to generate any planterflexion or dorsiflexion. However, the amount of sway during quiet stance was assessed by normalising angular sway of the shank to the range of motion of the ankle joint. This investigation looked closely into quiet stance and the movements recorded are very subtle. It was found that the bilateral angular sway of the shank was greater during dorsiflexion than plantarflexion of the ankle joint in both eyes open and eyes closed conditions. It can be inferred that ankle dorsiflexion occurred during anterior sway which is in accordance with the conclusions drawn by Gage et al. (2004).

In postural balance, considerable importance has been attached to torques generated at the ankle joint which can be both active and passive (Vette et al., 2010). Passive torque components are the result of tension/stiffness produced by muscles tones and by the stiffness of the surrounding tissue, such as ligaments and tendons (Masani et al., 2003). However, the stabilisation of quiet stance by passive torque alone is a very challenging task, and an active component is required to maintain stability (Pietro and Schieppati, 1999). The active torque component is controlled by the CNS, which controls muscle contractions based on the overall body kinematics and dynamics of spontaneous body sway that are influenced by external disturbances (Pietro and Schieppati, 1999; Winter, 1990; Winter et al., 1996). However, the torque generated during quiet stance, where there is absence of an externally applied force, can be considered passive in nature. During anterior sway, the torque generated is greater than that of posterior sway.

In order to have a clear understanding of anterior posterior sway during quiet standing EMG activity was measured for tibialis anterior, gastrocnemius lateralis,

gastrocnemius medialis and soleus muscles. There have been extensive studies on muscle activity during perturbed quiet stance (see reviews in Horak and Macpherson (1996); Scott Kelso and Kenneth (1981)) but only a few during unperturbed quiet stance (Gatev et al., 1999; Joseph, 1960; Joseph and Nightingale, 1952; Masani et al., 2003). These studies of muscle activity during unperturbed quiet stance have underlined the importance of tibialis anterior, gastrocnemius lateralis, gastrocnemius medialis and soleus muscles, congruous with the hypothesis that a single segment inverted pendulum would be an appropriate conjecture for quiet upright stance (Saffer et al., 2008) which is in accordance with the hypothesis presented in this thesis.

The tibialis anterior muscles was found to be "silent" on both eyes open and eyes closed conditions which is in accordance with previous literature Borg et al. (2007); Joseph (1960) contrary to the study by Giulio et al. (2009). However, the gastrocnemius lateralis, gastrocnemius medialis and soleus muscles showed some amount of activity. The experiment conducted shows that muscle activity in the triceps surae group is slightly greater during anterior sway than posterior sway which is accordance to the study conducted by Borg et al. (2007). As previously demonstrated, anterior sway evokes dorsiflexion at the ankle joint which could be an explanation as to the reason for marked EMG activity at the triceps surae muscle group which corroborates with the studies by Joseph (1960); Joseph and Nightingale (1952). The percentage of EMG activity of the triceps surae during quiet stance vs MVIC were found to be within the range Nagai et al. (2011); Panzer et al. (1995).

This preliminary case study evaluates the intrinsic model described in Chapter 3 as the model calculations were incorporated in the 3D model described in Section 6.2.5. However, the mechanical parameters such as the stiffness and damping of individual muscles, tendons and ligaments could not be measured with this experimental setup and is challenging as to obtain accurate measurements *in-vivo* studies need to be performed. The EMG values reported for the triceps surae muscle group are greater than tibialis anterior which was found to be silent. In the model simulations reported in Chapter 5, unit CD (consists of triceps surae) showed a significantly greater internal values as compared to unit AB (consists of tibialis anterior). Hence, it can be inferred that triceps surae plays

a dominant role in maintaining upright stance. In the experiments described in this chapter, internal perturbation could not be ruled out hence the destabilising gravitational torque generated have been compared with the simulation with internal perturbation in subsequent chapter to further evaluate the model.

This study is not without its limitations. During the motion capture experiments, there was minimal movement of the knee joint while the the inverted pendulum has considered the knee joint to be immobilised. There have been reports where knee joint movement have been considered to be a factor in maintaining quiet upright stance (Kimura and Kouzaki, 2013; Runge et al., 1999). The motion capture data would give anterior-posterior as well as medio-lateral sway data, however, medio-lateral sway is out of the scope in the present study as the inverted pendulum model is restricted to only anterior-posterior sway. In order for the inverted pendulum model to be validated more rigorous experiments need to be carried out with a large number of subjects with a robust statistical analysis. However, the basic experimental protocol and inclusion of the mathematical model into a 3D lower extremity model has been reported in this chapter which would serve as guidelines for future work. Model extension and its implications have been described in more detail in Chapter 8.

Chapter 7

Mass-spring-damper model simulations with internal perturbation

7.1   Introduction

This chapter evaluates the model further by using data obtained from the case study from Chapter 6. The simulation results in Chapter 5 show that the inverted pendulum model developed in this thesis is affected by the change in mechanical conditions of the system. It has been found that when the overall stiffness of the inverted pendulum was kept at 100% along with damping it was by far the most stable and plausible mechanical condition for quiet stance about the ankle joints. In this chapter the response of the same system will be further studied under internal perturbation to ascertain the conclusions drawn in Chapter 5.

As the human body is composed of multi-link segments any movement will cause involuntary perturbation of the equilibrium position. Internal perturbations are difficult to quantify experimentally (Nomura et al., 2013; Suzuki et al., 2012), hence random noise of low frequency was introduced into the mass-spring-damper system. In the past, various theoretical studies (Asai et al., 2009; Bottaro et al., 2008; Conforto et al., 2001; Schmid et al., 2004) have been undertaken to mimic internal perturbation and its effect on sway size, however, the effects of internal

perturbation on an intrinsic inverted pendulum modelling quiet stance has not been investigated. In this chapter, the applied internal perturbation will further determine which mechanical condition would be a plausible candidate for keeping the human body upright during quiet stance. In Chapter 5, it has been concluded that damping with 100% stiffness shows the best response for anterior-posterior sway during quiet stance. However, it has been known that internal perturbation will increase sway size (Asai et al., 2009; Bottaro et al., 2008) which would in turn increase the amount of destabilising gravitational torque.

In this current study, it is hypothesised that the internal perturbations will increase sway size and increase the gravitational torque attempting to destabilise the system, however, the internal torque generated would be still greater to maintain the system at its equilibrium position. The mechanical condition, damping with 100% stiffness, would be the plausible candidate for intrinsic inverted pendulum models for unperturbed quiet stance.

7.2   System response with internal perturbation condition

Postural equilibrium is the condition in which all the forces acting on the body are balanced such that the CoM is controlled relative to the base of support, either in a particular position or during movements. Control of balance, or equilibrium, can be reactive, that is, in response to external forces displacing the CoM, or proactive, as occurs in anticipation of internally generated, destabilising forces imposed by the body's own movements. Both external forces (including gravity and forces related to interaction with the environment) and internal forces (which are generated during all body movements, even respiration) ultimately act to destabilise the body by moving its CoM. The role of the nervous system is to detect and predict instability and produce the appropriate muscle forces that will complement and coordinate with all the other forces acting on the body so that the CoM is well controlled and balance is maintained. So far, the simulation was not comprised of any internal perturbations. In the subsequent sections of this chapter the responses of the mass-spring-damper system will de-

pict sway in the presence of an internal perturbation by adding random noise of $v = 0.01 \sin(2\pi f_g t + w)$, where the frequency f_g= 0.3 Hz and w is an independent random Gaussian variable having zero mean with variance of 0.5.
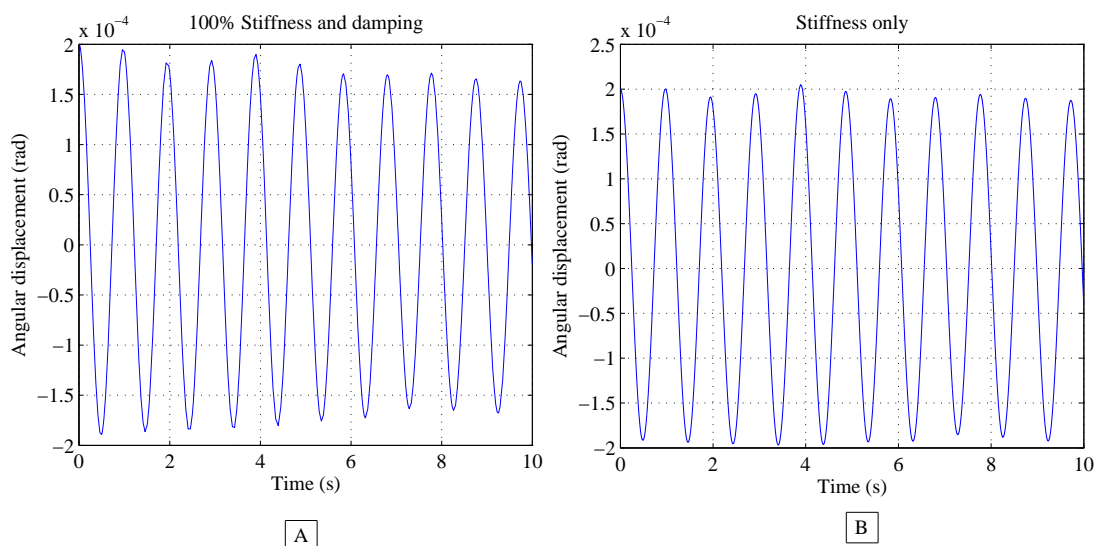
Figure 7.1: Angular displacement of the shank when $\alpha(0) = 0.0002$ rad during internal perturbation. Figure (A) shows the response of the system in the presence of damping and 100 % stiffness parameters of muscles, tendons and ligaments. Figure (B) shows the response of the system for stiffness only condition.

Figure 7.1 depicts the angular displacement response of the mass-spring-damper system for three different mechanical conditions. In Figure 7.1A, the maximum anterior sway was at 0.0002 rad and the maximum posterior sway was -0.0002 rad. There is a definite convergence towards the zero. However, in case of Figure 7.1B, the maximum anterior and maximum posterior sway peaked at 0.00024 rad and -0.0002 rad, respectively and slowly diverges away from the zero position.

Quiet stance is characterised by the anterior position of the centre of mass relative to the ankle. Accordingly, tonic postural activity is predominant in the posterior leg and trunk muscles. Such posture is probably a result of physical constraints imposed on maximal torques exerted differently by the ankle flexors and extensors. The length of the anterior portion of the foot (relative to the ankle

joint axis) is greater than that of the posterior portion. The anterior position of the centre of mass partially compensates for this asymmetry.
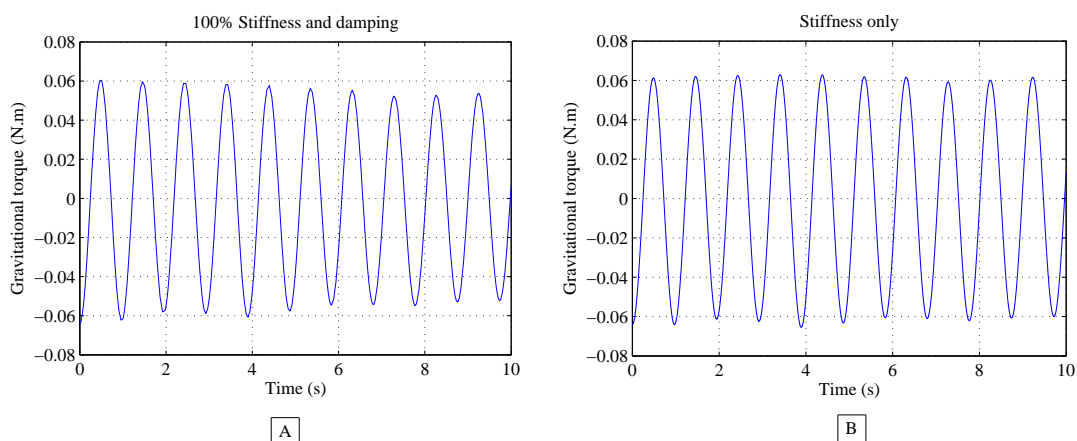
Figure 7.2: Torque generated due to gravity when $\alpha(0) = 0.0002$ rad during internal perturbation. Figure (A) shows the response of the system in the presence of damping and 100 % stiffness parameters of muscles, tendons and ligaments. Figure (b) shows the response of the system for the stiffness only condition.

Figure 7.2 depicts the gravitational torque generated during anterior-posterior sway of the mass-spring-damper system of the inverted pendulum during quiet standing. The negative torque here suggests an anterior position as the system started anteriorly when $\alpha(0) = 0.0002$ rad; conversely the generation of positive torque would be due to posterior sway of the mass-spring-damper system. This is true for both conditions. In the first instance shown in Figure 7.2(A), the maximum posterior torque generated was 0.06 N.m while the maximum anterior torque was -0.06 N.m. In the second instance shown in Figure 7.2(B), the gravitational torque acting on the system, the maximum posterior torque and maximum anterior torque values were 0.063 N.m and -0.07 N.m, respectively.

7.Mass-spring-damper model simulations with internal perturbation.
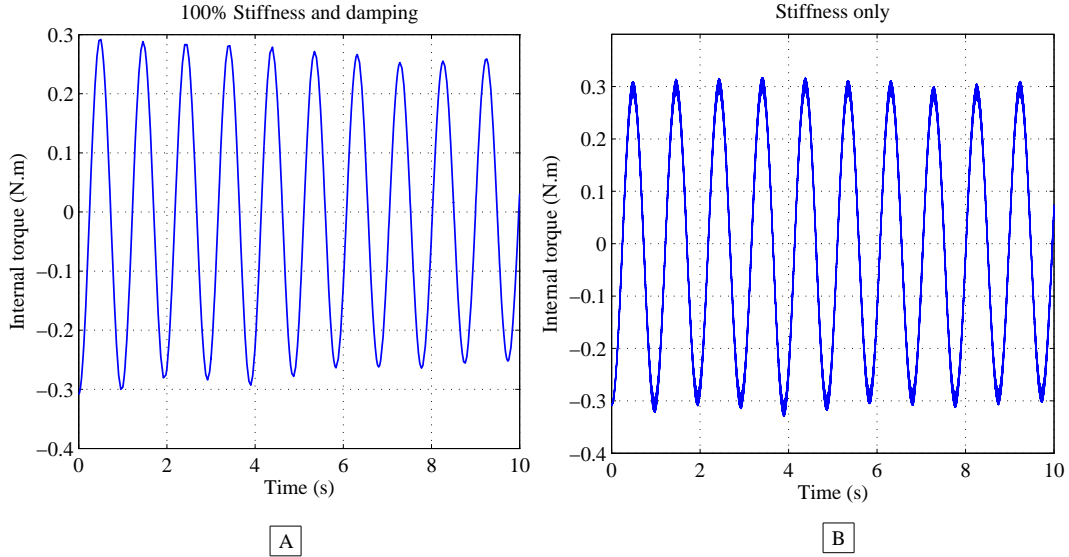
Figure 7.3: Total internal torque generated by the system when $\alpha(0) = 0.0002$ rad during internal perturbation. Figure (A) shows the response of the system in the presence of damping and 100 % stiffness parameters of muscles, tendons and ligaments. Figure (B) shows the response of the system under the stiffness only condition.

Figure 7.3 shows the response of the internal torque generated during anterior-posterior sway of the mass-spring-damper inverted pendulum model for quiet stance. Under the condition of damping with increased stiffness, Figure 7.3A recorded a maximum torque of -0.30 N.m for anterior sway and maximum internal torque of 0.30 N.m for posterior sway. In the second instance, for the stiffness only condition, Figure 7.3B shows a maximum torque of -0.33 N.m during anterior sway and 0.32 N.m for posterior sway.
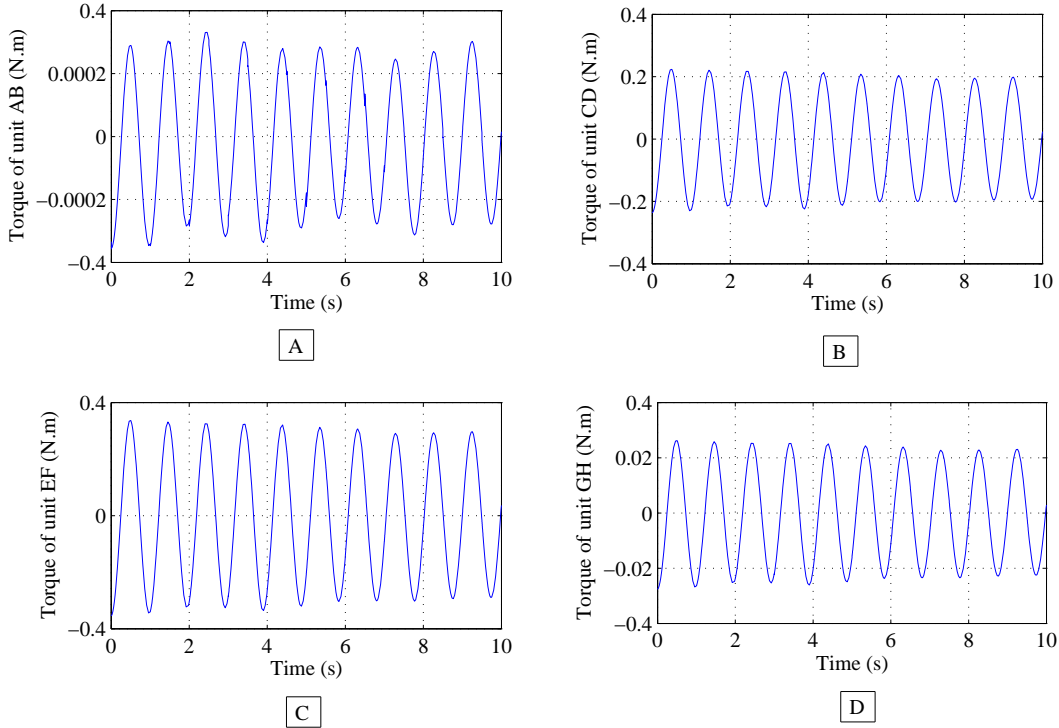
Figure 7.4: Internal torque generated at units AB, CD, EF and GH when $\alpha(0) = 0.0002$ rad during internal perturbation.

Figure 7.4 shows the internal torque response of unit AB under damping with 100% stiffness condition. Unit AB, positioned anteriorly to the shank, consists of tibialis anterior which is the dominant muscle of this unit. In Figure 7.4A, the maximum torque recorded (anterior sway) was -0.0004 N.m and the maximum torque for posterior sway was 0.0003 N.m. In Figure 7.4B, the maximum torques for anterior and posterior sway were -0.24 N.m and 0.22 N.m, respectively. In Figure 7.4C, the maximum anterior and posterior torques were recorded at -0.04 N.m and 0.04 N.m, respectively. Lastly, in Figure 7.4D the maximum anterior and posterior sway torques were -0.03 N.m and 0.03 N.m, respectively.

7.3 Discussion

When all the forces acting on the body are balanced for a set position or movement, i.e. the CoM of the body relative to its small base of support, the foot, it is deemed that postural equilibrium is attained (Horak et al., 1997). This equilibrium can be controlled either by reacting to externally applied forces such as gravity and forces generated because of environmental factors or proactive control, which regulates the position of the CoM of the whole body. Moreover, internal forces are generated during all body movements (including respiration) and ultimately act to destabilise the body (Horak et al., 1997). This thesis however is concerned with maintaining equilibrium during quiet stance without the application of external perturbations.

Quiet stance can be considered as the precursor to locomotion. The simulations conducted in this chapter demonstrated the influence of mechanical properties of muscles, tendons and ligaments during quiet stance. The model developed in this thesis is further evaluated by the results obtained through a preliminary case study described in Chapter 6. In the case of quiet stance, the intended equilibrium position was slightly anterior, $\alpha(0)$=0.0002 rad and the instability was gravity driven.

Most inverted pendulum models for quiet stance (Collins and De Luca, 1993; Flis and Peplowski, 2000; Gatev et al., 1999; Kiemel et al., 2002; Masani et al., 2003; Webber et al., 2004; Winter et al., 1998) do not report angular displacement and of anterior-posterior sway. When stiffness only condition was simulated the anterior angular displacement of the shank started to increase from the initial condition of $\alpha(0)$=0.0002 rad suggesting divergence from its precision point Figure 7.1, rendering the inverted pendulum system unstable. It has already shown in Chapter 5 that damping with 75% to 100% stiffness is better suited to simulate human bipedal quiet stance about the ankle joints. The simulation results with internal perturbation shows equivalency in results and does not destabilise the system. In the absence of damping shows that the system would oscillate away from its intial starting position and would eventually lead to a fall. However the presence of damping would suggest rigidity of the body. These conclusions drawn from this study are in accordance with the stiffness and damping study on an

inverted pendulum conducted by (Johansson et al., 1988).

Inverted pendulum models concerned with parametric estimation have earlier been modelled by Haldo (1979) and Ishida and Miyazaki (1987) where spontaneous sway was studied. There are, however, systematic statistical difficulties with analyses of spontaneous motion in closed loop control systems (Ljung, 1986; Soderstrom, 1984). These problems were overcome by developing an intrinsic inverted pendulum model in this thesis.

Considering only the ankle strategy for quiet stance, anticipatory postural adjustment was ignored because the movements are very subtle and furthermore in the absence of internal perturbation, the shank pivoted at the ankle joint connected by soft tissues (muscles, tendons and ligaments) constrained to act like a mass-spring unit (Scott Kelso and Kenneth, 1998). However, the addition of damping further brings out the viscoelastic properties of the soft tissues. The study by Asatryan and Feldman (1965) showed that variations of mass-spring account of limb localization minimises many problems confronted by theorists in movement control. One of the main reasons could be that it is intrinsically self-equilibrating; once set in motion the spring will always return to the same resting length for any particular load value. Neither an increase in initial deflection of the spring from its resting length nor temporary perturbations will prevent the achievement of equilibrium point, a property known as equifinality (von Bertalanffy, 1973).

It seems clear that when viscoelastic properties of muscles, tendons and ligaments are considered it is not the kinematic features, but the dynamic parameters of mass, stiffness and damping that take precedence for the regulation of movement. It is the specification of the dynamic parameters that determine kinematic details. Variability in these parameters will affect the equilibration process only in terms of the observed kinematics but not in terms of achievement of equilibrium position.

The figure 7.1 shows that under the mechanical condition, damping with 100 % stiffness, the shank angular displacement response is more plausible than the stiffness only condition. This is instrumental when comparing simulated (internal perturbation) gravitational torque values with experimental values calculate in Chapter 6. The model described in Chapter 3 of this thesis does not differentiate

between eyes open or eyes closed condition and it is assumed that ankle angle of the left leg and right leg were equal for anterior-posterior sway of the shank during quiet stance. The preliminary case study conducted in Chapter 6 revealed that average ankle angular displacement for 100s was α=0.0002 rad for both legs which became the initial starting point for the simulations. The simulations in this chapter revealed that the internal torque values of the system were considerably greater than the the gravitational torque which balances the shank at the equilibrium position.

Several models have proposed introducing noise as internal perturbation in order to mimic physiologically realistic conditions such as haemodynamics (Nomura et al., 2013) or a collective measure of internal perturbations (Suzuki et al., 2012; van der Kooij et al., 2005). The internal perturbation induced in the current model is much lower than those in Nomura et al. (2013); Suzuki et al. (2012); van der Kooij et al. (2005) in order to replicate plausible sway patterns during quiet stance (i.e. no exaggerated sways). The internal perturbation introduced in the current MSD model developed in this thesis further demonstrates that the damping with 100% stiffness is a more plausible mechanical condition that explains the biomechanical functionality of quiet stance. Most unperturbed quiet stance models (Kiemel et al., 2011; Masani et al., 2003; Maurer and Peterka, 2005; Van Der Kooij and De Vlugt, 2007; Vette et al., 2010) show that the involvement of the nervous system is bare minimum, hence the gravitational torque produced during anterior-posterior sway would be relatively small when compared against perturbed quiet stance. The EMG results reported in Chapter 6 also show very low muscle activity when compared with MVICs. This suggests that passive intrinsic inverted pendulum model developed in this thesis adheres to the biomechanical functionality of quiet stance at the ankle joints.

These findings suggest that the MSD inverted pendulum model serves to control joint torque rather than to control length of the muscle. This perspective meshes well with a dynamic analysis of movement at a limb segment level and suggests a characterisation of posture in terms of torque (Nashner, 1970). This torque implies two forces, compressive thrust and tension, with non-coincident lines of action so that they can act together as a "couple" (Nashner and McCollum, 1985). The tibia thrusts downward on the ankle joint and the Achilles

tendon pulls upward on the heel to develop torque across the ankle joint. The foot in turn thrusts down against the ground but there is no tension force between the foot and the ground. The ankle torque shifts the point of application of the thrust against the ground forward towards the ball of the foot. The centre of mass remains throughout in equilibrium over the support and no further correcting activity is called for, provided the forward thrust is countered by the internal torque generated by the body as shown repeatedly in the simulation results in this chapter. The hypothesis that internal torque has to be greater that the gravitational torque produced during quiet stance in order for the body to remain in upright position is in accordance with the conclusions drawn by Nashner and McCollum (1985). It is important to point out that the role played by internal torque for maintaining balance so far has been ignored in subsequent intrinsic models proposed till date.

7.3.1 Significance of AB, CD, EF and GH units in quiet stance

Tibialis anterior is the dominant muscle of unit AB and plays a functional role in maintaining balance (Day et al., 2013). However, during quiet stance, surface EMG recording revealed this muscles to be "silent" which was in accordance with Basmajian and DeLuca (1985); Borg et al. (2007); Joseph (1960). Simulations on the other hand demonstrated that the tibialis anterior did indeed generate internal torque and was less than the gravitational torque as shown in Figure 7.4. However, it is possible that surface EMG would yield a certain amount of muscle activity in tibialis anterior during quiet stance (Giulio et al., 2009). It shows that tibialis anterior muscle is does not play a major role in stablising upright posture during quiet stance.

Unit CD consists of the dominant triceps suare muscle group which consist of gastrocnemius lateralis, gastrocnemius medialis and soleus. Surface EMG measurements showed a certain amount of activity in these muscles during quiet stance as reported in Chapter 6. Simulations have showed that the internal torque generated by unit CD was the highest compared to AB, EF and GH as illustrated in Figure 7.4. This suggested that unit CD consisting of triceps surae

muscles and the Achilles tendon, played a crucial role in maintaining the equilibrium position of the shank during quiet stance (Gurfinkel et al., 1974; Loram and Lakie, 2002; Morasso and Sanguineti, 2002; Winter et al., 2001). One explanation could be that, as the person was in quiet stance, the line of gravity then lay anterior to the knee and ankle joints, therefore, the position of the CoM of the body would be in the anterior to the ankle joint. This would effectuate passive torque around the ankles, which would in turn facilitate activation of the triceps surae muscles and initiate a passive pull on the Achilles tendon, pulling the shank towards the equilibrium position initiating posterior sway. Mechanically, it would seem that the position of the shank, and in turn the centre of mass was being corrected continuously to counter the destabilising effects of the gravitational torque, hence making the shank oscillate at its equilibrium position

The remaining units EF and GH having a heavier concentration of ligaments than units AB (1 ligament) and CD (no ligaments) showed marked internal torque values as shown in Figures 7.4 and 7.4, which could be because they played more of a supporting role during anterior-posterior sway rather than being the primary controllers of plantarflexion and dorsiflexion of the ankle joint. These units play a passive role in guiding joint mobility during anterior-posterior sway contrary to ligaments originating from the extremities of the ankle joint which resist joint motion (Leardini et al., 1999a,b). The model developed in this thesis is concerned with only anterior-posterior sway, however, when the model is extended to mediolateral sway units EF and GH would be expected to produce higher torque values.

The 9-element instrinsic inverted pendulum model developed in this thesis investigates the anterior-posterior sway mechanism of unperturbed quiet stance. It was hypothesised that the human body can maintain its upright stance passively once the muscles in units AB, CD, EF and GH are activated. In order for the body to maintain its CoM at the equilibrium position the internal torque generated during anterior-posterior sway needs to be greater than the destabilising gravitational torque. The model in the current study, explored the effects of anterior-posterior sway during quiet stance by considering the intrinsic linear mechanical properties (stiffness and damping) of muscles, ligaments and tendons. This study demonstrates that the damping with 100% stiffness condition is a plausible mechanical condition that explains the biomechanics of anterior-posterior

sway during unperturbed quiet stance. The model was tested by applying an internal perturbation in the form of a Gaussian noise to replicate conditions such as respiration and haemodynamics. The intrinsic inverted pendulum developed in this thesis was able to maintain its equilibrium position passively without the need of an active control mechanism.

The current model is not without its limitations. This intrinsic model is restricted to anterior-posterior sway during quiet stance. In mass-spring-damper models, change in stiffness and damping parameters will significantly affect postural sway and hence care has to be taken while "tuning" spring and damper mechanical properties. The stiffness and damping dynamics were considered linear in this current model and there is a large difference in parametric values of muscles, tendons and ligaments in the literature. This model has considered only the ankle strategy with the assumption that the knee joints are immobilised. However, the model can be extended to take into account large sway excursions which would involve introducing a feedback control to maintain upright stance. Future model derivation would involve adding the hip strategy and the consideration of medio-lateral sways. Although, the current model does not differentiate between eyes open and eyes closed conditions during quiet stance, future work would involve introducing a sensory feedback to replicate eyes open and eyes closed conditions. A more detailed outlook on model limitations and future work is discussed in the next chapter.

Chapter 8

Conclusion, limit of the study and future work

8.1 Conclusion

Human bipedal stance, an inherently unstable system is made up of multiple flexible segments and maintains an erect posture with its CoM located high above a relatively small base of support, the ankle joint. The complexity of this system and its ability to maintain equilibrium, despite various perturbations (internal and/or external), have attracted the attention of many researchers in the field and have inspired various theories (Asatryan and Feldman, 1965; Clifford and Holder-Powell, 2010; Goswami, 1999; Imagawa et al., 2013; Kuo, 2007; Loram et al., 2007; Murnaghan et al., 2009; Nashner, 1970) that try to explain the control mechanism of bipedal quiet stance. However, the true nature of this control mechanism is still an object of discussion and controversy till date.

The model developed in this work is more biomechanically detailed than those in the existing literature (Jeka et al., 2004; Morasso and Sanguineti, 2002; Peterka, 2002; Winter et al., 1998, 2001). These previous models have only considered the effect of muscle stiffness with respect to postural balance and have attributed little or no importance to the role played by the damping nature of the muscle-tendon unit. The 2×4 9-element multiple-MSD model takes into account a variety of muscles, tendons and ligaments together with their damping co-efficients rendering

105

a more realistic approach towards the mechanical behaviour of postural balance with respect to the ankle joint. Moreover, this model can be used to estimate the amount of torque produced at various musculoskeletal groups about the ankle joint. This is useful when identifying muscle weakness groups and thus appropriate and timely biomechanical interventions could be prescribed; for strength conditioning exercises may be recommended to improve muscle performance in an aging population that is prone to falls and exhibits restricted mobility.

This study emphasises the need for detailed modelling of the ankle complex to understand postural control. In this model the connections have been made bilaterally between the shanks and feet by a number of MSD units. This would be instrumental in analysing and numerically simulating anterior-posterior sway during quiet stance, where the ankle acts as the fulcrum. The four units connect the shank (tibia and fibula) to the phalanges of the foot, and the posterior, lateral and to the medial aspects of the calcaneus. Each unit represented a group of muscles, tendons and ligaments which are represented by a 9-element MSD model. The series connection represented the muscle-tendon unit and the parallel MSD unit represented the ligaments. The anterior-posterior sway results in the geometrical change of length from the initial orientation of the four units. The Lagrange d' Alembert principle was used to derive 18 ordinary differential equations, along with 9 algebraic equations to describe the human body dynamics of anterior-posterior sway with respect to the ankle complex. The model was parameterised with respect to the length changes, mass, stiffness and damping coefficient of every identified muscles, tendons and ligaments responsible for postural control with respect to the movements about the ankle joints.

The ankle joint torque needed for the body to maintain its position at the equilibrium point during quiet stance can elicit either an active or passive response. Passive torque components can be thought as a product of the intrinsic mechanical property, i.e. stiffness and/or viscosity, produced by muscles and surrounding tissues, such as ligaments and tendons. It can be concluded that additional torque acts as an active torque, which may be generated by active muscle contraction. Since the CoM is located anterior to the ankle joint, plantar flexing torque acts perpetually to prevent the body from falling forward (Smith, 1957). However, the passive torque by itself is insufficient to ensure this required plantar

flexing torque. Therefore, an additional active torque, regulated by the central nervous system (CNS) and produced by the plantar flexors, is needed (Masani et al., 2006).

In this study, it has been shown that anterior-posterior sway during quiet stance can be modelled using intrinsic mechanical properties such stiffness and damping properties of muscles, tendons and ligaments. A novel approach has been taken by using Lagrange d' Alembert principle, to resolve that the humans acting as a classic inverted pendulum, can be balanced at its equilibrium point by internal torques produced during anterior-posterior motion. The use of a conventional control system has been avoided by assuming that the muscles are already engaged during anterior-posterior sway as the quiet stance involves an anterior tilt of the CoM, thus facilitates a passive contraction of the triceps surae muscle group.

Considering the theoretical aspect of inverted pendulum modelling, it has been observed that some models have considered non-symmetrical stiffness matrix (Rozendaal and van Soest, 2007; Thomas Edwards, 2007) which required low stiffness values of the segments and also they assumed the involvement of externally applied torques. Contrary to their assumption, the intrinsic inverted pendulum model consists of symmetrical stiffness matrix and no external active torque has been considered. This lead to the consideration of high stiffness values of muscles, tendons and ligaments which has been shown in the linear analysis in Chapter 5. The damping with 100% stiffness mechanical condition was shown to be the plausible candidate even under small internal perturbations as reported in Chapter 7.

This current model also considered the effect of friction as a dissipative function which so far no other single inverted pendulum model has taken into account. However, a study by van Soest and Rozendaal (2008) mentioned the role of friction as a possibility that could affect sway size. Based on the simulation results conducted in Chapter 5 of this thesis, it was found that friction had negligible effect on sway size on unperturbed quiet stance. Negligible effects of joint friction could be because of several reasons:-

(1) the joint is surrounded by ligaments to hold it in place reducing bone to bone contact;

(2) during quiet stance, there is not enough translation and rotation between the bone surfaces to increase frictional force;

(3) the high stiffness stiffness and damping values could perhaps mask the effect of friction in the system.

The simulations undertaken in this study reports the differences in sway size of the shank with respect to change in intrinsic muscle, tendon and ligament stiffness and damping properties. The model has taken into account specific muscles, tendons and ligaments and illustrates the effects it has on postural response based on their individual functionality, bringing about significant geometrical issues so far understudied to facilitate a more robust theoretical approach to the study of postural balance. The model demonstrates the dominant functionality of the calf muscles with respect to the mechanical aspect of postural balance during anterior-posterior sway. This model however, shows the difference between the unit CD (dominant muscle is triceps surae) and unit AB (dominant muscle tibialis anterior) by comparing their individual unit internal torque and the destabilising gravitational torque. These are quantifiable comparisons. However, other models like Jeka et al. (2004); Morasso and Sanguineti (2002); Winter et al. (1998, 2001) have only considered the effect of triceps surae muscle group based on low or negligible EMG activity of tibialis anterior. However, even though the tibialis anterior is a comparatively weaker muscle because of its smaller dimensions resulting in smaller moment arms (van Soest and Rozendaal, 2008) the stiffness of the model would be underestimated when ignoring tibialis anterior for modelling unperturbed quiet stance.

The current study puts forth a novel intrinsic model for unperturbed quiet stance with the focus on the ankle complex. This model has been tested for different mechanical conditions as mentioned in detail in Chapter 5.

Numerical simulations conducted show that damping with 100% stiffness is the more favourable mechanical condition for the human body to maintain upright posture during unperturbed quiet stance. The simulations were also performed under low frequency Gaussian noise that would mimic internal perturbation during quiet stance. These simulations showed that the sway size of the shank increased which in turn produced greater destabilising gravitational torque. However, the model was able to maintain its equilibrium position as the internal

torque generated was significantly greater than the gravitational torque induced at the ankle joint. The indirect measurements of internal torques of not only the ankle joints as a whole but also that of individual units helped to determine which muscle groups and the extent to which they were responsible for maintaining balance during unperturbed quiet stance.

A 3D model was built on the basis of the equations used in Chapter 3 using Visual 3D v5 (C-Motion, Rockville,US) where the using motion capture data for a preliminary case study. This helped in generating empirical values for bilateral ankle range of motion, gravitational torque and anterior-posterior sway size of the shank with reference to the ankle joint. The EMG data collected for triceps surae muscle group and tibialis anterior resulted in assessing which unit in the mathematical model played a dominant role in maintaining balance. This study lays the foundation for developing a 3D model based on intrinsic mechanical properties exhibited by muscles, tendons and ligaments. The model however has not been validated in this study. Model limitations and future work are discussed in the subsequent sections.

8.2 Modelling and experimental limitations of the study

The study has been limited to anterior-posterior sway during unperturbed quiet stance. The model derived is focused on the ankle strategy as during unperturbed quiet stance the sway size of the shank is quite small and the ankle strategy is enough to maintain upright posture (Alexandrov et al., 2005; Horak and Nashner, 1986; Horak et al., 1997). The stiffness and the damping parameters considered for muscles, tendons and ligaments were based on the concept of short-range stiffness (Loram et al., 2007; Rack and Westbury, 1974). However, there is apparent dearth in the current literature which required "tuning" of the mass-spring-damper parameters of the model within a physiological range determined from O'Brien et al. (2010). The model has not considered exact insertion and origin points of every muscle, tendon and ligament as they were grouped together

based on their biomechanical functionality.

The model developed in this study has not been validated, however, a preliminary case study was conducted to lay the ground work for future studies to be conducted and validate it. The experiments conducted was limited to the measurable parameters of the model. The motion capture experiment conducted could measure the gravitational torque, the ankle range of motion and the sway size of the shank relative to the ankle joints. The measurements were done bilaterally under the eyes open and eyes closed condition. However, the model developed does not differentiate between eyes open and eyes closed conditions as sensory feedback was not incorporated in the mathematical model. EMG recording were also undertaken however, they gave a measurable outcome of the percentage of muscle activity of tricpes surae and tibialis anterior and not the amount of force generated during anterior-posterior sway. However, the EMG recordings were useful in understanding that the trcipes surae muscle group generated comparatively more muscle activity than the tibialis anterior which was silent during unperturbed quiet stance. The surface EMG was able to detect clear muscle activity of only the above said muscles, however, it was difficult to detect reliable muscle activity in deep seated muscles specially during unperturbed quiet stance. The EMG and the motion capture experiments were not able to determine the stiffness and damping parameters of of individual muscles, tendons and ligaments.

Since, the experiments would include internal perturbations as a result of respiration and haemodynamics, the experimental data when compared to the mathematical model a low frequency internal perturbation was introduced. It is not possible to quantify the influence of internal perturbation on postural balance, however, based on the studies by Conforto et al. (2001); Schmid et al. (2004) a random Gaussian noise deemed fit to mimic anterior-posterior sway. The choice of noise as internal perturbation would account for the small difference in experimental and theoretical values.

8.3 Future work involving model extension and experimental validation

The model derived in this thesis lays the foundation upon which substantial studies (theoretical and experimental) on quiet stance can be undertaken to further validate the 9-element MSD model. Intrinsic postural models rely on the stiffness and damping parameters since they mimic the viscoelastic properties of muscles, tendons and ligaments. The models proposed by Jeka et al. (2004); Morasso and Sanguineti (2002); Winter et al. (1998, 2001) have not been able to clearly explain in their models the role played by the dorsiflexors and the plantarflexors during quiet stance. One of the main reasons for not having a robust postural models is because parameter values (stiffness and damping) have been understudied for unperturbed quiet stance. A study by Loram et al. (2007) classified that there are two types of stiffness, long-range stiffness which caters towards large postural sways and short-range stiffness, attributed to small postural sways. In order to obtain accuracy in stiffness and damping parameters for muscles, tendons and ligaments, it would be necessary to record *in-vivo* data during unperturbed quiet stance. It was been found that there is at least 2%-4% elongation of muscle fibres for small movements (Rack and Westbury, 1974), hence it can be expected that during quiet stance such small differences can be quantified and incorporated in intrinsic postural models.

The model can be extended to include various conditions which can be modelled in Visual 3D:-

(1) inclusion of the hip strategy;

(2) including medio-lateral sway;

(3) non-linear stiffness and damping models of muscles, tendons and ligaments.

The inclusion of the hip strategy will help in extending the understanding of postural balance during large sways, which would involve mixed strategies of ankle and hip. The large postural sways would see significant differences in the stiffness and damping parameters of muscles, tendons and ligaments. Exaggerated excursions of the sway path would then involve the CNS which would require the intrinsic inverted pendulum model to have a control system to stabilise the

system (Peterka, 2002). This modelling technique can then be applied to Visual 3D to create a 3D model to generate kinetic and kinematic data. The foundation for 3D model building has been described in detail in Chapter 6. The model can be used to determine the force generated during anterior-posterior and medio-lateral sways. This can be achieved by using the Lagrange-d'Alembert principle (Udwadia, 2000). The equations (3.10) and (3.11) will become:

$$M\ddot{q} + C\dot{q} + G(q) = \tau + F'\lambda, \tag{8.1}$$

$$f(q) = 0, \tag{8.2}$$

where vector q includes all joint variables, τ is the control torque vector, $F = \frac{\partial f(q)}{\partial q}$, and λ is the Lagrange multiplier. $F'\lambda$ represents the internal torque vector induced by the constraints.

Based on equations (8.1) and (8.2) the muscle, tendon and ligament model as shown in Figure 3.5 can be used determine the active and passive forces generated while maintaining upright stance. This would be useful when comparing perturbed and unperturbed quiet stance, exaggerated sways both in the eyes open and eyes closed conditions.

The extension of the intrinsic inverted pendulum model developed in this study and the experimental validation using motion capture synchronised with the EMG system will give further insight towards postural balance in terms of the following outcomes:-

(1) effects of non-linear stiffness and damping models on muscles, tendons and ligaments in terms of sway size;

(2) kinematic and kinetic measures during upright stance;

(3) control systems used while maintaining balance, and

(4) accuracy of active and passive forces generated at units AB, CD, EF and GH.

References

A.V. Alexandrov, A.A. Frolov, F.B. Horak, P. Carlson-Kuhta, and S. Park. Feedback equilibrium control during human standing. *Biological Cybernetics*, 93: 309–322, 2005. 72, 109

Y. Aramaki, D. Nozaki, K. Masani, T. Sato, K. Nakazawa, and H. Yano. Reciprocal angular acceleration of the ankle and hip joints during quiet standing in humans. *Experimental Brain Research*, 136:463–473, 2001. 1, 4, 9

Y. Asai, Y. Tasaka, K. Nomura, T. Nomura, M. Casadio, and P. Morasso. A model of postural control in quiet standing: robust compensation of delay-induced instability using intermittent activation of feedback control. *PLoS ONE*, 4:art. no. e6169, 2009. 93, 94

D.G. Asatryan and A.G. Feldman. Functional tuning of the nervous system with control of movement or maintenance of a steady posture: I. mechanographic analysis of the work of the joint or execution of a postural task. *Biofizika*, 10: 837–846, 1965. 100, 105

J. Babic and J. Lenarcic. In vivo determination of triceps surae muscle-tendon complex viscoelastic properties. *Eur J Appl Physiol*, 92:477–484, 2004. 45, 46, 72

A.J. Bailey and N.D. Light. Intermolecular cross-linking in fibrotic collagen. *Ciba Foundation Sympia*, 114:80–86, 1985. 43

F.A. Bandak, R.E Tannous, and T. Toridis. On the development of an osseoliga-

mentous finite element model of the human ankle joint. *International Journal of Solids and Structures*, 38:1681–1697, 2001. 47

J.V. Basmajian and C.J. DeLuca. *Muscles Alive: Their Functions Revealed By Electromyography.* Williams and Wilkins,Baltimore, MD, 1985. 102

E.V. Belaya. *Mekhanika Kompozitnykh Materialov.*, 4:737, 1979. 37

S. Bianchi and C. Martinoli. *Ultrasound of the musculoskeletal system.* Springer, 2007. 20

C. Bonifasi-Lista, S.P. Lake, M.S. Small, and J.A. Weiss. Viscoelastic properties of the human medial collateral ligament under longitudinal, transverse and shear loading. *Journal of Orthopaedic Research*, 23:67–76, 2005. 49

V. Bonnet, S. Ramdani, P. Fraisse, N. Ramdani, J. Lagarde, and G. Bardy Benoit. A structurally optimal control model for predicting and analyzing human postural coordination. *Journal of Biomechanics*, 44:2123–2128, 2011. 16

F. Borg, M. Finell, I. Hakala, and M. Herrala. Analyzing gastrocnemius emg-activity and sway data from quiet and perturbed standing. *Journal of Electromyography and Kinesiology*, 17:622–634, 2007. 91, 102

A. Bottaro, M. Casadio, Pietro G. Morasso, and V. Sanguineti. Body sway during quiet standing: Is it the residual chattering of an intermittent stabilization process? *Human Movement Science*, 24:588–615, 2005. 13

A. Bottaro, Y. Yasutake, T. Nomura, M. Casadio, and P. Morasso. Bounded stability of the quiet standing posture: an intermittent control model. *Hum. Movement Sci.*, 27:473495, 2008. 93, 94

R.A. Brand and R.D. Crowinshield. A model of lower extremity muscular anatomy. *J. Biomech*, 104:153–161, 1982. 42

A. Bryant, P. Tinley, and K. Singer. A comparison of radiographic measurements in normal,hallux valgus, and hallux limitus feet. *J Foot Ankle Surg*, 39:39–43, 2000. 38

B.D. Buch, M.S. Myerson, and S.D. Miller. Primary subtalar arthodesis for the treatment of comminuted calcaneal fractures. *Foot Ankle Int*, 17:61–70, 1996. 38

F.L. Buczek, M.J. Rainbow, K.M. Cooney, M.R. Walker, and J.O. Sanders. Implications of using hierarchical and six degree-of-freedom models for normal gait analyses. *Gait and Posture*, 31:57–63, 2010. 77

J.M. Burgers. *Mechanical Considerations model systems phenomenological theories of relaxation and viscosity.First Report on Viscosity and Plasticity,2nd edition.* Nordemann Publishing Company, Inc., New York., 1996. 41

A. Cappozzo, F. Catani, U.D. Croce, and A. Leardini. Position and orientation in space of bones during movement: anatomical frame definition and determination. *Clin Biomech (Bristol, Avon)*, 10:171–178, 1995. 77

M. Casadio, P.G. Morasso, and V. Sanguineti. Direct measurement of ankle stiffness during quiet standing: implications for control modelling and clinical application. *Gait Posture*, 21:410–424, 2005a. 8, 14

M. Casadio, G. Morasso Pietro, and V. Sanguineti. Direct measurement of ankle stiffness during quiet standing: implications for control modelling and clinical application. *Gait and Posture*, 21:410424, 2005b. 1, 2, 4, 71

A.M. Clifford and H. Holder-Powell. Postural control in healthy individuals. *Clinical Biomechanics (Bristol, Avon)*, 25:546551, 2010. 71, 105

J.J. Collins and C.J. De Luca. Open-loop and closed-loop control of posture: a random-walk analysis of center-of-pressure trajectories. *Exp Brain Res*, 95: 308318, 1993. 99

S. Conforto, M. Schmid, V. Camomilla, T. DAlessio, and A. Cappozzo. Hemodynamics as a possible internal mechanical disturbance to balance. *Gait and Posture*, 14:28–35, 2001. 93, 110

C. Coogler. Falls and imbalance. *Rehabilitation Management*, pages 53–79, 1992. 2, 3

F. Corazzaa, J.J O'Connor, A. Leardini, and V. Parenti Castelli. Ligament fibre recruitment and forces for the anterior drawer test at the human ankle joint. *Journal of Biomechanics*, 36:363–372, 2003. 44

B. Datta, R. Salleh, N. Mafulli, M. Neil, A. Butler, and W.R. Walsh. Mechanical properties of human flexor hallucis longus, peroneus brevis and tendo achilles tendons. *52nd Annual Meeting of the Orthopaedic Research Society,paper no:1889*, 1952. 45

H. David, Adam M. Butler, R. Mark Gillies, J. Bruce Warwick, and R. Walsh. William. Biomechanical and clinical evaluation of tendons and ligaments. *Orthopedic Biology and Medicine: Repair and Regeneration of Ligaments, Tendons, and Joint Capsule*, 2000. 45

J.T. Day, G.A. Lichtwark, and A.G. Cresswell. Tibialis anterior muscle fascicle dynamics adequately represent postural sway during standing balance. *Journal of Applied Physiology*, 115:117421750, 2013. 73, 102

P. de Leva. Adjustments to zatsiorsky-seluyanov's segment inertia parameters. *Journal of Biomechanics*, 29:1223–1230, 1996. 82

W.T. Dempster. *Space requirements of the seated operator: Geometrical, kinematic and mechanical aspects of the body with special reference to the limbs.* Wright-Patterson Air Force Base, US., 1955. 82

K. Devanshu and C. Markel David. The effect of posterior tibial slope on range of motion after total knee arthroplasty. *The Journal of Arthroplasty*, 21:809–813, 2006. 27, 40, 41

M. Arnold Edith and L. Delp. Scott. Fibre operating lengths of human lower limb muscles during walking. *Phil. Trans. R. Soc*, 366B:1530–1539, 2011. 45

D.R. Eyre, M.A. Paz, and P.M. Gallop. Cross-linking in collagen and elastin. *Annual Review of Biochemistry*, 53:717–748, 1984. 43

M. Ferdjallah, G.F. Harris, and J.J. Wertsch. Instantaneous postural stability characterization using time-frequency analysis. *Gait and Posture*, 10:129–134, 1999. 14

R. Fitzpatrick, D.K. Rogers, and D.I. McCloskey. Stable human standing with lower-limb muscle afferents providing the only sensory input. *Journal of Physiology-London*, 480(Pt 2):395–403, 1994. 1, 4, 9

R.C. Fitzpatrick, J.L. Taylor, and D.I. McCloskey. Ankle stiffness of standing humans in response to imperceptible perturbation: reflex and task dependent components. *Journal of Physiology*, 454:533547, 1992. 1

K. Flis and P. Peplowski. Identification of human postural sway. *Open Syst Inform Dyn*, 7:187–200, 2000. 99

G.F. Franklin, J.D. Powell, and A Emami-Naeini. *Feedback control of dynamic systems*. Pearson, sixth edition, 2010. 33

W.H. Gage, D.A. Winter, J.S. Frank, and A.L. Adkin. Kinematic and kinetic validity of the inverted pendulum model in quiet standing. *Gait and Posture*, 19:124–132, 2004. 13, 82, 90

P. Gatev, S. Thomas, T. Kepple, and M. Hallett. Feedforward ankle strategy of balance during quiet stance in adults. *Journal of Physiology-London*, 514(Pt 3):915–928, 1999. 1, 3, 13, 71, 91, 99

A. Gentili, S. Masih, L. Yao, and L.L. Seeger. Pictorial review: foot axes and angles. *Br J Radiol*, 69:968–974, 1996. 27, 38, 39

I.D. Giulio, C.N. Maganaris, V. Baltzopoulos, and I.D. Loram. The proprioceptive and agonist roles of gastrocnemius, soleus and tibialis anterior muscles in maintaining human upright posture. *J. Physiol.*, 587:2399–2416, 2009. 91, 102

P. Golano, J. Vega, Peter A. J. de Leeuw, F Malagelada, M.M. Cristina, Gotzens, and C.Niek van Dijk. Anatomy of ankle ligaments: a pictorial essay. *Knee Surg Sports Traumatol Arthrosc*, 18:557–569, 2010. 22

A. Goswami. An optimal control model for analyzing human postural balance. *Postural Stability of Biped Robots and the Foot-Rotation Indicator (FRI) Point.*, 18:523–533, 1999. 105

S. Grillner. The role of muscle stiffness in meeting the changing postural and locomotor requirements for force development by the ankle extensors. *Acta Physiologica Scandinavica*, 86:92–108, 1972. 14

V.S. Gurfinkel, M.I. Lipshits, and K.Y. Popov. Is the stretch reflex the main mechanism in the system of regulation of the vertical posture of man? *Biophysics*, 19:761–766, 1974. 71, 103

Ostlund Haldo. *A study of aim and strategy of stability control in quasistationary standing.* 1979. 100

J.H. Hicks. The mechanics of the foot.i. the joints. *J Anat*, 87:345–357, 1953. 71

J.H. Hicks. The foot as a support. *Acta Anat (Basel)*, 25:34–45, 1955. 71

F.B. Horak and J.M. Macpherson. *Postural orientation and equilibrium In Handbook of Physiology, section 12, Exercise: Regulation and Integration of Multiple Systems.* Oxford University Press, Oxford, 1996. 8, 14, 91

F.B. Horak and L.M. Nashner. Central programming of postural movements: Adaptation to altered support-surface configurations. *J Neurophysiol*, 55:1369–1381, 1986. 4, 72, 109

F.B Horak, M.S. Henry, and A. Shumway-Cook. Postural perturbations: New insights for treatment of balance disorders. *Physical Therapy*, 77:517–533, 1997. 99, 109

M.G. Hoy, F.E. Zajac, and M.E. Gordon. A musculoskeletal model of the human lower extremity: the effect of muscle,tendon,and moment arm on the moment-angle relationship of musculotendon actuators at the hip, knee and ankle. *Journal of Biomechanics*, 23:157–169, 1990. 47, 72

C.L. Hubley-Kozey, K.J. Deluzio, S.C. Landry, J.S. McNutt, and W.D. Stanish. Neuromuscular alterations during walking in persons with moderate knee osteoarthritis. *J Electromyogr Kinesiol*, 16:365–378, 2006. 80

L.R. Humphrey and H. Hemami. A computational human model for exploring the role of the feet in balance. *Journal of Biomechanics*, 43:3199–3206, 2010. 1, 2, 4, 8, 17, 18

H. Imagawa, S. Hagio, and M. Kouzaki. Synergistic co-activation in multi-directional postural control in humans. *Journal of Biomechanics*, 23:430–437, 2013. 18, 105

A. Ishida and S. Miyazaki. Maximum likelihood identification of a posture control system. *IEEE Trans. Biomed. Eng.*, 34:1–5, 1987. 100

L. Thomas James, W. Kunkel Mark, Robert Lopez, and Derrick Sparks. Radiographic values of the adult foot in a standardized population. *The Journal of Foot and Ankle Surgery*, 45:3–12, 2006. 27, 40

J. Jeka, T. Kiemel, R. Creath, F. Horak, and R. Peterka. Controlling human upright posture: velocity information is more accurate than position or acceleration. *J Neurophysiol*, 92:2368–2379, 2004. 13, 71, 105, 108, 111

R. Johansson, M. Magnusson, and M. Akesson. Identification of human postural dynamics. *IEEE Transcations on Biomedical Engineering*, 35:858–869, 1988. 72, 100

J. Joseph. *Man's posture:Electromygraphic studies.* Charles C. Thomas, Springfield,Ill, 1960. 91, 102

J. Joseph and A. Nightingale. Electromyography of muscles of posture: leg muscles in males. *J Physiol.*, 117:484–491, 1952. 91

L. Jozsa and P. Kannus. Human tendons: anatomy, physiology,and pathology. *Human Kinetics*, pages 16–64, 1997. 43

D. Karasick and K.L. Wapner. Hallux valgus deformity:preoperative radiologic assessment. *American Journal of Radiology*, 155:119–123, 1990. 39

A. Karlsson and T. Persson. The ankle strategy for postural control: A comparison between a model-based and a marker based method. *Computer Methods and Programs in Biomedicine*, 52:165–173, 1997. 1, 4, 8, 10, 11, 13

E. Kellis. Quantification of quadriceps and hamstring antagonist activity. *Sports Medicine*, 25:37–62, 1998. 43

R.F. Ker, M.B. Bennett, S.R. Bibby, R.C. Kester, and R.M. Alexander. The spring in the arch of the human foot. *Nature*, 325:147–149, 1987. 71

T. Kiemel, K. Oie, and J.J. Jeka. Multisensory fusion and the stochastic structure of postural sway. *Biol Cybernet*, 87:262–267, 2002. 99

T. Kiemel, Y. Zhang, and J. Jeka. Identification of neural feedback for upright stance in humans: stabilization rather than sway minimization. *J. Neurosci.*, 31:15144–15153, 2011. 101

T. Kimura and M. Kouzaki. Electrical noise to a knee joint stabilizes quiet bipedal stance. *Gait and Posture*, 37:634–636, 2013. 92

H.F.J.M. Klein, M.D.Horsman, F.C.T. Koopman, and H.E.J. Veeger van der Helm, L. Poliacu Prose. Morphological muscle and joint parameters for musculoskeletal modelling of the lower extremity. *Clinical Biomechanics*, 22:239–247, 2007. 42, 45

D.L. Korvick, J.F. Cummings, E.S. Grood, J.P. Holden, S.M. Feder, and D.L Butler. The use of an implantable force transducer to measure patellar tendon forces in goats. *Journal of biomechanics*, 29:557–561, 1996. 43

K. Kubo, H. Kanehisa, and T. Fukunaga. Effects of resistance and stretching training programmes on the viscoelastic properties of human tendon structures in vivo. *Journal of Physiology*, 538:219–226, 2002. 45

A.D. Kuo. An optimal control model for analyzing human postural balance. *IEEE Transactions on Biomedical Engineering.*, 42:87–101, 2007. 105

J.J. Kutch, A.D. Kuo, and W.Z. Rymer. Extraction of individual muscle mechanical action from endpoint force. *J Neurophysiol*, 103:3535–3546, 2010. 18

M. Lakie, N. Caplan, and I.D. Loram. Human balancing of an inverted pendulum with a compliant linkage: neural control by anticipatory intermittent bias. *J Physiol*, 551:357–370, 2003. 14, 72

G. Laporta, T. Melillo, and D. Olinsky. X-ray evaluation of hallux abducto valgus deformity. *J. Am.Podiatr. Assoc*, 64:544–566, 1974. 39

M.L. Latash, S.S. Ferreira, S.A. Wieczorek, and M. Duarte. Movement sway: changes in postural sway during voluntary shifts of the center of pressure. *Exp Brain Res*, 150:314–324, 2003. 3, 4

A. Leardini, J.J. O'Connor, F. Catani, and S. Giannini. Kinematics of the human ankle complex in passive flexion; a single degree of freedom system. *Journal of Biomechanics*, 32:111–118, 1999a. 43, 103

A. Leardini, J.J. O'Connor, F. Catani, and S. Giannini. A geometric model of the human ankle joint. *Journal of Biomechanics*, 32:585–591, 1999b. 43, 103

G.A. Lichtwark and A.M. Wilson. In vivo mechanical properties of the human achilles tendon during one-legged hopping. *The Journal of Experimental Biology*, 208:4715–4725, 2005. 45, 46, 72

F.A.Higgs Lintz, M. Millett, T. Barton, M. Raghuvanshi, M.A Adams, and Winson.I.J. The role of plantaris longus in achilles tendinopathy: A biomechanical study. *Foot and Ankle Surgery*, 17:252–255, 2011. 45, 47, 72

L. Ljung. *System Identijcation-Theory for the User. Ed:Englewood Cliffs*. Prentice-Hall, NJ, 1986. 100

I.D. Loram and M. Lakie. Direct measurement of human ankle stiffness during quiet standing: the intrinsic mechanical stiffness is insufficient for stability. *J Physiol*, 545:1041–1053, 2002. 2, 8, 13, 14, 103

I.D. Loram, C.N. Maganaris, and M. Lakie. Human postural sway results from frequent, ballistic bias impulses by soleus and gastrocnemius. *J Physiol*, 564: 295–311, 2005. 2, 4, 13, 14, 57

I.D. Loram, C.N. Maganaris, and M. Lakie. The passive, human calf muscles in relation to standing: the non-linear decrease from short range to long range stiffness. *Journal of Physiology*, 584:661675, 2007. 73, 105, 109, 111

C.N. Maganaris. Tensile properties of in vivo human tendinous tissue. *Journal of Biomechanics*, 35:1019–1027, 2002. 43

C.N. Maganaris and J.P. Paul. In vivo human tendon mechanical properties. *Journal of Physiology*, 521:307–313, 1999. 43

P. Malaviya, D.L. Butler, D.L. Korvick, and F.S. Proch. In vivo tendon forces correlate with activity level and remain bounded:evidence in a rabbit flexor tendon model. *Journal of biomechanics*, 31:1043–1049, 1998. 43

R.A. Mann. The great toe. *Orthop. Clin.*, 20:519–533, 1989. 39

K Masani, M.R. Popovic, K. Nakazawa, M. Kouzaki, and D. Nozaki. Importance of body sway velocity information in controlling ankle extensor activities during quiet stance. *Journal of Neurophysiology*, 90:3774–3782, 2003. 90, 91, 99, 101

K. Masani, A.H. Vette, and M.R. Popovic. Controlling balance during quiet standing: Proportional and derivative controller generates preceding motor command to body sway position observed in experiments. *Gait and Posture*, 23:164–172, 2006. 107

J. Massion. Postural control systems in developmental perspective. *Neuroscience and Biobehavioral Reviews*, 22:465–478, 1998. 72

C. Maurer and R. Peterka. A new interpretation of spontaneous sway measures based on a simple model of human postural control. *J. Neurophysiol.*, 93: 189–200, 2005. 101

John B. Medley. *The lubrication of normal human ankle joints.* PhD thesis, Department of Mechanical Engineering, The University of Leeds, 1981. 61, 62

C. Mkandawire, R. Ledoux William, J. Sangeorzan Bruce, and P.Ching. Randal. Foot and ankle ligament morphometry. *Journal of Rehabilitation Research and Development*, 42:809–820, 2005. 47

Bruce C. Moore. Principal component analysis in linear systems:controllability, observability and, model reduction. *IEEE Transactions On Automatic Control*, AC-26:17–31, 1981. 36, 66, 71

P. Morasso, L. Baratto, R. Capra, and G Spada. *Preventing the risk of falling in elderly people. In: Improving the quality of life for the European citizen-Technology for Inclusive Design and Equality.* IOS Press: Amsterdam, 1998. 3

P.G. Morasso and V. Sanguineti. Ankle muscle stiffness alone cannot stabilize balance during quiet standing. *J Neurophysiol*, 88:2157–2162, 2002. 8, 13, 14, 15, 71, 103, 105, 108, 111

P.G. Morasso, L. Baratto, R. Capra, and G. Spada. Internal models in the control of posture. *Neural Networks*, 12:1173–1180, 1999a. 2, 3, 15

P.G. Morasso, G. Spada, and R. Capra. Computing the com from the cop in postural sway movements. *Human Movement Science*, 18:759–767, 1999b. 8, 10, 11

C.D. Murnaghan, B. Elston, D.C. Mackey, and S.N. Robinovitch. Modeling of postural stability borders during heeltoe rocking. *Gait and Posture*, 30:161–167, 2009. 105

K. Nagai, M. Yamada, K. Uemura, Y. Yamada, N. Ichihashi, and T. Tsuboyama. Differences in muscle coactivation during postural control between healthy older and young adults. *Archives of Gerontology and Geriatrics*, 53:338–343, 2011. 91

L. Nashner and G. McCollum. The organization of postural movements:a formal basis and experimental synthesis. *Behavioral and Brain Sciences*, 26:135172, 1985. 1, 101, 102

L.M. Nashner. *Sensory feedback in human posture control.* 1970. 1, 4, 101, 105

T. Nomura, S. Oshikawa, Y. Suzuki, K. Kiyono, and P. Morasso. Modeling human postural sway using an intermittent control and hemodynamic perturbations. *Math Biosci.*, 245:86–95, 2013. 93, 101

T.D. O'Brien, N.D. Reeves, V. Baltzopoulos, D.A. Jones, and C.N. Maganaris. Mechanical properties of the patellar tendon in adults and children. *Journal of Biomechanics*, 43:1190–1195, 2010. 72, 109

J.J. O'Connor, F. Catani, S. Martelli, and S. Giannini. Fibre recruitment and articular contact at the ankle by an accurate 3d measurement system. *Journal of Biomechanics*, 31:10, 1998. 43

J.G. Oldroyd. On the formulation of rheological equations of state. *Annalon der Physik*, A:523–591, 1950. 41

V.P. Panzer, S. Bandinelli, and M. Hallett. Biomechanical assessment of quiet standing and changes associated with aging. *Arch Phys Med Rehabil*, 76:151–157, 1995. 75, 91

J.P. Paul. Tensile properties of the in vivo human gastrocnemius tendon. *Journal of Biomechanics*, 35:1639–1646, 2002. 43

B.de Freitas Paulo, M.S.F. Freitas Sandra, Marcos Duarte, L. Latash Mark, and M. Zatsiorsky Vladimir. Effects of joint immobilization on standing balance. *Human Movement Science*, 28:515–528, 2009. 9

A.W. 4th Pearsall, J.M. Hollis, and Scheer Z. Russell, G.V. Jr. A biomechanical comparison of three lower extremity tendons for ligamentous reconstruction about the knee. *The Journal of Arthroscopic and Related Surgery*, 19:1091–1096, 2003. 45, 72

R.J. Peterka. Sensorimotor integration in human postural control. *J Neurophysiol*, 88:1097–1118, 2002. 8, 13, 105, 112

M.R. Pierrynowski. *Analytic representation of muscle line of action and geometry.* Routledge, 1995. 23

G. Morasso Pietro and V. Schieppati. Can muscle stiffness alone stabilize upright standing? *J Neurophysiol*, 82:1622–1626, 1999. 13, 15, 90

T.E. Prieto, J.B. Myklebust, R.G. Hoffmann, E.G. Lovett, and B.M. Myklebust. Measures of postural steadiness: differences between healthy young and elderly adults. *IEEE Trans Biomed Eng.*, 43:956–966, 1996. 75

X. Qua, A. Nussbauma Maury, and L. Madigan Michael. A balance control model of quiet upright stance based on an optimal control strategy. *Journal of Biomechanics*, 40:35903597, 2007. 8, 10, 11

P.M. Rack and D.R. Westbury. The short range stiffness of active mammalian muscle and its effect on mechanical properties. *J Physiol*, 240:331350, 1974. 109, 111

A. Rainoldi, G. Melchiorri, and I. Caruso. A method for positioning electrodes during surface emg recordings in lower limb muscles. *Journal of Neuroscience Methods*, 134:37–43, 2004. 78, 79

K.R. Rajagopal. A note on a reappraisal and generalization of the kelvinvoigt model. *Mechanics Research Communications*, 36:232–235, 2009. 41

S. Rammelt, R. Grass, T. Zawadski, A. Biewener, and H. Zwipp. Foot function after subtalar distraction bone-block arthrodesis. a prospective study. *J Bone Joint Surg Br*, 86:659–668, 2004. 38

Rasch and Burke. *Movements of the ankle and foot.In:Kinesiology and Applied Anatomy.* Henry Kimpton, 1965. 49

F. LaPrade Robert, S. Bollom Timothy, A. Wentorf Fred, J. Wills Nicholas, and Keith Meister. Mechanical properties of the posterolateral structures of the knee. *The American Journal of Sports Medicine*, 33:1386–1391, 2005. 45, 46, 72

L.A. Rozendaal and A.J. van Soest. *Multi-segment stance can be stable with zero local ankle stiffness.* Proceedings of XXIst ISB Conference, Taipei, 2007. 107

C.F. Runge, C.L. Shupert, F.B. Horak, and F.E. Zajac. Ankle and hip postural strategies defined by joint torques. *Gait and Posture*, 10:161–170, 1999. 92

D.J. Rutherford, C.L. Hubley-Kozey, and W.D. Stanish. Maximal voluntary isometric contraction exercises: a methodological investigation in moderate knee osteoarthritis. *Journal of Electromyography and Kinesiology*, 21:154–160, 2011. 80

M. Saffer, T. Kiemel, and J. Jeka. Coherence analysis of muscle activity during quiet stance. *Exp Brain Res*, 185:215–226, 2008. 91

R. Ward Samuel, Carolyn Laura H. Smallwood, and L. Lieber. Richard. Are current measurements of lower extremity muscle architecture accurate? *Clin Orthop Relat Res*, 467:1074–1082, 2009. 45

S.K. Sarrafian. Biomechanics of the subtalar joint complex. *Clin Orthop Relat Res*, 290:17–26, 1993. 26

T. Schepers, A.Z. Ginai, P.G.H. Mulder, and P. Patka. Radiographic evaluation of calcaneal fractures: to measure or not to measure. *Skeletal Radio*, 36:847–852, 2007. 27, 38

M. Schmid, S. Conforto, D. Bibbo, and T. DAlessio. Respiration and postural sway: detection of phase synchronizations and interactions. *Hum. Movement Sci.*, 23:105–119, 2004. 93, 110

J.A. Scott Kelso and G.H. Kenneth. *Evidence for mass-spring model of human neuromuscular control. In: Psychology of Motor Behaviour and Sport.* New York: Plenum, 1981. 91

J.A. Scott Kelso and G.H. Kenneth. *Evidence for mass-spring model of human neuromuscular control. In: Psychology of Motor Behaviour and Sport.* Human Kinetics,Champaign,IL, 1998. 100

S. Siegler, J. Block, and D. Schneck Carson. The mechanical characteristics of the collateral ligaments of the human ankle joint. *Foot and Ankle*, 8:234–242, 1998. 47

J.W. Smith. The forces operating at the human ankle joint during standing. *Journal of Anatomy*, 91:545–564, 1957. 4, 106

T. Soderstrom. *Lecture notes in identification, automatatic. Control systems analysis group.* 1984. 100

C.W. Spoor, J.L. Van Leeuwen, W.J. Van Der Meulen, and A. Huson. Active force-length relationship of human lower-leg muscles estimated from morphological data:a comparison of geometric muscle models. *Eur. J. Morphol*, 29: 137–160, 1991. 42

Y. Suzuki, T. Nomura, Casadio.M, and P. Morasso. Intermittent control with ankle,hip,and mixed strategies during quiet standing: A theoretical proposal based on a double inverted pendulum model. *Journal of Theoretical Biology*, 310:55–79, 2012. 16, 93, 101

L. Haut Donahue Tammy, M. Howell Stephen, L. Hull Maury, and Colin Gregersen. A biomechanical evaluation of anterior and posterior tibialis tendons as suitable single-loop anterior cruciate ligament grafts. *The Journal of Arthroscopic and Related Surgery*, 18:589–597, 2002. 45, 72

W. Thomas Edwards. Effect of joint stiffness on standing stability. *Gait and Posture*, 25:432–439, 2007. 1, 2, 16, 107

J.I Thompson and J.T. Czernuszka. The effect of two types of cross-linking on some mechanical properties of collagen. *Biomedical Material Engineering*, 5: 37–48, 1995. 43

W. Thomson. On the elasticity and viscosity of metals. *Proc. Roy. Soc. London*, A:289–297, 1865. 41

F.E. Udwadia. Fundamental principles of lagrangian dynamics: Mechanical systems with non-ideal, holonomic, and nonholonomic constraints. *Journal of Mathematical Analysis and Applications*, 251:341–355, 2000. 19, 28, 30, 112

H. Van Der Kooij and E. De Vlugt. Postural responses evoked by platform perturbations are dominated by continuous feedback. *J. Neurophysiol.*, 98: 730–743, 2007. 101

H. van der Kooij, E. van Asseldonk, and F.C.T. van der Helm. Comparison of different methods to identify and quantify balance control. *J Neurosci Methods*, 145:175–203, 2005. 14, 101

A.J. van Soest and L.A. Rozendaal. The inverted pendulum model of bipedal standing cannot be stabilized through direct feedback of force and contractile element length and velocity at realistic series elastic element stiffness. *Biol Cybern*, 99:29–41, 2008. 14, 72, 107, 108

A.J. van Soest, W.P. Haenen, and L.A. Rozendaal. Stability of bipedal stance: the contribution of cocontraction and spindle feedback. *Biol Cybern*, 88:293–301, 2003. 14

R. Vanderwilde, L.T. Staheli, D.E. Chew, and V. Malagon. Measurements on radiographs of the foot in normal infants and children. *American Journal of Bone and Joint Surgery*, 70:407–415, 1988. 25, 27, 38, 39

G.V. Vasyukov. *A study of the mechanical properties of human skeletal muscles; Authors Abstract of Candidates Dissertation, Moscow.* PhD thesis, Mechanical Engineering, 1967. 37

A. Vette, K. Masani, K. Nakazawa, and M. Popovic. Neuralmechanical feedback control scheme generates physiological ankle torque fluctuation during quiet stance. *IEEE Trans. Neural Syst. Rehabil. Eng.*, 18:8695, 2010. 90, 101

W. Voigt. Ieber innere reibung fester korper, insbesondere der metalle. *Annalon der Physik*, 283:671–693, 1892. 41

von Bertalanffy. *General Systems Theory.* Penguin Press Books, London, 1973. 100

J.M. Wakeling, A.M. Liphardt, and B.M. Nigg. Muscle activity reduces soft-tissue resonance at heel-strike during walking. *Journal of Biomechanics*, 36: 1761–1769, 2003. 45, 49

J.H. Wang. Mechanobiology of tendon. *Journal of Biomechanics*, 39:1563–1582, 2006. 43

J.H. Wang, F. Jia, G. Yang, S. Yang, B.H. Campbell, D. Stone, and S.L. Woo. Cyclic mechanical stretching of human tendon fibroblasts increases the production of prostaglandin e2 and levels of cyclooxygenase expression: a novel in vitro model study. *Connective Tissue Research*, 44:128–133, 1998. 44

A. Webber, N. Virji-Babul, R. Edwards, and M. Lesperance. Stiffness and postural stability in adults with down syndrome. *Exp Brain Res*, 155:450–458, 2004. 99

E. Weber. U ber die langenverhaltnisse der fleischfasern der muskeln im algemeinen.berichte u. d. verh. d. konigl. sachs. ges. d. wiss. *Math.-Phys*, pages 5–86, 1851. 42

F. Wei, C. Hunley Stanley, W. Powell John, and C. Haut. Roger. Development and validation of a computational model to study the effect of foot constraint on ankle injury due to external rotation. *Annals of Biomedical Engineering*, 39:756–765, 2011. 47

T.L. Wickiewicz, R.R. Roy, P.L. Powell, and V.R Edgerton. Muscle architecture of the human lower limb. *Clin. Orthop*, pages 75–83, 1983. 42

D.A. Winter. *Biomechanics and Motor Control of Human Movement.* Toronto:Wiley, 1990. 90

D.A. Winter, F. Prince, J.S. Frank, C. Powell, and K.F. Zabjek. Unified theory regarding a/p and m/l balance in quiet stance. *Journal of Neurophysiology*, 75: 2334–2343, 1996. 1, 4, 13, 90

D.A. Winter, A.E. Patla, F. Prince, M. Ishac, and K. Gielo-Perczak. Stiffness control of balance in quiet standing. *J Neurophysiol*, 80:1211–1221, 1998. 8, 13, 14, 16, 72, 99, 105, 108, 111

D.A. Winter, A.E. Patla, S. Rietdyk, and M.G. Ishac. Ankle muscle stiffness in the control of balance during quiet standing. *J Neurophysiol*, 85:2630–2633, 2001. 8, 13, 14, 15, 71, 103, 105, 108, 111

W.G. Wright, Y.P. Ivanenko, and V.S. Gurfinkel. Foot anatomy specialization for postural sensation and control. *Journal of Neurophysiology*, 107:1513–1521, 2012. 71

A.S. Zilbergleit, I.N. Zlatina, V.S. Sinyakov, and M.I Khaikova. A method of measuring the modulus of elasticity of human muscle tissue. *ByulletenEksperimentalnoi Biologii Meditsiny*, 96:101–105, 1984. 37

Appendix A: Coefficient matrices in (3.10) and (3.11)

From the definition of p, direct calculations yield

$$
\frac{\partial p}{\partial q} =
\begin{bmatrix}
1 & 0 & 0 & 0 \\
0 & E & 0 & 0 \\
0 & 0 & 0 & E \\
1 & 0 & -1 & 0 \\
0 & \bar{E} & 0 & -\bar{E} \\
0 & 0 & -e & \tilde{E}
\end{bmatrix},
$$

$$
\left(\frac{\partial p}{\partial q} \right)^{-1} =
\begin{bmatrix}
1 & 0 & 0 & 0 & 0 & 0 \\
\bar{E}'\bar{D}e & E' & 0 & -\bar{E}'\bar{D}e & \bar{E}' & \bar{E}'\bar{D} \\
1 & 0 & 0 & -1 & 0 & 0 \\
\bar{E}'\bar{D}e & 0 & E' & -\bar{E}'\bar{D}e & 0 & \bar{E}'\bar{D}
\end{bmatrix},
$$

where

$$
\begin{aligned}
E &= \operatorname{diag}\left(e_1, e_1, e_1, e_1\right), \quad e_1 = \begin{bmatrix} 1 & 0 \end{bmatrix}, \\
\bar{E} &= \operatorname{diag}\left(\bar{e}_1, \bar{e}_1, \bar{e}_1, \bar{e}_1\right), \quad \bar{e}_1 = \begin{bmatrix} 0 & 1 \end{bmatrix}, \\
\tilde{E} &= D\bar{E}, \quad \bar{D} = D^{-1}, \quad D = 2\operatorname{diag}\left(\bar{y}_{r,1}, \bar{y}_{r,2}, \bar{y}_{r,3}, \bar{y}_{r,4}\right), \\
e &= 2 \begin{bmatrix} d_1 r_1 s_1 & d_2 r_2 s_2 & d_3 r_3 s_3 & d_4 r_4 s_4 \end{bmatrix}'
\end{aligned}
$$

with $\bar{y}_{r,i} = y_{r,i} + y^0_{r,i}$ for $i = 1, 2, 3, 4$, $s_1 = \sin(\alpha_r - \alpha_1)$ and $s_i = \sin(\alpha_r + \alpha_i)$ for $i = 2, 3, 4$. It is useful to note that $EE' = \bar{E}\bar{E}' = I$, $E\bar{E}' = 0$ and $E'E + \bar{E}'\bar{E} = I$.

Using the notation of block matrices and noting that Q_1 contains the first three block columns of $\left(\frac{\partial p}{\partial q}\right)^{-1}$ and that $EM_0\bar{E}' = 0$, direct calculations give $M_1 = \mathrm{diag}(M_{11}, M_{22}, M_{33})$ with

$$M_{11} = 2(\bar{I} + e'\bar{D}'\bar{E}M_0\bar{E}'\bar{D}e)$$

$$M_{22} = EM_0E'$$

Matrix C_1 is given by

$$C_1 = \begin{bmatrix} C_{11} & C'_{12} & C'_{12} \\ C_{12} & C_{22} & 0 \\ C_{12} & 0 & C_{22} \end{bmatrix} + \begin{bmatrix} \bar{C}_{11} & 0 & 0 \\ \bar{C}_{12} & 0 & 0 \\ \bar{C}_{12} & 0 & 0 \end{bmatrix}$$

with

$$C_{11} = 2e'\bar{D}'\bar{E}C_0\bar{E}'\bar{D}e = 2\sum_{i=1}^{4} t_i^2(c_{b,i} + c_{c,i}), \qquad t_i = \frac{d_i r_i s_i}{\bar{y}_{r,i}},$$

$$C_{12} = EC_0\bar{E}'\bar{D}e = \begin{bmatrix} t_1 c_{b,1} & -t_2 c_{b,2} & -t_3 c_{b,3} & -t_4 c_{b,4} \end{bmatrix}',$$

$$C_{22} = EC_0E' = \mathrm{diag}\left(c_{a,1} + c_{b,1}, \cdots, c_{a,4} + c_{b,4}\right),$$

and

$$\bar{C}_{11} = 2e'\bar{D}'\bar{E}M_0\bar{E}'\bar{D}\dot{e}, \qquad \bar{C}_{12} = EM_0\bar{E}\bar{D}\dot{e}.$$

Vector G_1 is given by $G_1 = \begin{bmatrix} g_1 & g_{1,l} & g_{1,r} \end{bmatrix}'$ with

$$
\begin{aligned}
g_1 &= e'\bar{D}'\bar{E}K_0(q_l + q_r) - \bar{g}(\sin\alpha_l + \sin\alpha_r) \\
&= \sum_{i=1}^{4} \frac{d_i r_i s_i}{\bar{y}_{r,i}}\left[(k_{b,i} + k_{c,i})(y_{l,i} + y_{r,i}) - k_{b,i}(x_{l,i} + x_{r,i})\right] - 2\bar{g}\sin\alpha,
\end{aligned}
$$

where $\alpha = \alpha_l = \alpha_r$, and

$$
\begin{aligned}
g_{1,l} &= EK_0 q_l = \mathrm{diag}(e_1 K_1, e_1 K_2, e_1 K_3, e_1 K_4) q_l = \begin{bmatrix} g_{l1} & g_{l2} & g_{l3} & g_{l4} \end{bmatrix}', \\
g_{1,r} &= EK_0 q_r = \begin{bmatrix} g_{r1} & g_{r2} & g_{r3} & g_{r4} \end{bmatrix}'
\end{aligned}
$$

with $g_{vi} = (k_{a,i} + k_{b,i}) x_{v,i} - k_{b,i} y_{v,i}$ for $v = l, r$ and $i = 1, 2, 3, 4$.

Appendix B: Inverse mapping of $q = p^{-1}(p)$

Recall that $p = \begin{bmatrix} p_1 \\ p_2 \end{bmatrix}$ with $p_2 = 0$, and denote $p_1 = \begin{bmatrix} p_{1,1} & \cdots & p_{1,9} \end{bmatrix}'$. Direct calculations give rise to

$$\alpha_l = \alpha_r = p_{1,1}\,, \qquad x_{l,i} = p_{1,1+i}\,, \quad x_{r,i} = p_{1,5+i}$$

and

$$y_{r,1} = \sqrt{d_1^2 + r_1^2 - 2d_1 r_1 \cos(\alpha - \alpha_1)} - y_{r,1}^0\,, \qquad y_{l,1} = y_{r,1} + y_{r,1}^0 - y_{l,1}^0$$

$$y_{r,i} = \sqrt{d_i^2 + r_i^2 - 2d_i r_i \cos(\alpha + \alpha_i)} - y_{r,i}^0\,, \qquad y_{l,i} = y_{r,i} + y_{r,i}^0 - y_{l,i}^0$$

for $i = 2, 3, 4$.

Appendix C: Coefficients of linearised model

Linearisation of a nonlinear function $f(x)$ about x_0 means to express $f(x) = f(x_0) + \frac{df}{dx}|_{x=x_0}(x - x_0)$ as an approximation. Applying this essential idea to the q_1-equation (3.15) implies linearisation of each of the three terms around $p_1 = 0$ and $\dot{p}_1 = 0$.

Linearisation of $M_1(p_1)\ddot{p}_1$ around $p_1 = 0$ gives $\bar{M}_1\ddot{p}_1$ with $\bar{M}_1 = Q_1'(0)MQ_1(0)$. Around $p_1 = 0$ and $\dot{p}_1 = 0$, linearisation of $C_1(p_1, \dot{p}_1)\dot{p}_1$ generates $\bar{C}_1\dot{p}_1$ with $\bar{C}_1 = Q_1'(0)CQ_1(0)$. Since $G_1 = Q_1'(p_1)G(p_1)$ and $G(0) = 0$, linearisation of G_1 around $p_1 = 0$ gives $Q_1'(0)\tilde{G}(p_1)$, where $\tilde{G}(p_1)$ is the linearisation of $G(p_1)$ around $p_1 = 0$. This leads to linearisation of G_1 as $\bar{G}_1 p_1$ with

$$\bar{G}_1 = Q_1'(0)\begin{bmatrix} \tilde{g} \\ K_0\tilde{Q} \\ \tilde{g} \\ K_0\tilde{Q} \end{bmatrix}, \quad \tilde{g} = \begin{bmatrix} \bar{g} & 0 & \cdots & 0 \end{bmatrix} \tag{3}$$

and

$$\tilde{Q} = \begin{bmatrix} 0 & 1 & 0 & 0 & 0 & 0 & 0 & 0 & 0 \\ \frac{\bar{r}_1}{y_{l,1}^0} & 0 & 0 & 0 & 0 & 0 & 0 & 0 & 0 \\ 0 & 0 & 1 & 0 & 0 & 0 & 0 & 0 & 0 \\ -\frac{\bar{r}_2}{y_{l,2}^0} & 0 & 0 & 0 & 0 & 0 & 0 & 0 & 0 \\ 0 & 0 & 0 & 1 & 0 & 0 & 0 & 0 & 0 \\ -\frac{\bar{r}_3}{y_{l,3}^0} & 0 & 0 & 0 & 0 & 0 & 0 & 0 & 0 \\ 0 & 0 & 0 & 0 & 1 & 0 & 0 & 0 & 0 \\ -\frac{\bar{r}_4}{y_{l,4}^0} & 0 & 0 & 0 & 0 & 0 & 0 & 0 & 0 \end{bmatrix}, \tag{4}$$

where $\bar{r}_i = d_i r_i \sin \alpha_i$ for $i = 1, \cdots, 4$.

Finally, with the nature of the defined input and output in (3.18) and (3.19), it is clear that $\bar{C} = \bar{B}' = \begin{bmatrix} 1 & 0 & \cdots & 0 \end{bmatrix}$.

Appedix D: MATLAB code for SIMULINK model

%Global parameter script file

$alpha = 0.01;$

$m = 75;$ % m = mass of total body

$h = 0.87;$ % e = 0.036, height of foot from ground

$g = 9.81;$ % acceleration due to gravity

$gg = 0.5 * m * g * h;$

$Izz = 1.89;$ % (3,3) element of total body moment of inertia

$Ia = 0.5 * (h^2 * m + Izz);$

%Dimensions of units AB, CD, EF and GH

$d1 = 128.47 * 10^-3;$

$d2 = 74.47 * 10^-3;$

$d3 = 79.76 * 10^-3;$

$d4 = 58.37 * 10^-3;$

$r1 = 21.2 * 10^-3;$

$r2 = 332 * 10^-3;$

$r3 = 32.5 * 10^-3;$

$r4 = 32.5 * 10^-3;$

$alpha1 = 26.88 * pi/180;$

$alpha2 = 102 * pi/180;$
$alpha3 = 55 * pi/180;$
$alpha4 = 55 * pi/180;$

%Parameters of mechanical properties of tendon=a, muscle=b, ligament=c

%Unit AB–1st unit

$ma1 = 0.054;$
$mb1 = 0.129;$
$mc1 = 0.004;$

$ka1 = 43300;$
$kb1 = 460000;$
$kc1 = 142000;$

$ca1 = 48.35;$
$cb1 = 243.60;$
$cc1 = 23.83;$

%Unit CD–2nd unit
% Tendons:- Achilles tendon + Plantaris
% Muscles:- Triceps surae + Tibialis posterior
% Ligaments:- None

$ma2 = 0.067+0.012;$
$mb2 = 0.225+0.056;$
$mc2 = 0;$
$ka2 = 364000+5710;$
$kb2 = 440000+379000;$
$kc2 = 0;$

$ca2 = 156.17+8.28;$

$cb2 = 314.64 + 145.68;$

$cc2 = 0;$

%Unit EF–3rd unit

% Tendon:-Flexor hallucis longus

% Muscle:-Flexor digitorium longus

% Ligaments:- Calcaneofibular (CFL) + Tibiocalcaneal (TCL)

$ma3 = 0.084;$

$mb3 = 0.034;$

$mc3 = 0.005 + 0.031;$

$ka3 = 43300;$

$kb3 = 43300;$

$kc3 = 127000 + 70000;$

$ca3 = 60.31;$

$cb3 = 38.37;$

$cc3 = 25.20 + 46.58;$

%Unit GH–4th unit

% Tendon:- Peroneus longus

% Muscle:- Extensor digitorium longus

% Ligaments:- Anterior tibiotalar (ATTL) + Posterior tibiotalar (PTTL) + Tibionavicular (TNL)

$ma4 = 0.086;$

$mb4 = 0.026;$

$mc4 = 0.02 + 0.01 + 0.005;$

$ka4 = 43600;$

$kb4 = 43300;$

$kc4 = 70000 + 39100;$

$ca4 = 61.23;$
$cb4 = 33.55;$
$cc4 = 37.41{+}48.37{+}13.98;$

%Constrained Dynamics

$Mo = blkdiag(ma1, mb1 + mc1, ma2, mb2 + mc2, ma3, mb3 + mc3, ma4, mb4 + mc4);$
$M = blkdiag(Ia, Mo, Ia, Mo);$

$Cd1 = [ca1 + cb1 - cb1;$
$- cb1cb1 + cc1];$

$Cd2 = [ca2 + cb2 - cb2;$
$- cb2cb2 + cc2];$

$Cd3 = [ca3 + cb3 - cb3;$
$- cb3cb3 + cc3];$

$Cd4 = [ca4 + cb4 - cb4;$
$- cb4cb4 + cc4];$

$Cb = 1 * eye(8);$
$Co = Cb * blkdiag(Cd1, Cd2, Cd3, Cd4);$
$C = blkdiag(0, Co, 0, Co);$

$K1 = [ka1 + kb1 - kb1;$
$- kb1kb1 + kc1];$

$K2 = [ka2 + kb2 - kb2;$
$- kb2kb2 + kc2];$

$K3 = [ka3 + kb3 - kb3;$
$- kb3kb3 + kc3];$

$K4 = [ka4 + kb4 - kb4;$
$- kb4kb4 + kc4];$

$Ko = 1 * blkdiag(K1, K2, K3, K4);$

%Calculating natural length when $alphal = alphar = 0$

% Right leg

$yro1 = sqrt(d1^2 + r1^2 - 2 * d1 * r1 * cos(alpha1));$
$yro2 = sqrt(d2^2 + r2^2 - 2 * d2 * r2 * cos(alpha2));$
$yro3 = sqrt(d3^2 + r3^2 - 2 * d3 * r3 * cos(alpha3));$
$yro4 = sqrt(d4^2 + r4^2 - 2 * d4 * r4 * cos(alpha4));$

% Left leg

$ylo1 = yro1;$
$ylo2 = yro2;$
$ylo3 = yro3;$
$ylo4 = yro4;$

$ybl1 = sqrt(d1^2 + r1^2 - 2 * d1 * r1 * cos(alpha - alpha1));$
$ybl2 = sqrt(d2^2 + r2^2 - 2 * d2 * r2 * cos(alpha + alpha2));$
$ybl3 = sqrt(d3^2 + r3^2 - 2 * d3 * r3 * cos(alpha + alpha3))$
$ybl4 = sqrt(d4^2 + r4^2 - 2 * d4 * r4 * cos(alpha + alpha4));$

$ybr1 = sqrt(d1^2 + r1^2 - 2 * d1 * r1 * cos(alpha - alpha1));$
$ybr2 = sqrt(d2^2 + r2^2 - 2 * d2 * r2 * cos(alpha + alpha2));$
$ybr3 = sqrt(d3^2 + r3^2 - 2 * d3 * r3 * cos(alpha + alpha3));$
$ybr4 = sqrt(d4^2 + r4^2 - 2 * d4 * r4 * cos(alpha + alpha4));$

$yr1 = ybr1 - yro1;$
$yr2 = ybr2 - yro2;$
$yr3 = ybr3 - yro3;$
$yr4 = ybr4 - yro4;$

$yl1 = ybl1 - ylo1;$
$yl2 = ybl2 - ylo2;$
$yl3 = ybl3 - ylo3;$
$yl4 = ybl4 - ylo4;$

$xl1 = (kb1/(ka1 + kb1)) * yl1;$
$xl2 = (kb2/(ka2 + kb2)) * yl2;$
$xl3 = (kb3/(ka3 + kb3)) * yl3;$
$xl4 = (kb4/(ka4 + kb4)) * yl4;$

$xr1 = xl1;$
$xr2 = xl2;$
$xr3 = xl3;$
$xr4 = xl4;$

%Assigning 'pp' to call later in the function blocks
$pp(1) = m;$
$pp(2) = h;$
$pp(3) = g;$
$pp(4) = gg;$
$pp(5) = d1;$
$pp(6) = d2;$
$pp(7) = d3;$
$pp(8) = d4;$
$pp(9) = r1;$
$pp(10) = r2;$
$pp(11) = r3;$

$$pp(12) = r4;$$
$$pp(13) = alpha1;$$
$$pp(14) = alpha2;$$
$$pp(15) = alpha3;$$
$$pp(16) = alpha4;$$
$$pp(17) = ma1;$$
$$pp(18) = mb1;$$
$$pp(19) = mc1;$$
$$pp(20) = ka1;$$
$$pp(21) = kb1;$$
$$pp(22) = kc1;$$
$$pp(23) = ca1;$$
$$pp(24) = cb1;$$
$$pp(25) = cc1;$$
$$pp(26) = ma2;$$
$$pp(27) = mb2;$$
$$pp(28) = mc2;$$
$$pp(29) = ka2;$$
$$pp(30) = kb2;$$
$$pp(31) = kc2;$$
$$pp(32) = ca2;$$
$$pp(33) = cb2;$$
$$pp(34) = cc2;$$
$$pp(35) = ma3;$$
$$pp(36) = mb3;$$
$$pp(37) = mc3;$$
$$pp(38) = ka3;$$
$$pp(39) = kb3;$$
$$pp(40) = kc3;$$
$$pp(41) = ca3;$$
$$pp(42) = cb3;$$
$$pp(43) = cc3;$$
$$pp(44) = ma4;$$

$pp(45) = mb4;$
$pp(46) = mc4;$
$pp(47) = ka4;$
$pp(48) = kb4;$
$pp(49) = kc4;$
$pp(50) = ca4;$
$pp(51) = cb4;$
$pp(52) = cc4;$
$pp(53) = yro1;$
$pp(54) = yro2;$
$pp(55) = yro3;$
$pp(56) = yro4;$
$pp(57) = ylo1;$
$pp(58) = ylo2;$
$pp(59) = ylo3;$
$pp(60) = ylo4;$
$pp(61) = Ia;$
$pp(62) = gg;$

%SIMULINK embedded math function block code

%Embedded MATLAB function 'q'

function $q = fcn2(p1, pp)$

$alpha1 = pp(13);$
$alpha2 = pp(14);$
$alpha3 = pp(15);$
$alpha4 = pp(16);$

$d1 = pp(5);$
$d2 = pp(6);$
$d3 = pp(7);$

$d4 = pp(8);$

$r1 = pp(9);$
$r2 = pp(10);$
$r3 = pp(11);$
$r4 = pp(12);$

$yro1 = pp(53);$
$yro2 = pp(54);$
$yro3 = pp(55);$
$yro4 = pp(56);$

$ylo1 = pp(57);$
$ylo2 = pp(58);$
$ylo3 = pp(59);$
$ylo4 = pp(60);$

$q = zeros(18, 1);$

$q(1) = p1(1);$
$q(2) = p1(2);$
$q(4) = p1(3);$
$q(6) = p1(4);$
$q(8) = p1(5);$
$q(10) = p1(1);$
$q(11) = p1(6);$
$q(13) = p1(7);$
$q(15) = p1(8);$
$q(17) = p1(9);$

$q(12) = sqrt(d1^2 + r1^2 - 2 * d1 * r1 * cos(q(10) - alpha1)) - yro1;$
$q(3) = q(12) + yro1 - ylo1;$
$q(14) = sqrt(d2^2 + r2^2 - 2 * d2 * r2 * cos(q(10) + alpha2)) - yro2;$

$q(5) = q(14) + yro2 - ylo2;$

$q(16) = sqrt(d3^2 + r3^2 - 2 * d3 * r3 * cos(q(10) + alpha3)) - yro3;$

$q(7) = q(16) + yro3 - ylo3;$

$q(18) = sqrt(d4^2 + r4^2 - 2 * d4 * r3 * cos(q(10) + alpha4)) - yro4;$

$q(9) = q(18) + yro4 - ylo4;$

%Embedded MATLAB function 'dq'

function $dq = fcn8(Q, dp1)$

$Q1 = Q(1 : 18, 1 : 9);$

$dq = Q1 * dp1$

%Embedded MATLAB function 'C'

function $[C2, C1, z] = fcn3(dq, M, C, Q, pp, q)$

eml.extrinsic('blkdiag');

$alpha1 = pp(13);$

$alpha2 = pp(14);$

$alpha3 = pp(15);$

$alpha4 = pp(16);$

$alphar = q(10);$

$d1 = pp(5);$

$d2 = pp(6);$

$d3 = pp(7);$

$d4 = pp(8);$

$r1 = pp(9);$

$r2 = pp(10);$

$r3 = pp(11);$
$r4 = pp(12);$

$yro1 = pp(53);$
$yro2 = pp(54);$
$yro3 = pp(55);$
$yro4 = pp(56);$

$ybr1 = q(12) + yro1;$
$ybr2 = q(14) + yro2;$
$ybr3 = q(16) + yro3;$
$ybr4 = q(18) + yro4;$

$s1 = sin(alphar - alpha1);$
$s2 = sin(alphar + alpha2);$
$s3 = sin(alphar + alpha3);$
$s4 = sin(alphar + alpha4);$

$ed1 = [01];$
$Ed = zeros(4, 8);$
$Ed = blkdiag(ed1, ed1, ed1, ed1);$

$Q1 = Q(1 : 18, 1 : 9);$
$Q2 = Q(1 : 18, 10 : 18);$

$c1 = cos(alphar - alpha1);$
$c2 = cos(alphar + alpha2);$
$c3 = cos(alphar + alpha3);$
$c4 = cos(alphar + alpha4);$

$z1 = (d1 * r1/ybr1^2) * (c1 * ybr1 - d1 * r1 * s1/ybr1) * dq(10);$
$z2 = (d2 * r2/ybr2^2) * (c2 * ybr2 - d2 * r2 * s2/ybr2) * dq(10);$
$z3 = (d3 * r3/ybr3^2) * (c3 * ybr3 - d3 * r3 * s3/ybr3) * dq(10);$

$z4 = (d4 * r4/ybr4^2) * (c4 * ybr4 - d4 * r4 * s4/ybr4) * dq(10);$

$z = [z1; z2; z3; z4];$

$dQ11 = [zeros(1, 9); Ed' * z \ zeros(8, 8)];$
$dQ1 = [dQ11; dQ11];$

$M1 = Q1' * M * Q1;$
$iM1 = inv(M1);$

$C1 = Q1' * (C * Q1 + M * dQ1);$
$C2 = Q2' * (eye(18) - M * Q1 * iM1 * Q1') * M * dQ1 + Q2' * C * Q1 - Q2' * M * Q1 * iM1 * C1;$

%Embedded MATLAB function 'G'

function $[G1, G2, G] = fcn4(Q, pp, q, Ko, M)$

eml.extrinsic('blkdiag');

$gg = pp(4);$

$GG11 = zeros(18, 18);$
$GG11 = blkdiag(0, Ko, 0, Ko);$

$gl = zeros(9, 1);$
$gl(1) = -gg * sin(q(1));$
$gr = zeros(9, 1);$
$gr(1) = -gg * sin(q(10));$
$gv = [gl; gr];$

$G = GG11 * q + gv;$

$Q1 = Q(1:18, 1:9);$
$Q2 = Q(1:18, 10:18);$

$G1 = Q1' * G;$

$M1 = Q1' * M * Q1;$

$G2 = Q2' * (eye(18) - M * Q1 * inv(M1) * Q1') * G;$

%Embedded MATLAB function 'lambda'

function $lambda = fcn9(C2, G2, dp1)$

$lambda = C2 * dp1 + G2;$

%Embedded MATLAB function 'ddp1'

function $ddp1 = fcn9(M, C1, G1, Q, dp1)$

$Q1 = Q(1:18, 1:9);$

$M1 = Q1' * M * Q1;$

%Embedded MATLAB function 'F'

function $F = fcn9(pp, q)$

$alpha1 = pp(13);$
$alpha2 = pp(14);$
$alpha3 = pp(15);$
$alpha4 = pp(16);$

$alphar = q(10);$

$$d1 = pp(5);$$
$$d2 = pp(6);$$
$$d3 = pp(7);$$
$$d4 = pp(8);$$

$$r1 = pp(9);$$
$$r2 = pp(10);$$
$$r3 = pp(11);$$
$$r4 = pp(12);$$

$$yro1 = pp(53);$$
$$yro2 = pp(54);$$
$$yro3 = pp(55);$$
$$yro4 = pp(56);$$

$$yr1 = pp(63);$$
$$yr2 = pp(64);$$
$$yr3 = pp(65);$$
$$yr4 = pp(66);$$

$$s1 = sin(alphar - alpha1);$$
$$s2 = sin(alphar + alpha2);$$
$$s3 = sin(alphar + alpha3);$$
$$s4 = sin(alphar + alpha4);$$

$$
F = \begin{pmatrix}
1 & 0 & 0 & 0 & 0 & 0 & 0 & 0 & 0 & -1 & 0 & 0 & 0 & 0 & 0 & 0 & 0 & 0; \\
0 & 0 & 1 & 0 & 0 & 0 & 0 & 0 & 0 & 0 & 0 & -1 & 0 & 0 & 0 & 0 & 0 & 0; \\
0 & 0 & 0 & 0 & 1 & 0 & 0 & 0 & 0 & 0 & 0 & 0 & 0 & -1 & 0 & 0 & 0 & 0; \\
0 & 0 & 0 & 0 & 0 & 0 & 1 & 0 & 0 & 0 & 0 & 0 & 0 & 0 & 0 & -1 & 0 & 0; \\
0 & 0 & 0 & 0 & 0 & 0 & 0 & 0 & 1 & 0 & 0 & 0 & 0 & 0 & 0 & 0 & 0 & -1; \\
0 & 0 & 0 & 0 & 0 & 0 & 0 & 0 & 0 & -2*d1*r1*s1 & 0 & 2*(yr1+yro1) & 0 & 0 & 0 & 0 & 0 & 0; \\
0 & 0 & 0 & 0 & 0 & 0 & 0 & 0 & 0 & -2*d2*r2*s2 & 0 & 0 & 0 & 2*(yr2+yro2) & 0 & 0 & 0 & 0; \\
0 & 0 & 0 & 0 & 0 & 0 & 0 & 0 & 0 & -2*d3*r3*s3 & 0 & 0 & 0 & 0 & 0 & 2*(yr3+yro3) & 0 & 0; \\
0 & 0 & 0 & 0 & 0 & 0 & 0 & 0 & 0 & -2*d4*r4*s4 & 0 & 0 & 0 & 0 & 0 & 0 & 0 & 2*(yr4+yro4);
\end{pmatrix}
$$

%Embedded MATLAB function 'F'lambda'

function $[z, zunits] = fcn9(F, lambda, q, pp)$

$alpha1 = pp(13);$
$alpha2 = pp(14);$
$alpha3 = pp(15);$
$alpha4 = pp(16);$

$alphar = q(10);$

$d1 = pp(5);$
$d2 = pp(6);$
$d3 = pp(7);$
$d4 = pp(8);$

$r1 = pp(9);$
$r2 = pp(10);$
$r3 = pp(11);$
$r4 = pp(12);$

$s1 = sin(alphar - alpha1);$
$s2 = sin(alphar + alpha2);$
$s3 = sin(alphar + alpha3);$
$s4 = sin(alphar + alpha4);$

$z = F' * lambda;$

$z6 = -d1 * r1 * s1 * lambda(6);$
$z7 = -d2 * r2 * s2 * lambda(7);$
$z8 = -d3 * r3 * s3 * lambda(8);$
$z9 = -d4 * r4 * s4 * lambda(9);$

zunits $=[z6z7z8z9]'$;

% Linearisation and model reduction of original system

$lalpha0 = 0$;

% Initial Conditions %
$p1 = zeros(9, 1)$;
$p10 = lalpha0$;
$p11 = xl1$;
$p12 = xl2$;
$p13 = xl3$;
$p14 = xl4$;
$p15 = xr1$;
$p16 = xr2$;
$p17 = xr3$;
$p18 = xr4$;

% Inverse mapping %
$q = zeros(18, 1)$;
$q1 = p10$;
$q2 = p11$;
$q4 = p12$;
$q6 = p13$;
$q8 = p14$;
$q10 = p10$;
$q11 = p15$;
$q13 = p16$;
$q15 = p17$;
$q17 = p18$;

$q12 = sqrt(d1^2 + r1^2 - 2 * d1 * r1 * cos(q10 - alpha1)) - yro1$;

$q3 = q12 + yro1 - ylo1;$

$q14 = sqrt(d2^2 + r2^2 - 2 * d2 * r2 * cos(q10 + alpha2)) - yro2;$

$q5 = q14 + yro2 - ylo2;$

$q16 = sqrt(d3^2 + r3^2 - 2 * d3 * r3 * cos(q10 + alpha3)) - yro3;$

$q7 = q16 + yro3 - ylo3;$

$q18 = sqrt(d4^2 + r4^2 - 2 * d4 * r3 * cos(q10 + alpha4)) - yro4;$

$q9 = q18 + yro4 - ylo4;$

$s1 = \sin(lalpha0 - alpha1);$
$s2 = \sin(lalpha0 + alpha2);$
$s3 = \sin(lalpha0 + alpha3);$
$s4 = \sin(lalpha0 + alpha4);$

% Coefficient matrices %

$e = 2 * [d1 * r1 * s1d2 * r2 * s2d3 * r3 * s3d4 * r4 * s4]';$
$D = 2 * blkdiag(ybr1, ybr2, ybr3, ybr4);$
$Db = inv(D);$

$e1 = [1 \quad 0];$
$ed1 = [0 \quad 1];$

$E = blkdiag(e1, e1, e1, e1);$
$Ed = blkdiag(ed1, ed1, ed1, ed1);$

$id = 0.5 * diag([1/ybr1, 1/ybr2, 1/ybr3, 1/ybr4]);$

$Q1 = [1 \quad zeros(1,8);$
$Ed' * id * e \quad E' \quad zeros(8,4);$
$1 \quad zeros(1,8);$
$Ed' * id * e \quad zeros(8,4) \quad E'];$

% Mass and inertia matrix and centrifugal and Coriolis torques %

$Mb = Q1' * M * Q1;$
$Cb = Q1' * C * Q1;$

$lyr1 = d1 * r1 * sin(alpha1)/yro1;$
$lyr2 = d2 * r2 * sin(alpha2)/yro2;$
$lyr3 = d3 * r3 * sin(alpha3)/yro3;$
$lyr4 = d4 * r4 * sin(alpha4)/yro4;$

$QL = [0 \quad 1 \quad 0 \quad 0 \quad 0 \quad 0 \quad 0 \quad 0 \quad 0$
$lyr1 \quad 0 \quad 0 \quad 0 \quad 0 \quad 0 \quad 0 \quad 0 \quad 0$
$0 \quad 0 \quad 1 \quad 0 \quad 0 \quad 0 \quad 0 \quad 0 \quad 0$
$lyr2 \quad 0 \quad 0 \quad 0 \quad 0 \quad 0 \quad 0 \quad 0 \quad 0$
$0 \quad 0 \quad 0 \quad 1 \quad 0 \quad 0 \quad 0 \quad 0 \quad 0$
$lyr3 \quad 0 \quad 0 \quad 0 \quad 0 \quad 0 \quad 0 \quad 0 \quad 0$
$0 \quad 0 \quad 0 \quad 0 \quad 1 \quad 0 \quad 0 \quad 0 \quad 0$
$lyr4 \quad 0 \quad 0 \quad 0 \quad 0 \quad 0 \quad 0 \quad 0 \quad 0];$

$QR = [0 \quad 0 \quad 0 \quad 0 \quad 0 \quad 1 \quad 0 \quad 0 \quad 0$
$lyr1 \quad 0 \quad 0 \quad 0 \quad 0 \quad 0 \quad 0 \quad 0 \quad 0$
$0 \quad 0 \quad 0 \quad 0 \quad 0 \quad 0 \quad 1 \quad 0 \quad 0$
$lyr2 \quad 0 \quad 0 \quad 0 \quad 0 \quad 0 \quad 0 \quad 0 \quad 0$
$0 \quad 0 \quad 0 \quad 0 \quad 0 \quad 0 \quad 0 \quad 1 \quad 0$
$lyr3 \quad 0 \quad 0 \quad 0 \quad 0 \quad 0 \quad 0 \quad 0 \quad 0$
$0 \quad 0 \quad 0 \quad 0 \quad 0 \quad 0 \quad 0 \quad 0 \quad 1$
$lyr4 \quad 0 \quad 0 \quad 0 \quad 0 \quad 0 \quad 0 \quad 0 \quad 0];$

$GG = [0 \quad 0 \quad 0 \quad 0 \quad 0 \quad 0 \quad 0 \quad 0 \quad 0$

$Ko * QL$

$0 \quad 0 \quad 0 \quad 0 \quad 0 \quad 0 \quad 0 \quad 0 \quad 0$

$Ko * QR];$

$Gg = [gg \quad 0 \quad 0 \quad 0 \quad 0 \quad 0 \quad 0 \quad 0 \quad 0$

$0 \quad 0 \quad 0 \quad 0 \quad 0 \quad 0 \quad 0 \quad 0 \quad 0$

$0 \quad 0 \quad 0 \quad 0 \quad 0 \quad 0 \quad 0 \quad 0 \quad 0$

$0 \quad 0 \quad 0 \quad 0 \quad 0 \quad 0 \quad 0 \quad 0 \quad 0$

$0 \quad 0 \quad 0 \quad 0 \quad 0 \quad 0 \quad 0 \quad 0 \quad 0$

$0 \quad 0 \quad 0 \quad 0 \quad 0 \quad 0 \quad 0 \quad 0 \quad 0$

$0 \quad 0 \quad 0 \quad 0 \quad 0 \quad 0 \quad 0 \quad 0 \quad 0$

$0 \quad 0 \quad 0 \quad 0 \quad 0 \quad 0 \quad 0 \quad 0 \quad 0$

$0 \quad 0 \quad 0 \quad 0 \quad 0 \quad 0 \quad 0 \quad 0 \quad 0$

$gg \quad 0 \quad 0 \quad 0 \quad 0 \quad 0 \quad 0 \quad 0 \quad 0$

$0 \quad 0 \quad 0 \quad 0 \quad 0 \quad 0 \quad 0 \quad 0 \quad 0$

$0 \quad 0 \quad 0 \quad 0 \quad 0 \quad 0 \quad 0 \quad 0 \quad 0$

$0 \quad 0 \quad 0 \quad 0 \quad 0 \quad 0 \quad 0 \quad 0 \quad 0$

$0 \quad 0 \quad 0 \quad 0 \quad 0 \quad 0 \quad 0 \quad 0 \quad 0$

$0 \quad 0 \quad 0 \quad 0 \quad 0 \quad 0 \quad 0 \quad 0 \quad 0$

$0 \quad 0 \quad 0 \quad 0 \quad 0 \quad 0 \quad 0 \quad 0 \quad 0$

$0 \quad 0 \quad 0 \quad 0 \quad 0 \quad 0 \quad 0 \quad 0 \quad 0$

$0 \quad 0 \quad 0 \quad 0 \quad 0 \quad 0 \quad 0 \quad 0 \quad 0];$

$Gb = Q1' * (GG + Gg);$

% Transfer function %

$b = [1$

$zeros(8, 1)];$

$A = [zeros(9, 9) \quad eye(9)$

$- inv(Mb) * Gb \quad - inv(Mb) * Cb];$

$B = [zeros(9, 1)$

$inv(Mb) * b];$

$CC = [b'\quad zeros(1, 9)];$

$D = 0;$

$[num, den] = ss2tf(A, B, CC, D);$

$T = tf(num, den);$

$[z, p, k] = tf2zp(num, den);$

% Model Reduction %

$rsys = balred(T, 2);$

$[num1, den1] = tfdata(rsys, 'v');$

$n = 2;$

$zz = -2 * ones(1, n);$

$c = zeros(n + 1, 1); \quad c(1) = 1;$

$for j = 1 : n$

$c(2 : j + 1) = c(2 : j + 1)\text{-}zz(j) * c(1 : j);$

end

$numb = den1(2 : n + 1) - c(2 : n + 1)';$

$denb = [1 c(2 : n + 1)'];$

$Tb = tf(numb, denb);$

Appendix E: Determination of accuracy and reliability of biomechanical equipment used in postural balance assessment

To determine the accuracy and reliability of the Qualysis motion capture system a set of distance and angular tests were conducted. Ten cameras captured raw kinematic data at 100 Hz. The system was calibrated as normal. The signals were then processed in Qualysis using Moving average algorithm per 11 frames. For the distance trials, a wand of a known length was moved throughout the measurement volume 10 times for 10 seconds each. The distance between two markers (14mm diameter) was calculated. The known distance between markers on the wand was 498.7mm. The measurements of the wand, Table 1, the mean ($\pm$ SD) difference between the known length and measured length was 0.44 $\pm$ 0.33 mm and the RMS was 0.54. The coefficient of variation was 0.75. However, if the coefficient of variation was calculated for the absolute mean difference, it was 0.68.

Table 1: Measurement of wand length using Qualysis

Trial	Wand length (mm)	Difference (mm)	Absolute difference (mm)
01	498.43	0.27	0.27
02	497.62	1.08	1.08
03	498.34	0.36	0.36
04	497.91	0.79	0.79
05	498.42	0.28	0.28
06	498.77	-0.07	0.07
07	498.49	0.21	0.21
08	498.16	0.54	0.54
09	498.42	0.28	0.28
10	498.04	0.66	0.66
Mean	498.26	0.44	0.45
S.D.	0.33	0.33	0.31

For the angular trials, three reflective markers (14 mm diameter) were placed onto a plastic goniometer. One marker was placed at the apex of each of the two arms of the goniometer and one marker at the vertex. The goniometer was adjusted at the following known angles: 45, 90 and 180 and was moved throughout the measurement volume 10 times for 10 seconds each.

Table 2: Angle (45 °)measured using Qualysis.

Trial	Angle °	Difference °	Absolute difference °
01	45.08	-0.08	0.08
02	44.97	0.03	0.03
03	45.00	0.00	0.00
04	44.90	0.10	0.10
05	44.90	0.10	0.10
06	45.10	-0.10	0.10
07	45.10	-0.10	0.10
08	45.06	-0.06	0.06
09	45.06	-0.06	0.06
10	45.06	-0.06	0.06
Mean	45.023	-0.02	0.07
S.D.	0.08	0.08	0.03

For the 45° angle, Table 2, the mean ($\pm$ SD) difference between the known and measured angles was $0.02 \pm 0.08°$ and the coefficient of variation was 0.50.

Table 3: Angle (90 °)measured using Qualysis.

Trial	Angle °	Difference °	Absolute difference °
01	89.89	0.11	0.11
02	89.89	0.11	0.11
03	89.89	0.11	0.11
04	89.91	0.09	0.09
05	89.91	0.09	0.09
06	89.99	0.01	0.01
07	89.89	0.11	0.11
08	89.91	0.09	0.09
09	89.91	0.09	0.09
10	89.91	0.09	0.09
Mean	89.91	0.09	0.03
S.D.	0.00	0.30	0.30

For the 90° angle, Table 3, the mean (± SD) difference between the known and measured angles was $0.09 \pm 0.03°$ and the coefficient of variation was 0.33.

Table 4: Angle (180 °)measured using Qualysis.

Trial	Angle °	Difference °	Absolute difference °
01	178.90	1.10	1.10
02	178.80	1.20	1.20
03	178.80	1.20	1.20
04	178.90	1.10	1.10
05	178.70	1.30	1.30
06	178.70	1.30	1.30
07	178.90	1.10	1.10
08	178.90	1.10	1.10
09	178.90	1.10	1.10
10	178.80	1.20	1.20
Mean	178.83	1.17	1.17
S.D.	0.08	0.08	0.08

For the 180° angle, Table 4, the mean (± SD) difference between the known and measured angles was $1.17 \pm 0.08°$ and the coefficient of variation was 0.07.

In order to determine the accuracy of the Kistler force plates, static weights were placed onto the respective force plates and the vertical force was recorded. The following known weights were used: (5 kg), (10 kg), (25 kg), (50 kg), (70 kg). The force for each weight was calculated 10 times for 10 seconds each. The mean and standard deviation (S.D.) have been summarized in Table 5. The coefficient of variation between the two plates was found to be zero for all cases.

Table 5: Measurement of known loads through Qualysis.

Applied load	5 (kg)	10 (kg)	25 (kg)	50 (kg)	70 (kg)
Mean measured					
Kistler (plate 1)	46.55	99.47	245.28	490.48	686.74
S.D.	0.19	0.29	0.24	0.26	0.23
Mean measured					
Kistler (plate 2)	46.62	99.52	245.04	490.33	686.38
S.D.	0.19	0.27	0.26	0.27	0.21